GPR183 controls spatial organization and survival of hepatic conventional dendritic cells within hepatic portal regions *via* M-CSF and Gas6

Dissertation

zur

Erlangung des Doktorgrades (Dr. rer. nat.)

der

Mathematisch-Naturwissenschaftlichen Fakultät

der

Rheinischen Friedrich-Wilhelms-Universität Bonn

vorgelegt von

Sumit Sheoran, MSc

aus

Bhagana, INDIA

January, 2023

Angefertigt mit Genehmigung der Mathematisch-Naturwissenschaftlichen Fakultät der Rheinischen Friedrich-Wilhelms-Universität Bonn

Erstgutachter: Prof. Dr. Andreas Schlitzer

Zweitgutachterin: Prof. Dr. Evi Kostenis

Tag der Promotion: 03.04.2023

Erscheinungsjahr: 2023

Table of Contents

Acknowledgements

Firstly, I would like to express my sincere gratitude to my supervisor **Prof. Dr. Andreas Schlitzer** for conceptualizing this wonderful project and for giving me the opportunity to work on this wonderful and exciting project. Thank you for always encouraging and motivating me during the time of my PhD studies and for providing good insights on my experimental setups and science. Your knowledge sharing and patience throughout my research work gave me more confidence in myself and made me work independently during my PhD studies. You always have new ideas and answers to all my problems in the lab. Thank you for always believing in me and for being proud to call me your student and being happy for my achievements (PS. I still remember that hug you gave me when I won the best poster award in Munster!). Thank you for all the good times, support and the supervision for last 3 years.

I would like to thank **Prof. Dr. Evi Kostenis** and **Prof. Dr. Alexander Pfeifer** for being my second supervisor and mentors at the graduate school. Thank you for your suggestions and comments on my work during our GRK meetings and symposiums. This work would have not been possible without your efforts and support. I would also like to express gratitude to **Prof. Dr. Eva Kiermaier** and **Prof. Dr. Veronika Lukacs-Kornek** for agreeing to be a part of my doctoral committee.

Living far away from the family is always hard, but I had my friends and colleagues at **Schlitzer lab** around me, whom I could call my family in Bonn. Thank you, **David, the dbchen and Hannah, the flamy**, for these wonderful years of togetherness and companionship. I will always cherish the friendship we have and the times we enjoyed together in the lab and outside the lab. You guys always made the working environment so pleasant and comfortable. Cheers to ours trips together with **Tobi** and **Rodders**, it was a fun time with you guys in Belgium, Netherlands and not to forget in INDIA. Thank you all for being such amazing friends

and for coming all the way to India for my special day. Thank you so much for always listening to my problems, heartbreaks, my crying and what not. You guys have always supported me and treated me like a family. It would be hard to express my feelings with words here. Love, ALWAYS!

I would like to thank everyone in the Schlitzer lab for creating such friendly and pleasant working environment. Thank you, **Lili** for helping me initially with the project and for being with me in the lab until late hours. Thanks to **Jiangyan** for helping me with running my R scripts and **Maria** for always taking care of genotyping and transporting mice and reagents. Special thanks to **Martina** for helping with lab organization and for those warm hugs every time I returned back from India after holidays. Thank you for being so friendly and nice and for teaching me German. I would like to also thank **David, Marie** and **Jake** for reading and correcting my thesis and for providing the valuable inputs to my work.

Thank you, **Anna** for sharing the apartment with me for last 3 years. You were a nice flat mate and a wonderful friend. Thanks for all the memories and outings together. Thanks, **Ziad** for being my only Indian friend in Bonn. Thank you for being the friend I can always count upon anytime.

Last but not the least, I would like to thanks my family for always believing in me and supporting me during my PhD and thanks to my beloved wife **Neha** for being such a nice support.

I had a nice time in Germany during my PhD and it would not have been possible without the contribution of my supervisors, collaborators, colleagues, friends and family. Thanks to everyone for their valuable contribution in this wonderful journey. Signing off!

vielen Dank!

Abstract

G protein-coupled receptor 183 (GPR183) recognizes 7α,25-dihydroxycholesterol (7α,25-OHC) and exerts chemotactic action upon recognition. Recent studies have shown that GPR183 is highly expressed in T, B and dendritic cells (DCs) and is essential for the correct positioning of splenic DCs within the marginal zones of spleen. Nevertheless, whether GPR183 plays a similar role in positioning and regulating DC homeostasis in the cholesterol-rich microenvironment of the murine liver remains elusive. Therefore, we set out to investigate the role of GPR183 on murine liver resident dendritic cells during homeostasis.

To understand the role of GPR183 in hepatic DC maintenance, we analyzed the abundance and phenotype of liver resident DCs in WT, *Gpr183*$^{-/-}$, *Gpr183*$^{flox/flox}$-*Zbtb46*-cre^{+} *Ch25h*$^{-/-}$, *Cyp7b1*$^{-/-}$ animals by means of high dimensional flow cytometry coupled to transcriptomics and spatial imaging analyses.

Our data shows that lack of GPR183 resulted in increased abundance of hepatic cDC and DC progenitors due to their increased in-situ proliferation and impaired apoptosis. Next, we investigated whether an active production of 7α,25-OHC is needed to maintain normal DC numbers in the liver and we assessed the liver-resident DC compartment of *Ch25h*$^{-/-}$ and *Cyp7b1*$^{-/-}$ mice. Here we observed an increased abundance of hepatic DCs within these mice. Furthermore, analysis of chimeric experiments revealed that the radioresistant stromal compartment is crucial for maintaining the DC pool size and that DCs are closely associated with 7α,25-OHC producing endothelial cells in the portal regions of the liver. Next, our single-cell transcriptomics data and NIchenet-based in-silico receptor-ligand inference alongside spatial analyses identified M-CSF-M-CSFR and Gas6-Axl endothelial cell-DC interactions as crucial to the control of DC pool size within the murine liver. Additionally, blocking the gut-

liver axis cholesterol transport also showed similar M-CSF and Gas6 dependent increase in hepatic DC numbers. Finally, to understand the role of GPR183 in disease and pathophysiological conditions we fed WT and *Gpr183*$^{flox/flox}$-*Zbtb46*-cre^{+} animals on CDAA-HFD and our data showed a significantly increased lipid content and decreased ALT and AST serum concentration in KO animals compared to their WT counterparts.

Taken together, these findings demonstrate that GPR183 plays a cell-intrinsic role in organization and survival of hepatic DCs in murine liver. Additionally, M-CSF and Gas6 produced by endothelial cells in the portal regions act as the guiding niche factor for positioning and survival of cDCs within the portal regions of liver. Our data also shows possible implication of GPR183 in health and disease and could pave ways for developing novel therapeutic targets for liver diseases.

Keywords: GPR183, Dendritic cells, Mononuclear phagocytes, Cholesterol, Homeostasis, M-CSF, Gas6, Niche, Microenvironment, Endothelial cells

Abbreviations

In the order they appear in the text

Abbreviation	Full form
PRRs	Pattern-Recognition Receptors
MAMPs	Microbe-Associated Molecular Patterns
PAMPs	Pathogen-Associated Molecular Patterns
NK	Natural Killer
KC	Kupffer Cell
HSCs	Hepatic Stellate Cells
DC	Dendritic Cells
ILCs	Innate Lymphoid Cells
APCs	Antigen Presenting Cells
TCRs	T Cell Receptors
BCRs	B Cell Receptors
MPs	Mononuclear Phagocytes
MHCII	Major Histocompatibility Class II
HSPCs	Hematopoietic Stem and Progenitor Cells
BM	Bone Marrow
CLPs	Common Lymphoid Progenitors
CMPs	Common Myeloid Progenitors
cDCs	Classical DCs
pDCs	Plasmacytoid DCs
Flt3	Fms-Like Tyrosine Kinase 3
MDP	Macrophage Dendritic Cell Progenitors
MPS	Mononuclear Phagocyte System
CDP	Common DC Progenitor
ID2	DNA-Binding 2
ZBTB46	Zinc Finger and Btb Domain Containing 46
IFN	Interferon
IRF8	Interferon Regulatory Factor 8
TCF4	Transcription Factor 4
BATF3	Basic Leucine Zipper ATF-Like Transcription Factor 3
IRF4	Interferon Regulatory Factor 4
KLF4	Krüppel-like factor 4
Inf-DCs	Inflammatory DCs
XCR1	X-C Motif Chemokine Receptor 1
Zeb2	Zinc Finger E-Box Binding Homeo Box 2
RelB	V-Rel Avian Reticuloendotheliosis Viral Oncogene Homolog
LT- β	Lymphotoxin
LN	Lymph Node
Thf	T Follicular Helper
AREG	Amphiregulin

VSV	Vesicular Stomatitis Virus
MCMV	Murine Cytomegalovirus
LCMV	Lymphocytic Choriomeningitis Virus
MHV	Mouse Hepatitis Virus
HSV	Herpes Simplex Virus
MoMFs	Monocyte-Derived Macrophages
TNF	Tumor Necrosis Factor
NASH	Nonalcoholic Steatohepatitis
IL	Interleukin
MCP-1	Monocyte Chemoattractant Protein 1
GPR183	G-Protein Coupled Receptor 183
EBI2	Epstein-Barr Virus-Induced G Protein-Coupled Receptor 2
EBV	Epstein-Barr Virus
7α,25-OHC	7α,25-Dihydroxycholesterol
CH25H	Cholesterol-25-Hydroxylase
CYP7B1	Cytochrome P450 Oxysterol 7-Alpha-Hydroxylase
HSD3B7	Hydroxy-Delta-5-Steroid Dehydrogenase, 3 Beta- And Steroid Delta-Isomerase 7
MAP	Mitogen-Activated Protein
ERK	Extracellular-Signal-Regulated Kinase
SRE	Serum Response Element
NFAT	Nuclear Factor of Activated T Cells
NFκB	Nuclear Factor Kappa B
ILC3s	Innate Lymphoid Cells 3
ICOS	Inducible Co-Stimulator
WT	Wild Type
KO	Knockout
DSS	Dextran Sulfate Sodium
SPF	Specific Pathogen-Free
H&E	Hematoxylin and Eosin
FVD	Fixable Viability Dye
HDL-C	High-Density Lipoprotein Cholesterol
CDAA	Choline-Deficient, L-Amino Acid-Defined
ILF	Isolated Lymphoid Follicles
LPS	Lipopolysaccharide
NAFLD	Non-Alcoholic Fatty Liver Disease

List of Figures

1. Introduction

1.1. The immune system

The immune system is a defense network system to detect, destroy and protect the body from various invading foreign pathogens along with its ability to distinguish self from non-self to prevent autoimmunity [1, 2]. This complex immune network functions as a regulator of tissue homeostasis and remodeling, restoring tissue function after encountering an immune challenge [3]. Over the time, the pathogenic microbes have considerably evolved and so has the mammalian immune system to readily respond and adapt accordingly in order to mount an appropriate immune response. Responding to any invading pathogenic insult is carried out by various cell types in the immune system. To fully coordinate this rapid response, immune cells communicate efficiently via cell-cell interactions [4] and also through a wide array of cytokines and chemokines acting as messengers functioning at local, as well as distant sites in the body [5]. The immune system broadly consists of innate and adaptive responses which contain myeloid and lymphoid cells. While the innate immune compartment recognizes selective microbial components at a very broad spectrum [6], the adaptive immune compartment can recognize very specific pathogenic components which are unique to a class of pathogens [7]. Although innate and adaptive arms are functionally two different entities, they are inter-connected and there is ample cross-communication between the two compartments through arrays of cytokines and chemokines to eliminate the invading pathogens efficiently [8, 9].

1.1.1. Innate Immunity

The innate immune compartment is responsible for rapidly sensing and consequently eliminating the invading pathogens and it provides a broader but precise recognition between self and non-self antigens. Innate immune function is mediated by various germline-encoded pattern-recognition receptors (PRRs) which recognize microbe or pathogen-associated molecular patterns (MAMPs or PAMPs) as their targets on microorganisms [10]. The innate immune system consists of various cells such as natural killer (NK) cells, monocytes, macrophages, dendritic cells (DCs) and innate lymphoid cells (ILCs)[10]. NK cells are cytotoxic cells with the ability to kill and produce arrays of cytokines. Macrophages and DCs are known as antigen presenting cells (APCs), which internalize the antigens, and present them to the T cells along with co-stimulatory signals [11]. More about DCs, their development, functional and phenotypical diversity will be discussed in more details in section 1.2.

1.1.2. Adaptive Immunity

The adaptive immunity is characterized by the recognition of antigens by cells with distinct specificity, which then proliferate to produce a large number of identical or nearly identical clones [12]. Upon infection few of these cells remain, forming an immune memory which is a hallmark of the adaptive immunity. This acquired immunity comes with the ability of the immune system to rapidly respond to forthcoming immune insults in a better and efficient way. The adaptive immune system consists of T and B cells which recognize antigens *via* specific receptors, T cell (TCRs) and B cell receptors (BCRs) that are produced by rearrangement of germline-encoded genes, resulting in diverse lymphocyte clones [13, 14]. After their development, maturation of B cells occurs in the bone marrow, whereas T cells

exit to the thymus to undergo further processes of selection and maturation [15, 16]. Primarily, B cells produce antibodies against invading pathogens, which function to neutralize the antigens or specifically target them to be killed by the components of the innate response, such as macrophages or complement proteins [17]. TCR activation triggers the ability of T cells to proliferate, thereby allowing them to either directly kill the infected cells or coordinate their actions with innate APCs [18].

1.2. Dendritic cells (DCs): translating innate to adaptive immunity

DCs are a crucial part of the innate mononuclear cells within the mononuclear phagocytes (MPs). They are capable of sensing, processing and presenting antigens to T cells to orchestrate the adaptive immune response, thereby linking the innate and adaptive immune systems [19]. Initially, DCs were described morphologically by the presence of dendrites and their ability to adhere to the surface[20]. Later studies precised the identification of DCs by the expression of major histocompatibility class II (MHCII) [21] and CD11c [22]. These two markers provided a convenient, yet accurate approach to distinguish DCs from other MPs. In the recent years, due to the advancement of technologies such as mouse models, multi-parameter flow cytometry-based phenotyping and characterization, transcriptome profiling, and mass cytometry, the identification of DCs has become more precise. Collectively, all these methods have allowed to delve deeper into the DC biology and broadened the knowledge of mouse and human DCs and their implications in health and disease.

1.3. Ontogeny of Dendritic cells

Like all other hematopoietic cells, DCs develop from the hematopoietic stem and progenitor cells (HSPCs) in the bone marrow (BM) [23-25]. Over the past few decades, it has been proven

that DCs develop from a different lineage than the other leukocytes, establishing the DC compartment as a distinct hematopoietic branch of the immune system [24]. Common lymphoid progenitors (CLPs) and common myeloid progenitors (CMPs) are considered as the very early committed progenitors giving rise to DCs. This was confirmed with the adoptive transfer of CLPs and CMPs into lethally irradiated mice, as well as with *in vitro* studies that showed the production of classical DCs (cDCs) and plasmacytoid DCs (pDCs) [26-28] in a Fms-like tyrosine kinase 3 (Flt3) ligand-dependent manner [29-31] **(Fig 1.1).**

Development of macrophage dendritic cell progenitors (MDPs) from CMPs marks the commitment of myeloid progenitors to the mononuclear phagocyte system (MPS), giving rise to both, monocytes and DC progeny [32]. MDPs further give rise to common DC progenitor (CDP) which was confirmed with an adoptive transfer experiment of MDPs and CDPs into a non-irradiated recipient. CMPs gave rise to MDPs, CDPs, and pre-cDCs, whereas MDPs only generated CDPs, pre-cDCs and pDCs. Furthermore, CDPs only produced pre-cDCs and pDCs committed lineages [33]. Another similar study also showed and validated that adoptive transfer of CDPs gave rise to cDCs and pDCs and had no potential to produce macrophages [33]. Taken together, these results indicate that CDPs are downstream of MDPs, and that MDPs are more developmentally restricted to early myeloid progenitors than to pDCs, DCs and macrophages. On the other hand, CDPs give rise to pDCs and cDC progenitors [24, 34]. Moreover, different transcription factors have been shown to regulate the development and differentiation of DCs **(Fig 1.1)**. For example, downregulation of DNA-binding protein 2 (ID2) and zinc finger and btb domain containing 46 (ZBTB46), together with the upregulation of interferon (IFN) regulatory Factor 8 (IRF8) and transcription factor 4 (TCF4) results in terminally differentiated pDCs within the BM itself. These pDCs then migrate to peripheral locations [35]. On the other hand, pre-cDCs commitment to pre-cDC1 and pre-cDC2 occurs

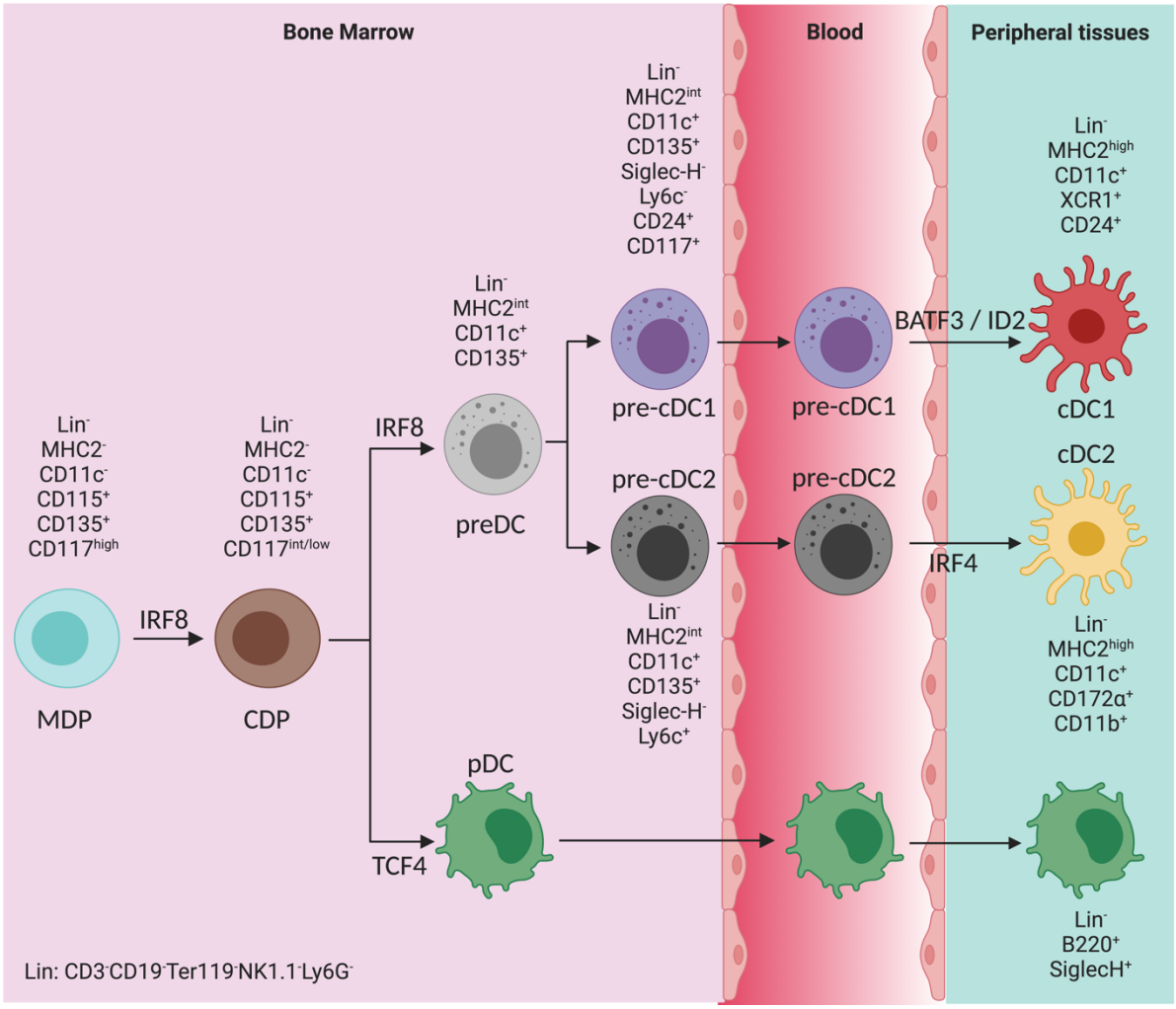

Figure 1.1: Developmental scheme of murine DCs from the early progenitors towards lineage committed tissue resident DCs (adapted from: [36-38]). cDCs and pDCs develop in the BM in a sequential manner. CDP gives rise to MDP in the BM which is regulated by a transcription factor IRF8. CDP further gives rise to preDC and mature pDC which is regulated by IRF8 and TCF4 respectively. pDC is then seeded into peripheral tissue via the blood stream and contribute towards tissue resident pDC pool. Pre-DC splits into cDC1 committed pre-cDC1 and cDC2 which is committed towards pre-cDC2 in the BM itself. These committed pre-cDCs then exit the bone marrow depending on the tissue specific signals they received and become cDC1s and cDC2s in the peripheral tissue. Development of cDC1 is regulated by BATF3 and ID2, while IRF4 is crucial for cDC2s development.

within the BM. These pre-cDCs leave the BM *via* the blood stream to the peripheral tissues, where they differentiate into mature cDC1s and cDC2s depending on the tissue microenvironment and various transcription factors [39]. Maturation of cDC1s is mainly

regulated by IRF8, ID2 and basic leucine zipper ATF-like transcription factor 3 (BATF3) [40, 41], whereas maturation of cDC2s is driven by interferon regulatory factor 4 (IRF4), NOTCH2 and Krüppel-like factor 4 (KLF4) [42].

1.4. Classification and phenotypical diversity of Dendritic Cells

Considering the heterogeneous nature of DCs, based on their ontogeny, cell surface marker expression, transcription factors and functional specialization, DCs are broadly classified as conventional DCs (cDCs), plasmacytoid DCs (pDCs) and inflammatory DCs (inf-DCs).

1.4.1. Conventional Dendritic Cell subsets (cDCs)

The morphology of cDCs is characterized by long dendrite extensions. They express high levels of MHCII and CD11c [22, 43, 44], and also express CD26 extensively in multiple tissues [45]. The transcription factor, ZBTB46 was identified as a canonical marker for cDCs and the reporter mouse model for gene *Zbtb46* was initially used for the identification of progenitors with potential for only one type of cDC, excluding pDCs [46, 47]. cDCs, as well as the other DC subsets, perform antigen presentation function by presenting the antigens to T and B cells *via* MHC class I and II molecules. cDCs are phenotypically and functionally heterogeneous, express different surface markers, and have a variable ontogeny, thus they are further divided into cDC1 and cDC2 subsets [48]. This modern nomenclature is widely followed across various tissues and species.

1.4.1.1. Conventional Dendritic Cell subset 1 (cDC1)

cDC1 subset is a more homogeneous population which resides across multiple tissues. cDC1s are generally characterized by the expression of CD11c, MHCII, CD8α, and CD103 in various tissues [24, 48]. CD103 is thought to be a marker for the migratory DCs and is generally expressed by cDC1 residing in the skin, lung, liver, and kidney [49-53]. On the other hand CD8α is considered as a marker for lymphoid resident DCs and is usually expressed by cDC1 subset in the spleen or other lymphoid organs [54]. Furthermore, the expression of chemokine receptor X-C Motif Chemokine Receptor 1 (XCR1) has been shown to be restricted to cDC1s in various tissues and is largely conserved across species [45, 55, 56]. Additionally, *bona fide* cDC1s can be further delineated by the expression of CD24 and CD26 across different tissues [45].

cDC1 subset generally function as cross-presenting DCs and various studies have shown their ability of cross-presentation of antigens from dying cells and to mount anti-tumor immune responses [57]. The role of cDC1s in humans as cross-presentation is still not very clear as the assumptions are based on *in-vitro* studies, but several studies have shown similar roles of cDC1s in human as well [58-61]. Furthermore, the ability of murine and human cDC1s to produce high levels of type III interferon in response to poly I:C stimulation suggests that they might play a crucial role in antiviral immunity [62].

The development of cDC1 subset is highly dependent on IRF8 [63, 64], ID2 [65] and BATF3 [41, 66]. cDC1 subset expresses low level of IRF4 and Zinc Finger E-Box Binding Homeo box 2 (Zeb2) but expresses high levels of Zbtb46 [46]. Furthermore, Notch signaling plays and important role in cDC1 differentiation and maturation [67, 68]. Murine splenic cDC1s are capable of producing IL-12 in response to viral stimulation but the human cDC1 subset does not respond to poly I:C viral stimulation [67]. Deletion of either IRF8 or DC-specific IL-12

production resulted in increased susceptibility towards *Toxoplasma gondii* infection [69, 70]. Furthermore, by using *Batf3*$^{-/-}$: *Il12p40*$^{-/-}$ mixed BM chimeras it was shown that these defects were intrinsic to only cDC1 subset and not to other DC subsets [71]. In addition, studies using mice which were lacking BATF3 demonstrated that cDC1s are critical for cross-presentation of exogenous antigen to CD8^{+} T cells, which in turn are required for antiviral and antitumor responses [72]. cDC1s also express Clec9a, which helps CD8α^{+} DCs to recognize a preformed signal exposed on necrotic cells thereby playing important role in clearing necrotic and tumor cells *via* cross-priming CD8^{+} T cells [73].

1.4.1.2. Conventional Dendritic Cell subset 2 (cDC2)

cDC2 subset resides in lymphoid as well as non-lymphoid tissues and is more heterogeneous than the cDC1 subset. cDC2s are characterized by the expression of CD4, MHCII, CD11c, CD11b, CD26 and SIRPα (CD172α) [45, 74]. Several tissue-specific subpopulations of cDC2s have been identified based on the expression of other markers. For example, splenic cDC2 can be further delineated based on the expression of CLEC12A, ESAM, and DCIR1 with diverse functional specializations [75, 76]. An intestinal CD11b^{+} DC subpopulation co-expressing CD103 in the small and large intestine has also been identified [77, 78]. Although development of cDC2s requires several transcriptional factors, up to date there is not a single mutant murine model in which cDC2 subset can be selectively ablated genetically. V-Rel Avian reticuloendotheliosis viral oncogene homolog B (RelB) was the first transcription factor which was discovered to specifically contribute the development of cDC2 subset [79, 80]. Unlike cDC1s, CD11b^{+} cDC2 subset exhibit tissue specific transcription factors and cytokines requirements. Recent studies have shown RelB as a critical player for the development of CD4^{+}ESAM^{+} cDC2 within the spleen in a cell-intrinsic manner[81]. Additionally, these cells are

also dependent on Notch2 [82] and lymphotoxin β (LT-β) receptor signaling [83]. On the contrary, $CD11b^{+}CD103^{+}$ cDC2s within the intestine and lung are dependent on IRF4 for their development and maintenance which is required for instructing Th2 [84] and IL-17 responses in mouse as well as human [42, 85]. IRF4 also controls CCR7 expression in dermal DCs, which in turn promotes their migration to the skin-draining lymph node (LN) [86]. Furthermore, antigen processing and presentation on either MHC class I or MHC class II is driven by the IRF8-IRF4 axis [86]. Under steady state conditions, *Klf4* expression is indispensable for the development of cDC2s in lung and migratory cDC2s in the skin-draining LN. Interestingly, depletion of these cells resulted in enhanced lung inflammation during house dust mite challenge and significantly increased susceptibility to helminth infection [87]. $CD301b^{+}$ cDC2 is also known as another subpopulation within the cDC2 compartment which has been described in multiple tissues such as murine skin, lung and LN. Interestingly, $CD301b^{+}$ cDC2s are important for determining $CD4^{+}$ T cell fate, driving Th2 cell-mediated immune responses [88], and suppressing T follicular helper (Tfh) cells and antibody responses to antigens [89]. Recently, two different subpopulations within the cDC2 subset have been reported based on their expression of transcription factors T-bet and RORγt. They are termed as cDC2A ($T\text{-}bet^{+}$) and cDC2B ($T\text{-}bet^{-}$ $ROR\gamma t^{+}$)[90]. $T\text{-}bet^{-}$ cDC2B are similar to $CD301b^{+}$ cDC subset and exhibit a pro-inflammatory profile, whereas the cDC2A DC subset is distinguished from the cDC2B by the expression of amphiregulin (AREG) and is critical for tissue repair.

1.4.2. Plasmacytoid Dendritic Cell subset (pDCs)

pDCs were first discovered in human LN in the early 1950s [91] and were initially labelled as "plasma cells" and "interferon-producing cells" because of their similar morphology with B cells [92, 93]. pDCs are characterized by having high levels of rough endoplasmic reticulum

and secreting high amounts of IFNs during viral infections [93, 94]. pDCs are continuously produced in the BM and are seeded as mature cells in the periphery, where they are non-proliferative and terminally differentiated having very short lifespan [95]. Phenotypically, murine pDC subset expresses Siglec-H, CD45R (B220), CD45RA, Ly6C and BST2 (CD317) [96].

Several *in-vitro* studies on pDCs have shown a central role for controlling systemic viral infections, but the *in-vivo* results on the role of pDCs in viral infections have been controversial. For instance, pDCs are dispensable for the *in-vivo* control of vesicular stomatitis virus (VSV), murine cytomegalovirus (MCMV), lymphocytic choriomeningitis virus (LCMV) and influenza infections [97-99] because cDCs alone were able to compensate for the loss of pDCs in MCMV [100] and ectromelia viral infections [101] . However, genetic ablation and antibody blocking-based pDC depletion studies have shown that pDCs are necessary for controlling the mouse hepatitis virus (MHV) [99, 102]. Furthermore, pDCs are required for early production of IFN-I (within 8–12 hours), proinflammatory cytokine production, NK cell activation and CD8 T cell responses during systemic herpes simplex virus (HSV) infection [103].

Similar to their cDC counterpart, Flt3L alone is sufficient for the development of pDCs. Additionally, for further development, functional specification, and maintenance, pDCs require high-level expression of TCF4 (also known as E2-2), IRF8 and BCL11A [40, 104-107]. To allow the generation of pDCs from CDPs, the expression of the ID2, which inhibits the activity of the major pDC transcription factor (i.e. TCF4), needs to be suppressed [108, 109].

1.4.3. Inflammatory Dendritic Cells (Inf-DCs)

Inf-DCs are not present under the steady state conditions and are usually derived from circulating Ly6C high monocytes under inflammation, infection and cancer [24, 110-112]. Mouse Inf-DCs display a similar phenotype as the cDC2 subset with high expression levels of

CD11b, CD11c and MHCII. Additionally, they also express CD206, CD115, Ly6C, F4/80, CD107b, FcεRI, and CD64 [113]. Alike cDCs, murine Inf-DCs also express the transcription factor Zbtb46, therefore, FcεRI becomes a useful marker to discriminate Inf-DCs from cDCs and macrophages [114]. Functionally, Inf-DCs are different from macrophages and they migrate to LN in a CCR7-dependent manner and activate T cells [115, 116]. Various studies have shown that Inf-DCs usually express TLR2, TLR4, TLR6, TLR8 and TLR9 and they respond to LPS, peptidoglycans, and R848 thereby producing various inflammatory cytokines [113].

1.5. Organization of the hepatic immune microenvironment

The liver is a primary metabolic organ, with a high degree of vascularization within, resulting in slow blood flow, and highly permeable fenestrated endothelia that allows direct bloodstream access to liver tissue cells [117]. The liver is frequently exposed to external inflammatory cues from food or the gut microbiota, which in conjunction with the ongoing presence of bacterial endotoxins would elicit an immune response. However there exists a specialized system within the liver which guards against unnecessary immune activation and still provides the necessary immunosurveillance for pathogens and malignant cells [118].

The liver contains a unique network of myeloid and lymphoid immune cells in steady state **(Fig 1.2)**. Approximately 80% of the body's macrophages are found in the liver, which is also watched by other myeloid cells such blood monocytes, which scan the liver vasculature before infiltrating the tissue [119]. Although monocyte-derived cells can give rise to monocyte-derived macrophages (MoMFs) or liver DCs [120], they do not contribute to the liver's local resident macrophage population, known as Kupffer cells (KCs) [121]. KCs develop from resident stem cells derived from the embryonic yolk sack [121-123] and produce a self-

renewing pool of organ-resident macrophages independent of the myeloid monocytic compartment [119].

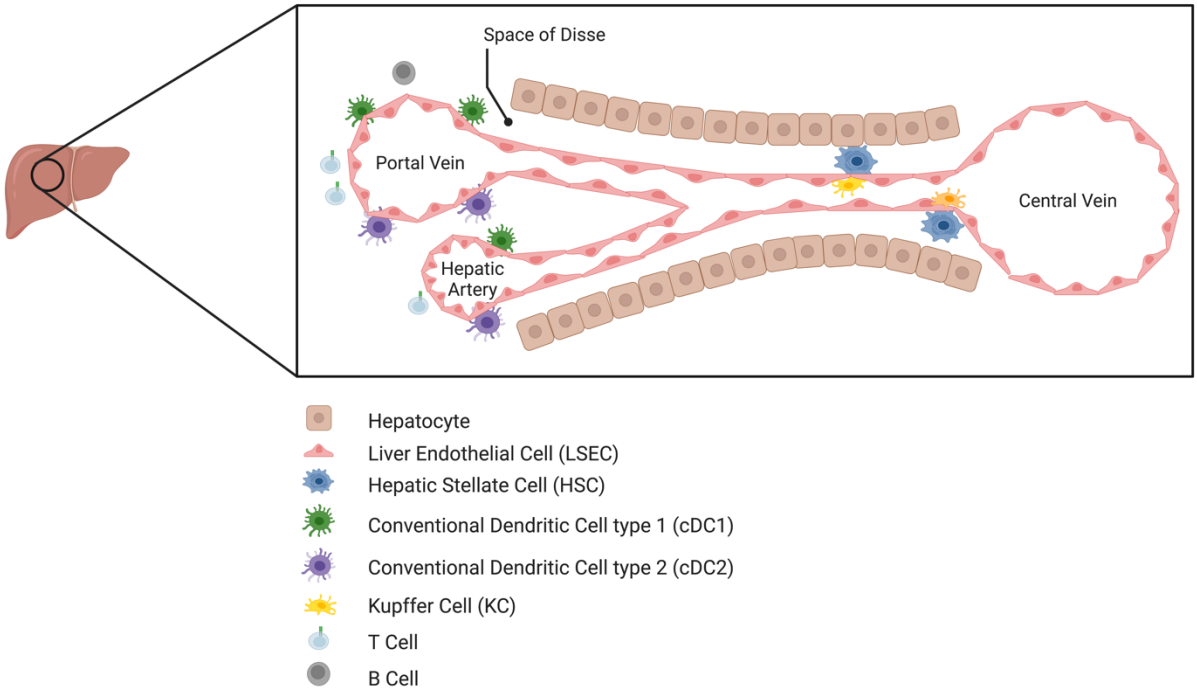

Figure 1.2: Schematic representation of distribution and organization of MPS within murine liver at steady state homeostasis. HSCs are located within the space of disse and are in close contact with LSECs and KCs. KCs are mainly found in the periportal and central vein regions. DCs are positioned around the portal veins within the portal regions of liver. Other immune cells, such as T cells and B cells are also positioned in the portal regions.

Under steady state conditions, KCs are organized in the periportal hepatic region and are closely associated with liver endothelial cells (LSECs) and hepatic stellate cells (HSCs) [124, 125]. DCs are positioned around portal tracks and they develop periportal lymphoid structures in response to inflammatory signals, which act as a priming location for liver-infiltrating T cells **(Fig 1.2)** [126-128]. Under pathophysiological conditions such as liver fibrosis, DCs have the tendency to activate T and NK cells *via* increased Tumor necrosis factor (TNF) and IL-6 secretion to circumvent liver protection by preventing tumor growth [129]. In another similar study of murine fibrosis model by Henning *et.al*, it was shown that DCs under

Nonalcoholic steatohepatitis (NASH) conditions activate $CD4^+$ T cells *via* secretion of immuno-modulatory cytokines such as TNFα, interleukin (IL)-10, IL-6 and monocyte chemoattractant protein 1 (MCP-1), thereby modulating the development of hepatitis and fibrosis in NASH [130]. In addition, DCs also play an essential role in liver tissue repair and regeneration. For instance, depletion of $CD11^+$ cells in a carbon tetrachloride liver injury model showed delayed fibrosis regression. Conversely, DC stimulation by Flt3L or adoptive transfer of DCs resulted in significantly increased liver fibrosis regression on a matrix metalloproteinase (MMP)-9-dependent manner [131]. Taken together, myeloid cells within the hepatic microenvironment are positioned very precisely in their niche, where they perform their tasks depending on the location where they reside and the signals they receive from the surrounding. However, the exact mechanisms by which they strategically position themselves in their hepatic niche are poorly understood.

Interestingly, G-protein coupled receptor 183 (GPR183), a chemotactic receptor, has been identified as a guiding niche factor which regulates tissue homeostasis. Prior studies have shown that GPR183 is essential for correct positioning of B cells and DCs in spleen [132].

1.6. GPR183 signaling cascade and its function

G protein-coupled receptor 183 (GPR183), also known as Epstein-Barr virus-induced G protein-coupled receptor 2 (EBI2) is a seven-transmembrane receptor which was first discovered in 1993 in a screening of genes induced by *in-vitro* Epstein-Barr virus (EBV) infection of a Burkitt's lymphoma cell line [133]. Recent studies have identified oxysterols as

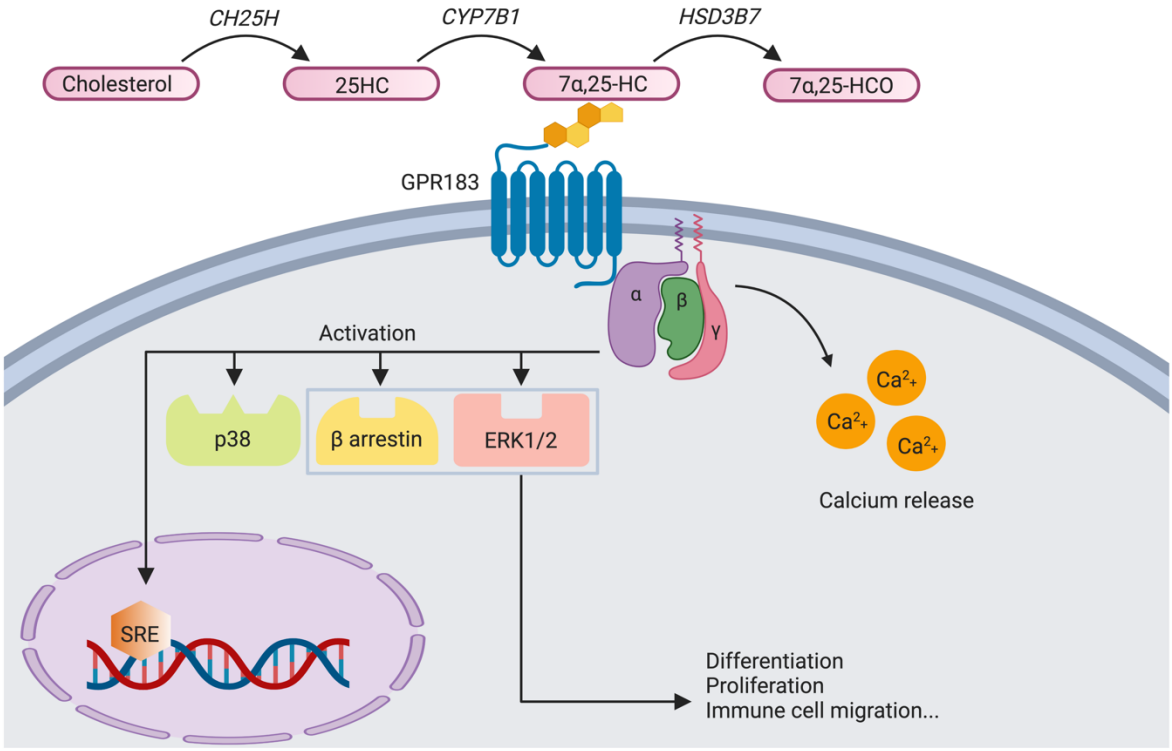

Figure 1.3: Schematic representation of oxysterol-GPR183 signaling axis pathway. Oxysterol (7α,25-OHC) is one of the potent ligands of GPR183, synthesized *via* sequential hydroxylation of cholesterol by enzymes CH25H and CYP7B1 and degraded by HSD3B7. Upon activation by 7α,25-OHC, GPR183 signals via $G_{i\alpha}$ protein, which leads to activation of SRE, ERK1/2, p38, β-arrestin along with calcium release. Activation of signaling cascade controls various functional responses, such as cell differentiation, proliferation and migration.

natural ligands for GPR183 and among them, 7α,25-dihydroxycholesterol (7α,25-OHC) is one of the most potent ligands displaying higher affinity to GPR183 **(Fig 1.3)** [134, 135]. 7α,25-OHC is generated *via* sequential hydroxylation of cholesterol by the enzymes cholesterol-25-hydroxylase (CH25H) and cytochrome P450 oxysterol 7-alpha-hydroxylase (CYP7B1), which is then further degraded to 7α,25-HCO by the enzyme Hydroxy-delta-5-steroid dehydrogenase, 3 beta- and steroid delta-isomerase 7 (HSD3B7) for bile acid synthesis for the liver [136, 137]. Under homeostatic conditions, CH25H is highly expressed by stromal cells in the murine spleen, whereas CYP7B1 expression is abundant in the murine liver [134, 135]. GPR183 is exclusively attached to the G_i protein and once it is activated, along with intracellular calcium

release, it activates two mitogen-activated protein (MAP) kinases, p38, β-arrestin, extracellular-signal-regulated kinase (ERK1/2), and the nuclear transcription factor serum response element (SRE) in a pertussis toxin (Ptx)-sensitive manner **(Fig 1.3)** [138-140]. Collectively, the downstream activity of GPR183 leads to various immune responses, cellular proliferation, cell migration and inflammation. Interestingly, no signaling *via* nuclear factor of activated T cells (NFAT) or nuclear factor kappa B (NFκB) has been observed or reported so far [139-141].

1.7. Immune regulation of GPR183 and oxysterols

GPR183 is expressed abundantly by the majority of innate and adaptive immune cells such as innate lymphoid cells 3 (ILC3s), DCs, T cells and B cells [132, 142-145]. Recent studies have highlighted the role of GPR183 signaling in various immune processes, such as immune cell migration, inflammation, cellular proliferation, autoimmunity, and chemotactic distribution and positioning of immune cells within secondary lymphoid organs. For example, lack of GPR183 in B cells leads to disruption of B cells positioning in the spleen, wherein B cells lacking GPR183 failed to move to the outer follicle after activation, and instead were positioned in the follicle center leading to reduced T cell-dependent antibody responses [144, 145]. Moreover, similar to *Gpr183*$^{-/-}$ mouse, mice lacking *Ch25h* failed to position activated B cells within the spleen to the outer follicle and mounted a reduced plasma cell response after an immune challenge [134]. Furthermore, Gatto and colleagues have also shown that GPR183 acts in synergy with CXCR5 and CCR7 to direct B cell migration and positioning within follicles and germinal center of murine spleen [146]. In another similar study, it has been shown that GPR183 and its agonist 7α,25-OHC facilitate positioning of activated CD4^{+} T cells at the interface of the follicle and T zone, where they interact with activated DCs and are exposed

to Tfh cells, promoting inducible co-stimulator (ICOS) ligand synthesized by $ICOSL^{hi}$ $CD25^{+}$ DCs [147].

In addition to T cells localization and positioning, it has been shown that expression of GPR183 is important for DC homeostasis, localization, and for mounting appropriate T and B cell responses. Interestingly, mice lacking *Gpr183* and *Ch25h* had fewer $CD4^{+}$ DCs when compared to their wildtype (WT) counterparts [132]. Furthermore, another study has also highlighted the role of *Cyp27a1* and 7α,27-HC in positioning of cDC2s within the murine spleen. *Cyp27a1* deficient mice were shown to have significantly less $DCIR^{+}$ cDC2 and a critical role for the expression of *Cyp27a1* by the stromal compartment in the regions where naïve DC localize in steady-state was identified. Moreover, oxysterol metabolism by Batf3-dependent DCs was also important for GPR183-dependent positioning of activated $DCIR2^{+}$ cDC2 [148].

During pathophysiological conditions GPR183 signaling plays a role as well. For example, patients with ulcerative colitis and mice treated with dextran sulfate sodium (DSS) showed elevated mRNA levels of *Gpr183* and oxysterol synthesizing enzymes, *Cyp7b1* and *Ch25h*. Additionally, mice lacking *Gpr183* showed a decrease of colonic lymphoid structures compared to WT control group and showed defects in inflammation-induced accumulation of lymphoid structures [149]. In a different study, a similar phenotype was obtained wherein mice lacking *Gpr183* were less susceptible to development of colitis in an innate model of intestinal inflammation [142]. Taken together, there are ample evidences so far that GPR183 is a guiding niche factor which guides the immune cells to localize themselves in precise locations within the secondary lymphoid organs. Nevertheless, whether GPR183 plays similar role in other tissues, especially in organs with a cholesterol-rich environment such as the liver remains elusive. Therefore, this project aims to study the role of GPR183 in maintenance of hepatic DC homeostasis.

2. Materials and methods

2.1. Materials

2.1.1. Mice

Gpr183$^{-/-}$, *Ch25h*$^{-/-}$ and *Gpr183*$^{fl/EGFP}$ were bred and housed in the Genetic Resources Center (GRC) at the Life and Medical Sciences (LIMES) Institute, University of Bonn, Germany. *Zbtb46*-cre and CD45.1 animals were purchased from Jackson laboratory and then bred and housed in the GRC facility. Dendritic cell specific depletion of Gpr183 was done by breeding *Gpr183*$^{fl/fl}$ animals with *Zbtb46*-cre animals. *Abca1*$^{fl/fl}$ and *Abca1*$^{fl/fl}$-*Vil1-cre* animals were bred at mouse facility of Washington University, St. Louis, USA.

All the experimental animals were bred and housed in a specific pathogen-free (SPF) condition rooms at 22-24°C and 50-60% humidity with a 12 hours light and dark cycle. 6-14 weeks animals were used for the experiments and tissue harvesting. All animal experiments were performed according to the protocols (2019.A256- Untersuchung der Rolle von GPR183 für die Entwicklung und Funktion von lungenresidenten dendritischen Zellen, 2017.A347- Einfluss der Gedächtnissfunktion des angeborenen Immunsystems auf die Entwicklung und schwere von akuter und chronischer Entzündung in der Lunge) approved by Landesamt für Natur, Umwelt und Verbraucherschutz Nordrhein Westfalen.

2.1.2. General consumables used in methods

Product	Source
1.5 ml microcentrifuge tubes	Eppendorf
2 ml microcentrifuge tubes	Greiner Bio-One

5 ml microcentrifuge tubes	Greiner Bio-One
15 ml Falcon tubes	Greiner Bio-One
50 ml Falcon tubes	Greiner Bio-One
Aluminum foil	Carl Roth
Cryo tubes	Carl Roth
Cell freezing container	Corning
Cell strainer 70um	Greiner Bio-One
Cell filter	MERCK
Cell culture plates	Greiner Bio-One
Coverslips	Marienfeld
Cryomolds	Science Services
Disposable autoclave bags	Carl Roth
Disposable tissue wipes	Carl Roth
FACS tubes	SARSTEDT
Gloves	SemperGuard
Microscope slides	Thermo Scientific
Parafilm	Carl Roth
Pasteur pipettes	VWR
PCR tubes	VWR
Pipette tips	STARLAB
Reflotron GPT strips	Roche
Reflotron GOT/ ASAT strips	Roche
Syringes	B/Braun

Syringe needles	B/Braun
Serological pipettes	Greiner Bio-One
Weighing dishes	Carl Roth

2.1.3. Lab equipments used in methods

Equipment	**Source**
Autoclave	H+P Varioklav Dampfsterilisator EP-2
autoMACS Pro Separator	Miltenyi Biotec
Biosafety Hood	BDK
Brightfield Microscope	Nikon ECLIPSE TS100
Centrifuges	Eppendorf
Centrifuge balances	Kern & Sohn
Cell counter	La Fontaine via Labotec
Cell culture incubator	Binder
Confocal microscope LSM880	Zeiss
CODEX microscope	Akoya Biosciences
Faxitron CP160	Faxitron
Flow cytometer (LSRII)	BD Biosciences
Flow cytometer (Symphony A5)	BD Biosciences
Flow cytometry sorter (AriaIII)	BD Biosciences
Fluorescence microscope	KEYENCE
Incubators	Memmert

Leica CM3050 S	Leica
Microwave	Panasonic
Microplate reader	TECAN
PCR cycler	Bio-Rad
Pipette controller	BRAND
Reflotron Plus hematology analyzer	Roche
Thermo block	Eppendorf
Vortex	Vortex Genie2
Water bath	Julabo SW22

2.1.4. Reagents and kits used in methods

Reagent	**Source**
Albumin Bovine Fraction	SERVA
Agarose (Low Melting Point)	Promega
Ammonium Chloride	Carl Roth GmbH
Collagenase type IV	Sigma-Aldrich
Cryo-PAN	PAN Biotech
Deoxyribonuclease I (DNase I)	Sigma-Aldrich
Direct PCR Lysis Reagent	VIAGEN Biotech
Donkey Serum	Sigma-Aldrich
DPBS 10x	Carl Roth GmbH
DRAQ7™	BioLegend

DreamTaq Green PCR Master Mix	ThermoFisher Scientific
Ethanol	Carl Roth
Ethanol absolute for molecular biology	AppliChem
Ethylenediaminetetraacetic acid (EDTA)	Thermo Fisher Scientific
Fixation/ Perm Diluent	eBioscience
Fixation/ Permeabilization Concentrate	eBioscience
Fixable Viability Dye eFluor™ 660	eBioscience
Fixable Viability Dye eFluor™ 780	eBioscience
Isopropanol	AppliChem
GeneRuler 1kb Plus DNA Ladder	Thermo Fisher Scientific
Goat Serum	MERCK
GoTaq qPCR master mix	Promega
HBSS	PAN-Biotech
Hydrogen Peroxide	Sigma-Aldrich
Mouse Serum	Sigma-Aldrich
MojoSort™ Streptavidin Nanobeads	Biolegend
Mounting Medium	ThermoFisher Scientific
Penicillin-Streptomycin	Thermo Fisher Scientific
Permeabilization Buffer (10x)	eBioscience
Precision Count Beads™	Biolegend
Proteinase K Solution	Panreac AppliChem
Rabbit Serum	Sigma-Aldrich
Rat Serum	Sigma-Aldrich

Recombinant Murine Flt3-Ligand	PeproTech
Recombinant Murine M-CSF	PeproTech
Recombinant Murine Gas6	PeproTech
RPMI-1640	PAN Biotech
RTU Animal-Free Block and Diluent	VECTOR
Sodium Hydrogen Carbonate (NaHCO3)	Carl Roth GmbH
SYBR™ Safe DNA Gel Stain	ThermoFisher Scientific
Tissue-Tek O.C.T Compound	Sakura Finetek
TruStain fcX™	Biolegend
Triton X	Sigma-Aldrich
Tween-20	Sigma-Aldrich
UltraPure™ EDTA	Invitrogen

2.1.5. Buffers used in methods

Buffer	**Contents**
1X PBS	100 ml 10X PBS 9000 ml Distilled water
0.5M EDTA	186.1 g EDTA 20 g NaOH 1L H2O pH 8.0
4% PFA	40 g PFA 1L 1 X PBS pH 7.4
Blood Collection Buffer	500 ml 1 X PBS 1.86 g EDTA
Complete RPMI 1640	RPMI Medium 10% FCS 1% Penicillin-Streptomycin
FACS Buffer	1 X PBS

	0.5% BSA 2mM EDTA
Histology Washing Buffer	0.01% Tween-20 1 X PBS
Permeabilization Buffer	0.1 % Triton X In 1X PBS
Photobleach Solution	4.5 ml Hydrogen Peroxide (H_2O_2) 0.8ml 1M Sodium Hydroxide 25ml 1X PBS
Red Blood Cell Lysis Buffer	8.32g NH4CL 0.84g NaHCO3 0.043g EDTA 1L H2O
Tail Lysis Buffer	0.1 M Tris 5 mM EDTA, pH 8,0 0,2 % SDS 0.2 M NaCl 0,1 mg/ml Proteinase K

2.2.6. Antibodies used for FACS and histology staining

Antibody	Fluorophore	Source	Clone
B220	BV421	BioLegend	RA3-6B2
B220	APC	BioLegend	RA3-6B2
B220	APC/Cy7	BioLegend	RA3-6B2
Caspase3	FITC	BD Bioscience	C92-605
CD3	APC	BioLegend	17A2
CD3	APC/Cy7	BioLegend	145-2C11
CD4	PerCP/Cy5.5	BioLegend	RM4-5
CD4	APC/Cy7	BioLegend	GK1.5
CD8a	BV650	BioLegend	53-6.7
CD11b	BV421	BioLegend	ICRF44
CD11b	BUV737	BD Bioscience	M1/70

CD11c	PerCp/Cy5.5	BioLegend	N418
CD11c	BV650	BioLegend	N418
CD11c	Unconjugated	BioLegend	N418
CD11c	Unconjugated	CST	D1V9Y
CD11c	Unconjugated	BD Bioscience	HL3
CD19	PE/Cy7	BioLegend	6D5
CD19	APC/Cy7	BioLegend	6D5
CD26	PE	BioLegend	H194-112
CD31	Unconjugated	R & D	Polyclonal
CD45	FITC	BioLegend	I3/2.3
CD45	BUV395	BD Bioscience	30-F11
CD45.1	BUV395	BioLegend	A20
CD45.2	BV711	BD Bioscience	104
CD64	PE/Cy7	BioLegend	X54-5/7.1
CD64	Unconjugated	BioLegend	X54-5/7.1
CD68	Unconjugated	BioLegend	FA-11
CD73	Unconjugated	BioLegend	TY/11.8
CD80	BUV615	BD Bioscience	B7-1
CD86	BUV805	BD Bioscience	GL1
CD115	PE/Dazzle 594	BioLegend	AFS98
CD117	PE/Cy7	BioLegend	2B8
CD135	PE	eBioscience	A2F10
CD172a	APC	BioLegend	P84
CD172a	PE/Cy7	BioLegend	P84
Desmin	Unconjugated	Abcam	Polyclonal
Desmin	Unconjugated	R&D Systems	Polyclonal

EpCAM	Unconjugated	BioLegend	G8.8
F4/80	BV786	BioLegend	BM8
F4/80	Unconjugated	BioLegend	BM8
Gas6	Unconjugated	BioLegend	Polyclonal
Ki-67	BV421	BD Bioscience	B56
Ly6C	BV605	BioLegend	HK1.4
Ly6C	BV570	BioLegend	HK1.4
Ly6G	APC	eBioscience	RB68C5
Ly6G	APC/Cy7	BioLegend	1A8
M-CSF	Unconjugated	BioLegend	Polyclonal
MHCII	Unconjugated	BioLegend	M5/114.15.2
MHCII	FITC	BioLegend	M5/114.15.2
MHCII	BV510	BioLegend	M5/114.15.2
NK1.1	APC/Cy7	BioLegend	PK136
NK1.1	Alexa Fluor 700	BioLegend	PK136
pSTAT3	BC421	BioLegend	13A3-1
pSTAT5	PE	Invitrogen	SRBCZX
Siglec-F	BUV395	BD Biosciences	E50-2440
Siglec-F	PE-CF594	BioLegend	E50-2440
Siglec-H	PerCp/Cy5.5	BioLegend	551
Ter-119	APC/Cy7	BioLegend	TER-119
TCR-b	PE	BioLegend	H57-597
TIM4	APC	BioLegend	RMT4-54
XCR1	BV650	BioLegend	ZET
XCR1	APC	BioLegend	ZET

2.2. Methods

2.2.1. Isolation of tissue resident immune cells

Blood:

The mouse was anaesthetized with 1:3 dose of ketamine and xylazine according to the animal´s body weight. 150-200 µl of blood was collected by directly inserting the insulin syringe into the heart and was transferred into a FACS tube containing blood collection buffer. Blood was then centrifuged at 1350 rpm for 5 mins at 4°C to pellet down the immune cells. Cells were then further processed for flow cytometry staining.

Bone Marrow:

To isolate the cells from the bone marrow, femurs and tibias were collected from the anaesthetized mouse and were flushed with HBSS using a 24G needle and 5 ml syringe until the bones turned white. Collected cells were then spun down at 1350 rpm for 5 mins at 4°C. Cells were ready for flow cytometry staining.

Hepatic LNs:

To isolate the hepatic LN, the gut was carefully removed and placed to the left to locate the LN around the portal vein. Complete LN were then carefully picked without allowing them to burst the inside content. LN were placed in a 70 µm cell strainer and were meshed with a syringe plunger in circular motions alongside washing with FACS buffer. Cells were collected in a 50 ml tube and were spun at 1350 rpm for 5 mins at 4°C to collect the cell pellet for further processing of flow cytometry staining.

Liver:

The largest lobe of the liver from the mouse was excised, weighed and was transferred to a 2 ml microcentrifuge tube containing 1 ml HBSS buffer. Tissue was then minced in small pieces using a scissor and was transferred to 12 well plate containing 2 ml digestion buffer

supplemented with 0.2 mg/ml collagenase type IV and 50 μg DNase I. Tissue was digested for 40 minutes at 37°C in an incubator and after digestion, tissue was homogenized using a 19G needle and syringe to obtain a single cell suspension. Cell suspension was then collected in a 50 ml tube via 70 μm cell strainer, alongside washing with FACS buffer. Collected cells were spun at 50g for 3 minutes at 4°C to pellet down the hepatocytes. Immune cells were carefully collected in a FACS tube from the top by using a pasteur pipette without disturbing the hepatocyte pellet. Collected immune cells were spun down at 1350 rpm for 5 minutes at 4°C and were further processed with flow cytometry staining.

2.2.2. Preparation and cryopreservation of fresh frozen liver tissue

Mouse was anaesthetized with 1:3 dose of ketamine and xylazine according to the animal´s body weight. Liver was perfused sequentially with first 10-15 ml of cold 4% PFA and then with 10-15 ml of DPBS by using safety winged IV needle until the liver turned to white in color. The left liver lobe was transferred to cold 4% PFA and was fixed at 4°C overnight. Next day, the tissue was washed thrice with PBS and then transferred to 30% sucrose solution and was incubated at 4°C overnight in fridge. Next, the liver tissue was transferred to 50% sucrose solution and was incubated at 4°C overnight or until the tissue sinks at the bottom of the tube. Next day, the tissue was taken out of the 50% sucrose solution, was wiped with tissue wipes to remove the excess of sucrose content and was imbedded in the optimal cutting temperature compound (Tissue-Tek) into the cryomolds. Cryomolds were kept on the dry ice for 5-10 minutes until the OCT froze and were then stored at -80°C until further use.

2.2.3. Hematoxylin and eosin (H&E) staining

Cryomolds were transferred to the cryostat machine chamber in a cryobox and temperature was maintained to -20°C. Tissue block was taken out and was stuck on the tissue holder using OCT, which was then inserted on top of the cryostat blade and screwed tightly. Tissue block was first trimmed until reaching the tissue border and 5 μm thick sections were sliced and mounted on SuperFrostPlus slides. For H & E staining, the tissue slides were fixed in 10% formalin solution for 20 minutes and washed in water. Slides were then immersed in GILL II Hematoxylin for staining the nuclei for 5 minutes, followed by washing the sections with running tap water until the water was clear without any blue tint. Next, sections were immersed in 95% ethanol for 30 seconds and then immersed in Eosin dye to stain the cytoplasm for 3 minutes. Sections were then dipped quickly into water once and dehydrated by immersing in 1 change of 95% ethanol for 1 minute, and then 3 changes of 100% ethanol for approximately 10 dips each. Sections were immersed in citrosol for 3 changes for 2 minutes each and then were mounted with FlourMount mounting medium using a glass coverslip. Images were analyzed and captured using light microscope.

2.2.4. Dietary challenge models

Where specified, mice were fed with CDAA-HFD to induce liver inflammation and liver steatosis. All the experimental animals for dietary challenge model were housed in a SPF condition rooms at 22-24°C and 50-60% humidity with a 12 hours light and dark cycle in the animal facility at the Institute of Molecular Medicine and Experimental Immunology (IMMEI), University of Bonn, Germany. Where mentioned, mice were fed with either chow diet or CDAA-HFD for 5 weeks or 12 weeks and all the experimental mice were monitored thrice a week to keep track of body weight.

2.2.5. Measurement of ALT and AST

200-300 µl blood was drawn directly from the heart of mouse by using an insulin syringe and was transferred to a Microvette clotting activator gel tube. Tubes were then spun down for 10-15 minutes at 15000 rpm at room temperature to separate the serum and serum was collected in separate microcentrifuge tubes. 30 µl of serum sample was applied on Reflotron ALT and AST measuring strips and was placed in the Automatic hematology analyzer Reflotron Plus machine (Roche). Measurement of ALT and AST were taken and plotted using Graphpad Prism.

2.2.6. Masson's trichrome staining of liver sections

Tissue slides from -20 storage were taken out and were dried for 5 minutes at room temperature. Tissues were then treated with sequential treatment of 80% and 70% ethanol for 2 minutes each and then washed thrice in distilled water. Sections were then immersed in preheated Boulin´s solution at 56°C for 15 minutes or at room temperature overnight. Next, the slides were washed in running tap water to remove the yellow color and were stained in working solution of Weigert's iron hematoxylin for 5 minutes. After washing with running tap water, sections were stained with Biebrich Scarlet-Acid Fuchsin for 5 minutes at room temperature. Next, the sections were washed and stained with working phosphotungstic/phosphomolybdic acid solution for 5 minutes, then stained with aniline blue solution for 5 minutes. Next, the sections were placed in 1% acetic acid for 2 minutes at room temperature and finally dehydrated in sequential steps of 80%, 90%, 95%, 100% ethanol and then in Xylene. Tissue was mounted with mounting medium and images were captured for analysis of liver fibrosis.

2.2.6. Immunofluorescence microscopy

Cryomolds were transferred to the cryostat machine chamber in a cryobox and temperature was maintained to -20°C. Tissue block was taken out and was stuck on the tissue holder using OCT, which was then inserted on top of the cryostat blade and screwed tightly. Tissue block was first trimmed until reaching the tissue border and 14 μm thick sections were sliced and mounted on SuperFrostPlus slides. Sections were incubated at room temperature for 5 minutes and were fixed in chilled isopropanol for 5 minutes. Sections were then washed twice for 3 minutes in 0.1% tween-20 in PBS and were incubated in photobleach solution twice for 45 minutes each and changing the solution with LED light ON during both the cycles. Next, the tissue sections were washed with 0.1% tween-20 in PBS solution thrice for 3 minutes each and the sections were blocked with blocking serum containing 1-2% of goat, rabbit, rat and donkey serum for 2 hours at room temperature. Sections were then incubated overnight with primary unconjugated antibodies (CD11c, MHCII, CD31) overnight at 4°C. Next day, the slides were washed thrice with 0.1% tween-20 in PBS for 3 minutes each and the sections were stained with secondary antibodies (Donkey anti-rabbit IgG, Donkey anti-rat IgG and Donkey anti-goat IgG) for 1.5 hours at room temperature. Sections were then washed thrice with 0.1% tween-20 in PBS for 3 minutes each, dried and wiped with tissue wipes and were mounted with mounting medium containing DAPI. Images were captured on Zeiss LSM880 confocal microscope with 20X or 43X oil objective. All captured images were then analyzed and quantified with ImageJ and IMARIS softwares.

2.2.7. Flow cytometry analysis

Surface staining:

After digestion with collagenase type IV and DNase, the single cell suspension of immune cells was blocked with CD16/32 for 15 minutes and cells were then stained with an antibody cocktail (BUV395-anti-CD45, BV786-anti-F4/80, BV650-anti-XCR1, BV605-anti-Ly6C, BV510-anti-MHCII, BV421-anti-CD11b, PerCp-Cy5.5-anti-CD11c, PE/Cy7-anti-CD64, PE-CF594-anti-CD172α, PE-anti-CD26, APC-anti-Tim4) of cell surface markers for myeloid cells in murine liver for 30 minutes at 4°C in dark. Next, cells were washed with 3-5 ml of FACS buffer and resuspended in 2 ml RBCs lysis buffer and incubated for 3 minutes at room temperature in dark. Cells were washed and stained with dead cell labeling dye Draq7 for 5-10 minutes at room temperature in dark. Cells were then filtered through a 70 μm mesh, 5 μl precision counting beads were added in 400 μl cell suspension and cells were acquired on BD FACS symphony flow cytometry machine on a low to medium flow rate. Data collected was analyzed by using FlowJo version 10 and absolute cell numbers were calculated by knowing the number of beads used in 5 μl beads in the cell suspension. Formula used for calculating the absolute cell number was: cells per g of tissue= (number of cells in specific gate X number of beads in 5 μl beads)/ (number of beads in specific gating X weight of the tissue used for staining).

Intra-cellular staining:

Cell suspension was obtained after digesting the tissue, the cells were blocked with CD16/32 and were then stained with fixable viability dye (FVD)780 for 15 minutes at 4°C in dark. Cells were washed with FACS buffer and were stained with cell surface markers for 30 minutes at 4°C in dark. Next, the cells were washed and fixed and permeabilized with BD cytofix/cytoperm 30 minutes at 4°C in dark by using intracellular staining kit (BD Biosciences)

according to the manufacturer´s instructions. Cells were then washed and were stained with the intracellular antibodies cocktail for 30 minutes at 4°C in dark. Cells were washed and resuspended into 400 µl FACS buffer, filtered through 70 µm mesh and were acquired on BD FACS symphony flow cytometry machine on a low to medium flow rate.

Intra-nuclear staining:

After digestion, the single cell suspension was blocked withCD16/32 for 15 minutes and the cells were stained with fixable viability dye (FVD)780 for 15 minutes at 4°C in dark. Cells were washed with FACS buffer and were stained with cell surface markers for 30 minutes at 4°C in dark. Cells were fixed with intracellular fixation buffer (eBioscience) for 30 minutes at room temperature in dark. Next, the cells were washed and permeabilized with 1X permeabilization buffer (eBiosciences) for 30 minutes at room temperature in dark and were stained with intranuclear antigens for 30 minutes at 4°C in dark. Cells were then filtered through 70 µm mesh and were acquired on BD FACS symphony flow cytometry machine on a low to medium flow rate.

2.2.8. Adoptive transfer of BM cells

To isolate the cells from the bone marrow, femurs and tibias were collected from the anaesthetized mouse under the sterile conditions and were flushed with DPBS using a 24G needle and 5 ml syringe until the bones turned white. Collected cells were then spun down at 1350 rpm for 5 mins at 4°C. Cells were then treated with sterile RBC lysis buffer, washed and resuspended in sterile DPBS at a concentration of 1 million cells per 100 µl.

CD45.1 B6 recipient animals were lethally irradiated with a 10 Gy X-Rays by using Faxitron CP160 X-Ray machine according to manufacturer's instructions. 100 µl PBS containing 1 million WT or KO BM cells were injected via an intravenous injection through the tail vein

after 8 hours of irradiation. Mice were then monitored every day according to the animal lenience approval by The University of Bonn. Blood chimerism of Ly6G granulocytes was accessed after 4 weeks of reconstitution and the animals with more than 80% chimerism were analyzed after 18 weeks of reconstitution.

2.2.9. *In-silico* prediction of ligand-receptor interaction of DCs and stromal compartment

To predict and understand the possible ligan-receptor interaction regulating the DC abundance within the murine liver, NicheNet algorithm on a recently published and publicly available scRNA murine liver dataset (GSE156059)[150] from liver cell atlas (https://www.livercellatlas.org). The Seurat package (V3.1.5) was applied to identify *Gpr183*$^{+}$ cDCs and the stromal cells expressing *Ch25h* and *Cyp7b1* enzymes.

CD45^{-} and CD45^{+} populations from the datasets of standard diet animals were sequentially loaded into Seurat package. UMAPs were then generated with a resolution of 0.5 and clusters were annotated using signature DE genes. *MHCII*, *Itgae* and *Gpr183* expressing clusters were annotated as cDCs. From the CD45^{-} population dataset, the clusters expressing *Ch25h* and *Cyp7b1* were annotated and DE genes were determined withing the clusters expressing high levels of both the enzymes. Next, the DCs and stromal cells expressing *Ch25h* and *Cyp7b1* were chosen for the downstream analysis. cDCs were defined as receiver cells and endothelial cells expressing *Ch25h* and *Cyp7b1* were considered as receiver cells. Next, the NicheNetr package of version V0.1.0 was applied according to the user manual for the prediction of potent ligand receptor interactions regulating the DC abundance within the murine liver.

2.2.10. Statistics

Statistical significance was determined using the two-tailed unpaired Student's T-test with at least 95% confidence. One-way analysis of variance was initially performed to determine whether an overall statistically significant change existed before using unpaired T-test. All statistical analyses were performed using the GraphPad Prism V8. Data were shown as mean ± SEM. *P < 0.05, **P < 0.01, ***P < 0.001, and ****P < 0.0001 were all considered significant.

3. Results

3.1. Flow cytometry based phenotypic characterization of hepatic mononuclear phagocytes

The liver harbors various types of myeloid cells such as KCs, monocytes, basophils, eosinophils and DCs, which are crucial players for the maintenance of tissue homeostasis and immunity. Flow cytometry-based discrimination of MPS based on their surface marker expression is challenging due to their high degree of phenotypic plasticity and extensive overlapping of surface markers. The distinction of *bona fide* DC subsets and macrophages is particularly difficult in multiple tissues. Therefore, a comprehensive multi-color flow cytometry panel to strategically identify and discriminate the populations of myeloid cells based on their surface markers within the murine liver was designed **(Fig 3.1-A)**. Bulk immune cells were first gated based on forward and sideward scatter to remove debris and doublets and lineage negative (Lin^-) cells were gated to exclude dead cells and cells expressing lineage markers (CD19, CD3, B220, NK1.1, Ter119, and Ly6G). Next, total $CD45^+$ cells were gated from Lin^- cells and based on the expression of Ly6C (monocyte marker) and CD11b, $Ly6C^-CD11b^+$ cells were gated. To further remove the macrophage contamination, these were excluded by using the macrophage-specific marker CD64. The residual $Ly6C^-CD64^-$ cells were used to gate *bona fide* cDCs based on their high expression levels of CD11c and MHCII. CD26 has been recently reported to be highly expressed by the cDC compartment [45]. To further validate the gating strategy and to identify cDCs, the expression of CD26 on total $CD11c^+MHCII^+$ cDCs was analyzed and showed that 80-85% of cDC subset expressed CD26. To further delineate the cDC subclasses, cDC1 and cDC2 subsets, the expression of XCR1 and CD172α (SIRPα) was

utilized. cDCs expressing XCR1 were gated as cDC1 subset and cDCs expressing CD172α were gated as cDC2 subset **(Fig 3.1-A)**.

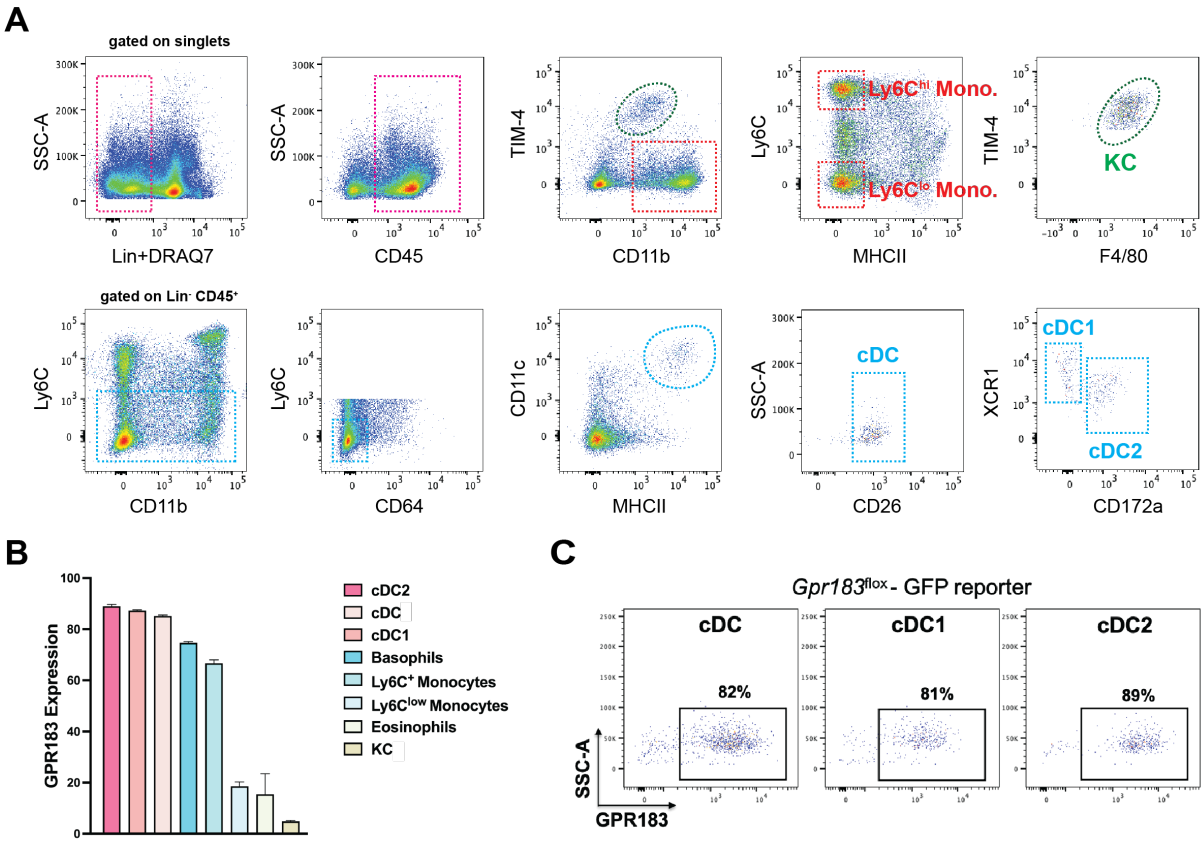

Figure 3.1: Identification of myeloid cell subsets with flow cytometry and expression patterns of GPR183 in myeloid cells within murine liver. The murine liver was enzymatically digested, cells were then stained with cell surface markers and analyzed with flow cytometry. **(A)** Gating strategy to discriminate various myeloid cell subsets. After excluding the doublets, dead cells and Lin cells were excluded and Lin$^-$ cells were gated (Lin: CD3, CD19, Ter119, NK1.1, B220, Ly6G). CD45$^+$ cells were further gated and based on cell surface marker expression, various myeloid cell subsets such as KC, cDC, cDC1, cDC2, Ly6C^{hi} monocytes, Ly6C^{lo} monocytes were gated. **(B)** Expression pattern of GPR183 in cDC, cDC1, cDC2, basophils, Ly6C^{hi} monocytes, Ly6C^{lo} monocytes, eosinophils and KCs. **(C)** Representative flow cytometry plots showing the expression of GPR183 in cDC, cDC1 and cDC2 subsets. (*n*=4-6, error bars represent mean ± SEM).

To further characterize the macrophage-monocyte compartment, resident KCs and monocyte populations were gated. From total Lin$^-$CD45$^+$ immune cells, TIM4$^+$ cells were gated and to

further validate their identity, the expression of F4/80, a canonical marker for macrophages, was analyzed. Cells expressing both TIM4 and F4/80 were gated as KCs. To identify the monocyte populations, $CD11b^{+}$ cells were gated from total $Lin^{-}CD45^{+}$ cells and sequentially subdivided based on the expression of Ly6C and MHCII. $Ly6C^{+}MHCII^{-}$ cells were gated as Ly6C high monocytes and $Ly6C^{-}MHCII^{-}$ cells were gated as Ly6C low monocytes. Overall, we were successfully able to define monocytes, KC, macrophages, and cDC subsets at the steady state condition, which will allow us to further study the role of GPR183 on various myeloid subsets **(Fig 3.1-A)**.

3.2. GPR183 is abundantly expressed by hepatic cDC, cDC1 and cDC2 subsets and not by Kupffer cells

Recent studies have shown that GPR183 is expressed by splenic cDC subsets [132], but their expression patterns in the murine liver is unidentified. Next, the expression pattern of GPR183 within the myeloid compartment of the murine liver was examined **(Fig 3.1-B, C)**. For this purpose, *Gpr183*^{flox}-GFP reporter mice, which faithfully reports the expression of GPR183, were used. By using the previously established myeloid cells flow cytometry panel, the expression patterns of GPR183 in the hepatic mononuclear phagocytes was determined using GFP as a surrogate marker. These analyses revealed that cDCs expressed high levels of GPR183, and within the cDC compartment, 81% of cDC1 and 89% of cDC2 subsets expressed GPR183 **(Fig 3.1-B, C)**. On the contrary, resident KCs, eosinophils and $Ly6C^{lo}$ monocytes expressed very low levels of GPR183 and basophils and $Ly6C^{hi}$ monocytes expressed intermediate levels of GPR183 **(Fig 3.1-B, C)**.

3.3. *Gpr183* ablation results in increased cDC abundance within murine liver

The previous results suggested that myeloid cells, particularly DC subsets, express high levels of GPR183. Recent studies have shown that GPR183 regulates immune cell homeostasis within the secondary lymphoid organs and it controls the positioning of DCs in a niche-specific manner. Therefore, to assess the role of GPR183 in the regulation of immune cell homeostasis within murine liver, hepatic tissue from WT and *Gpr183*$^{-/-}$ mice was analyzed at a cellular level by using multi-color flow cytometry and confocal microscopy. Flow cytometry analyses of hepatic mononuclear phagocytes showed that ablation of *Gpr183* resulted in significantly increased abundance of overall cDC compartment at both, percentage as well as absolute cell number levels **(Fig 3.2-A, B)**. To assess if the increase in total cDCs was biased towards cDC1 or cDC2 lineage, the expression of XCR1 and CD172α for cDC1 and cDC2 subclasses, respectively, was quantified. The percentage as well as absolute cells numbers of both cDC1 and cDC2 subclasses in murine liver were significantly increased in *Gpr183*$^{-/-}$ mice when compared with WTs **(Fig 3.2-A, B)**.

Next, to further validate these findings and visualize changes in the spatial distribution of DC subsets, liver sections were prepared for microscopy. Fresh frozen sections were immunostained with antibodies against CD11c, MHCII, F4/80, and CD31, and were subsequently visualized by confocal microscopy. In the WT control, DCs (identified as CD11c^{+} MHCII^{+} F4/80^{-} cells) were primarily observed at or in the vicinity of large vessels **(Fig 3.2-C)**. Ablation of *Gpr183* did not alter the location of DCs, but in agreement with the flow cytometry quantification, more CD11c^{+} MHCII^{+} F4/80^{-} signals were observed. This was confirmed by manual quantification in multiple random areas of the same size, validating the previous results **(Fig 3.2-D)**.

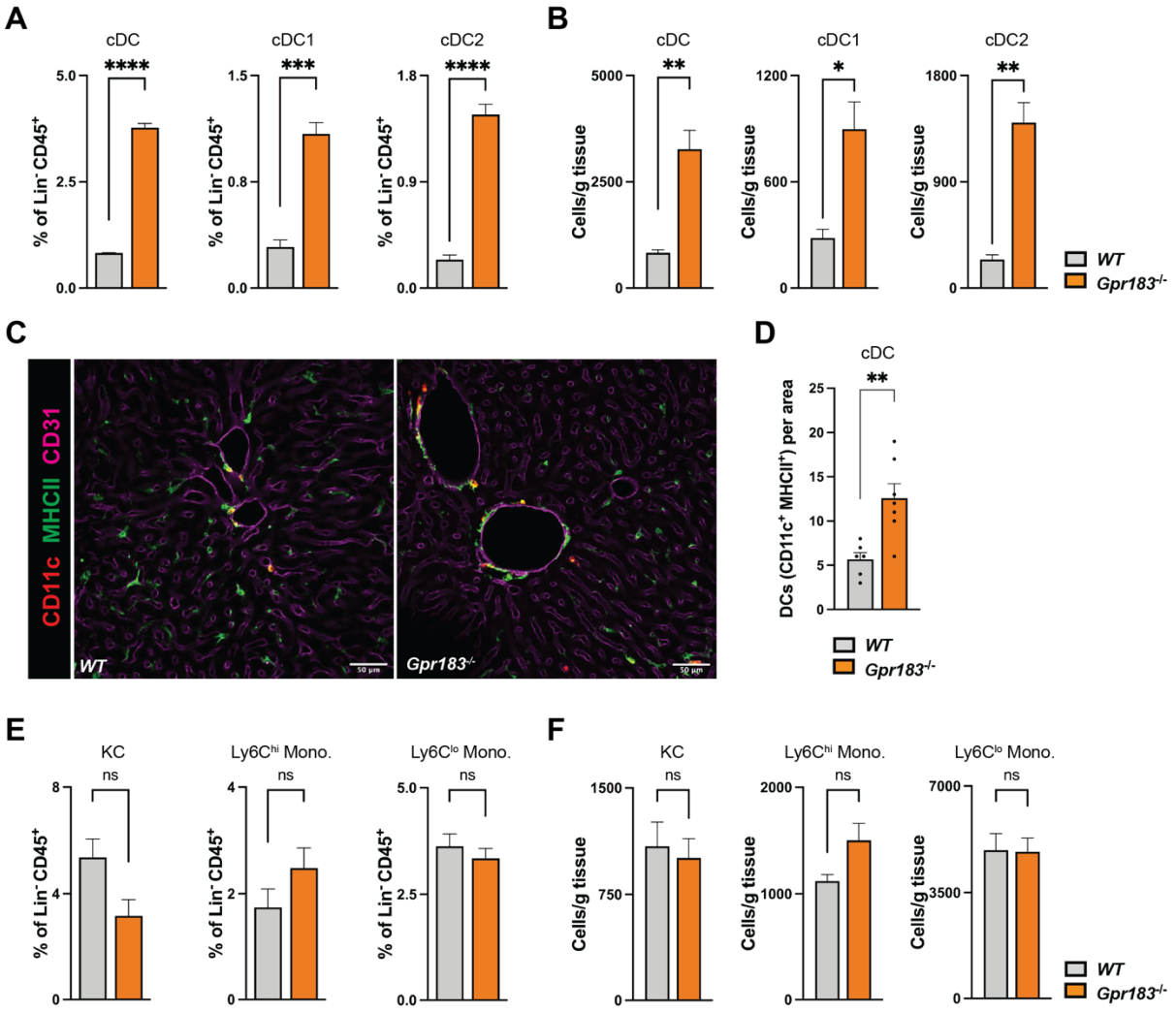

Figure 3.2: *Gpr183* ablation results in increased cDC abundance within murine liver. The murine liver was enzymatically digested, cells were then stained with cell surface markers and analyzed with flow cytometry. **(A-B)** Frequency (A) and absolute cell numbers (B) of cDC, cDC1 and cDC2 subsets within the liver of WT and *Gpr183*$^{-/-}$ animals (*n*=10-12, error bars represent mean ± SEM). **(C)** Representative confocal microscopy images of fresh frozen liver sections from WT and *Gpr183*$^{-/-}$ animals. Sections were immunostained using anti-CD11c (red), anti-MHCII (green) and anti-CD31 (magenta) antibodies to visualize cDCs in the liver sections. Scale bars represent 50 µm. **(D)** Quantification of cDC numbers per area (425.10 x 425.10 µm) in fresh frozen liver sections from WT and *Gpr183*$^{-/-}$ animals (*n* = 6-7, each dot represents one area, error bars represent mean ± SEM). **(E-F)** Frequency (E) and absolute cell numbers (F) of KC, Ly6C^{hi} monocytes and Ly6C^{lo} monocytes subsets within the liver of WT and *Gpr183*$^{-/-}$ animals (*n*=10-12, error bars represent mean ± SEM). **P < 0.05, **P < 0.01, ***P < 0.001, ****P < 0.0001.*

Since the quantification of GPR183 levels with the reporter mice showed expression in other cell types, the effect of *Gpr183* ablation on other hepatic myeloid cells was assessed by flow cytometry in the same KO model. The percentage and absolute cell numbers of KCs, Ly6C^{hi} monocytes, Ly6C^{lo} monocytes were not affected **(Fig 3.2-E, F)**. Taken together, this data shows that GPR183 regulates cDC pool size within the murine liver, whereas other myeloid cells are unaffected.

3.4. *Gpr183* ablation results in increased migratory cDC subsets in hepatic LNs

Activated tissue resident cDCs have a tendency to migrate to LNs in a CCR7-dependent manner to prime T cells. As the abundance of hepatic cDC subset increased upon genetic ablation of *Gpr183*, draining LNs were analyzed to determine (i) if a similar phenotype was observed here and (ii) if the increase observed in the hepatic tissue was due to a defective migration to draining LNs. For this purpose, hepatic LNs were harvested and analyzed for cDC abundance by flow cytometry. This quantification showed an increased percentage as well as absolute cell numbers of total migratory cDC (M-cDC), migratory cDC1 (M-cDC1) and migratory cDC2 (M-cDC2) subsets within the hepatic LNs **(Fig 3.3-A, B)**. Altogether, these results suggested that deficiency of *Gpr183* did not alter the migratory tendency of cDC subsets to the hepatic LNs and excluded any migratory defect leading to the accumulation of cDCs within the liver.

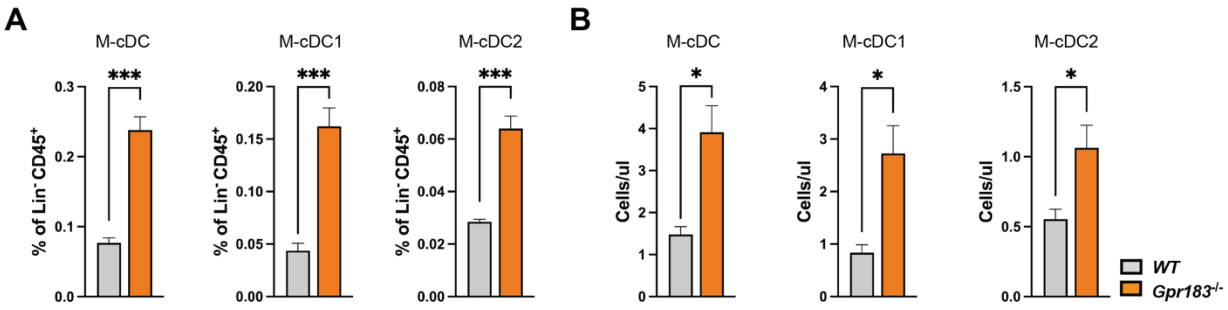

Figure 3.3: *Gpr183* ablation results in increased migratory cDC subsets within the hepatic draining LN. The murine LN was isolated and a cell suspension was obtained. Cells were then stained with cell surface markers and analyzed with flow cytometry. **(A-B)** Frequency (A) and absolute cell numbers (B) of M-cDC, M-cDC1 and M-cDC2 subsets within the LN of WT and *Gpr183*$^{-/-}$ animals (*n*=10-12, error bars represent mean ± SEM). **P < 0.05, ***P < 0.001*.

3.5. Cell intrinsic expression of GPR183 is crucial for the maintenance of increased hepatic cDC pool size in the liver

To further understand whether the increased DC numbers was a cell intrinsic process specific to the DC compartment and if expression of GPR183 in DC subset was crucial for the maintenance of increased DC pool size in the liver, a DC-specific knockout mouse line was generated by crossing *Gpr183*$^{flox/flox}$ animals with *Zbtb46*-cre reporter line. *Zbtb46* is one of the transcription factors expressed by cDCs and their precursors but not by other myeloid cells. The offsprings were then analyzed by flow cytometry as before to dissect the hepatic immune compartment. The flow cytometry phenotyping data showed an increase in percentage as well as in absolute cell numbers of total cDC, cDC1, and cDC2 subsets **(Fig 3.4-A, B)** within the liver tissue of *Gpr183*$^{flox/flox}$-*Zbtb46*-cre^{+} animals when compared with *Zbtb46*-cre^{+} littermate control groups, which is in line with the phenotype observed in *Gpr183*$^{-/-}$ animals. These results were further validated by visualizing frozen liver sections by using confocal microscopy. Immunostaining of DC markers showed increased CD11c^{+} MHCII^{+} F4/80^{-} cDCs around the portal regions of liver in DC-specific KO animals when compared to the control group **(Fig 3.4-C, D)**. Similar to the global KO animals, KCs, Ly6C^{hi} monocytes and Ly6C^{lo} monocytes frequency and absolute cell numbers were not altered. To further understand whether increased cDCs within the liver upon DC-specific genetic ablation of *Gpr183* required a cell intrinsic expression of GPR183, BM chimeras were generated by injecting one million

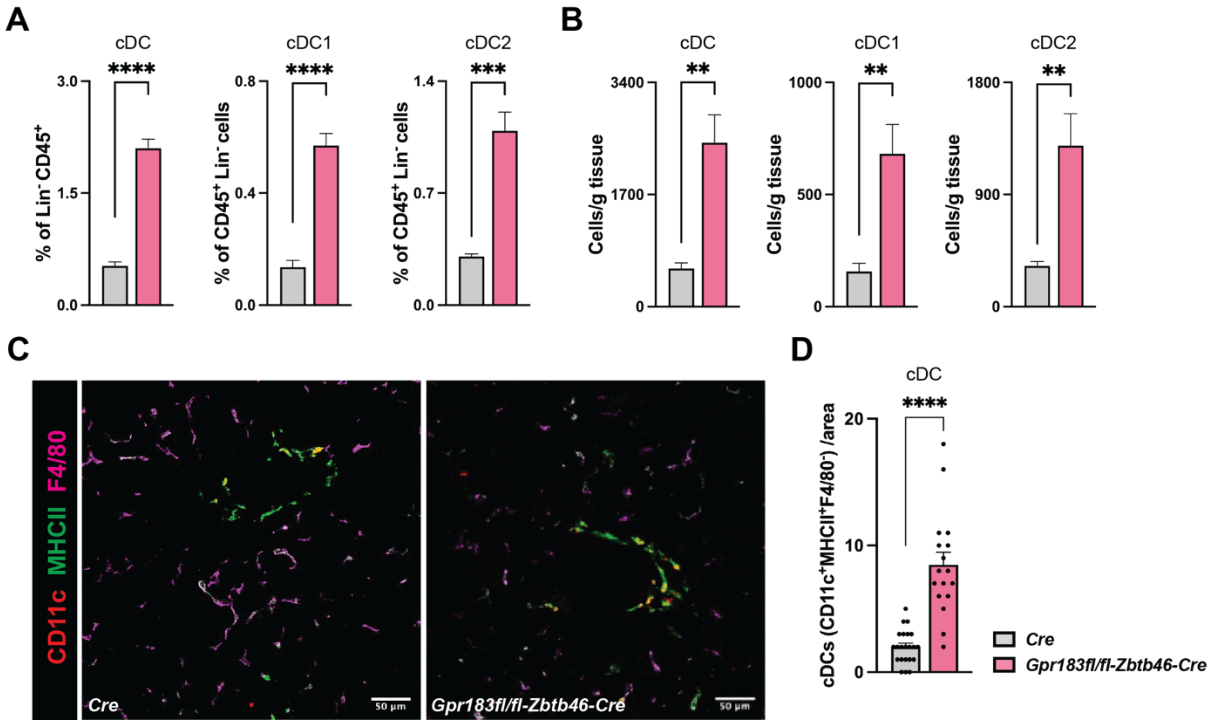

Figure 3.4: DC specific ablation of *Gpr183* results in increased cDC abundance in murine liver. The murine liver was enzymatically digested with collagenase type IV, cells were then stained with cell surface markers and analyzed with flow cytometry. **(A-B)** Frequency (A) and absolute cell numbers (B) of cDC, cDC1 and cDC2 subsets within the liver of *Zbtb46*-cre^{+} and *Gpr183*$^{flox/flox}$-*Zbtb46*-cre^{+} animals (*n*=12-14, error bars represent mean ± SEM). **(C)** Representative confocal microscopy images of fresh frozen liver sections (14 µm) from *Zbtb46*-cre^{+} and *Gpr183*$^{flox/flox}$-*Zbtb46*-cre^{+} animals. Sections were immunostained using anti-CD11c (red), anti-MHCII (green) and anti-F4/80 (magenta) antibodies to visualize cDCs in the liver sections. Scale bars represent 50 µm. **(D)** Quantification of cDC cell numbers per area (425.10 x 425.10 µm) in fresh frozen liver sections (14 µm) from *Zbtb46*-cre^{+} and *Gpr183*$^{flox/flox}$-*Zbtb46*-cre^{+} animals (*n* = 18-24, each dot represents one area, error bars represent mean ± SEM). **P < 0.05, **P < 0.01, ***P < 0.001, ****P < 0.0001.*

donor BM cells from either *Zbtb46*-cre^{+} or from *Gpr183*$^{flox/flox}$-*Zbtb46*-cre^{+} animals having a CD45.2 background (Ly5.2) into lethally irradiated WT host animals with CD45.1 (Ly5.1) background **(Fig 3.5-A)**. 8 weeks after reconstitution, the livers of both chimera groups were analyzed by flow cytometry to check for cDC abundance. The host animals which received *Gpr183*$^{flox/flox}$-*Zbtb46*-cre^{+} donor BM cells had higher frequency and increased absolute cell

numbers of cDC, cDC1, and cDC2 subsets within the tissues when compared with the group which received the *Zbtb46*-cre^{+} donor BM cells **(Fig 3.5-B, C)**.

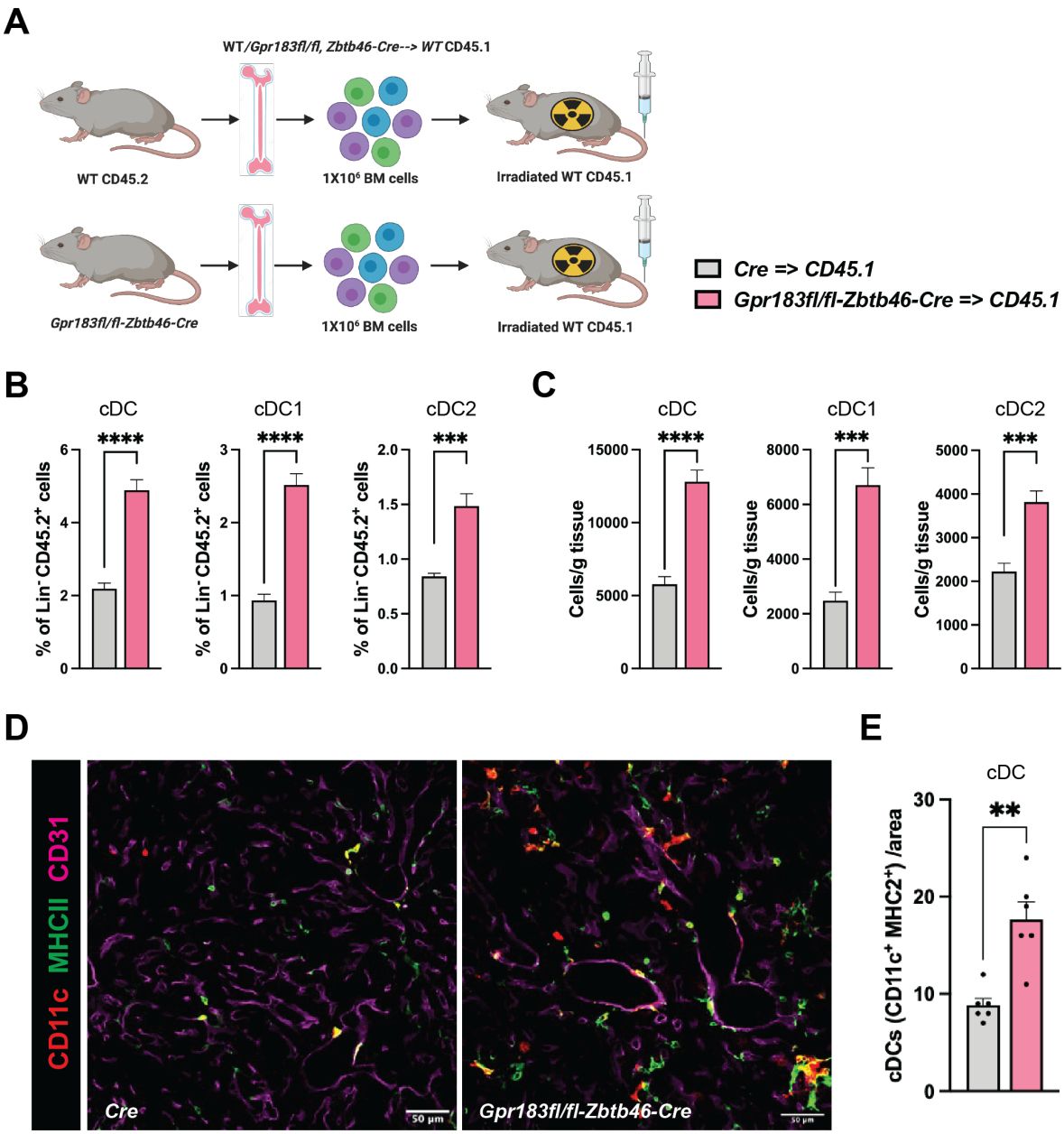

Figure 3.5: Maintenance of hepatic cDC subsets is dependent on cell-intrinsic expression of GPR183. (A) Schematic illustration of *Zbtb46*-cre^{+} and *Gpr183*$^{flox/flox}$-*Zbtb46*-cre^{+} chimera generation. 1 million CD45.2 donor BM cells either from *Zbtb46*-cre^{+} or *Gpr183*$^{flox/flox}$-*Zbtb46*-cre^{+} mice were intravenously injected into lethally irradiated CD45.1 recipient mice. After 8 weeks, recipients with more than 85% BM reconstitution were selected and number of cDC, cDC1 and cDC2 subsets were assessed in the livers of chimeras. **(B-C)** Frequency (B) and absolute cell numbers (C) of cDC, cDC1 and cDC2 subsets within the liver of *Zbtb46*-cre^{+} and *Gpr183*$^{flox/flox}$-*Zbtb46*-cre^{+} animals (*n*=12-14, error bars represent mean ± SEM). **(D)** Representative confocal microscopy

images of fresh frozen liver sections (14 µm) from *Zbtb46*-cre^{+} and *Gpr183*$^{flox/flox}$-*Zbtb46*-cre^{+} chimera animals. Sections were immunostained using anti-CD11c (red), anti-MHCII (green) and anti-CD31 (magenta) antibodies to visualize cDCs in the liver sections. Scale bars represent 50 µm. **(E)** Quantification of cDC cell number per area (425.10 x 425.10 µm) in fresh frozen liver sections (14 µm) from *Zbtb46*-cre^{+} and *Gpr183*$^{flox/flox}$-*Zbtb46*-cre^{+} chimera animals (*n* = 6, each dot represents one area, error bars represent mean ± SEM). **P < 0.05, **P < 0.01, ***P < 0.001, ****P < 0.0001.*

Furthermore, frozen livers of both chimera groups were sectioned, immunostained, and visualized by confocal microscopy. This revealed significantly increased numbers of CD11c^{+} MHCII^{+} cDCs in the portal regions of animals which received the BM cells from *Gpr183*$^{flox/flox}$-*Zbtb46*-cre^{+} donor animals when compared to the control groups which received the BM cells from the *Zbtb46*-cre^{+} animals **(Fig 3.5-D, E)**. Taken together, these results indicated that the increase of cDC subsets within the liver upon *Gpr183* ablation is a cell intrinsic process and *Gpr183* expression on hepatic cDC subsets is crucial for their homeostasis.

3.6. DC specific genetic ablation of *Gpr183* results in increased *in-situ* proliferation and impaired apoptosis of cDC subsets

To determine if ablation of *Gpr183* altered the proliferative and apoptotic capacity of DC subsets, the expression of Ki-67 and STAT3/5 on hepatic cDC subsets was examined by flow cytometry. These analyses showed an increase in the frequency and absolute cell numbers of Ki-67^{+} cDC1 and cDC2 subsets in livers of *Gpr183*$^{flox/flox}$-Zbtb46-cre^{+} animals when compared to the Zbtb46-cre^{+} littermate control group **(Fig 3.6-A, B)**. Furthermore, an increase in frequency and absolute cell numbers of cDC precursors, pre-cDC1 and pre-cDC2, was also observed, further validating the observed phenotype **(Fig 3.6-B, C)**.

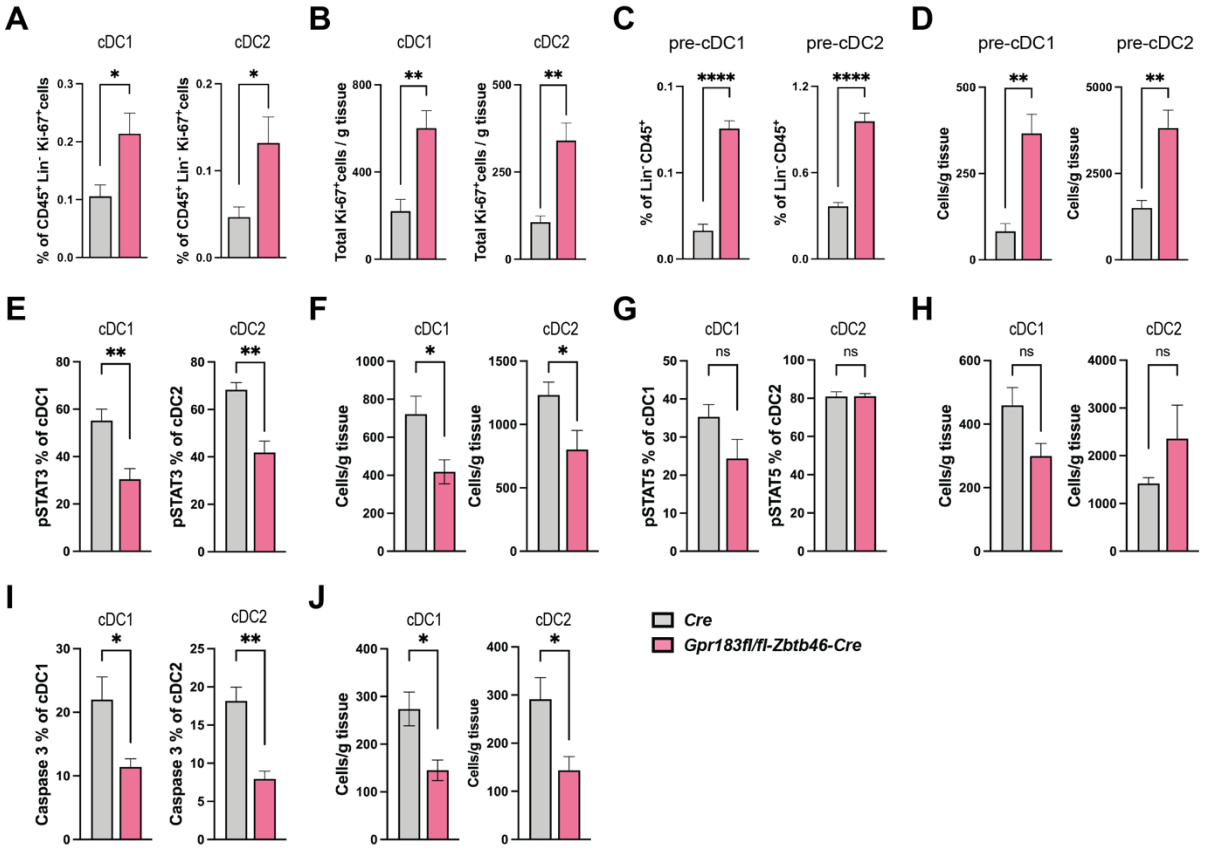

Figure 3.6: Lack of *Gpr183* results in increased proliferation and impaired apoptosis of hepatic cDC subsets. The murine liver was enzymatically digested with collagenase type IV, cells were then stained with cell surface markers, and intracellular markers and were analyzed with flow cytometry. **(A-B)** Frequency (A) and absolute cell numbers (B) of Ki-67 expressing cDC1 and cDC2 subsets within the liver of *Zbtb46*-cre^{+} and *Gpr183*$^{flox/flox}$-*Zbtb46*-cre^{+} animals (*n*=6, error bars represent mean ± SEM). **(C-D)** Frequency (C) and absolute cell numbers (D) of pre-cDC1 and pre-cDC2 subsets within the liver of *Zbtb46*-cre^{+} and *Gpr183*$^{flox/flox}$-*Zbtb46*-cre^{+} animals (*n*=6, error bars represent mean ± SEM). **(E-F)** Frequency (E) and absolute cell numbers (F) of pSTAT3 expressing cDC1 and cDC2 subsets within the liver of *Zbtb46*-cre^{+} and *Gpr183*$^{flox/flox}$-*Zbtb46*-cre^{+} animals (*n*=6, error bars represent mean ± SEM). **(G-H)** Frequency (G) and absolute cell numbers (H) of pSTAT5 expressing cDC1 and cDC2 subsets within the liver of *Zbtb46*-cre^{+} and *Gpr183*$^{flox/flox}$-*Zbtb46*-cre^{+} animals (*n*=6, error bars represent mean ± SEM). **(I-J)** Frequency (I) and absolute cell numbers (J) of caspase 3 expressing cDC1 and cDC2 subsets within the liver of *Zbtb46*-cre^{+} and *Gpr183*$^{flox/flox}$-*Zbtb46*-cre^{+} animals (*n*=6, error bars represent mean ± SEM). **P < 0.05, **P < 0.01, ***P < 0.001, ****P < 0.0001*.

It has been previously shown that STAT3 and STAT5 modulate DC maintenance and their immune functions [151-154]. For example, decreased STAT3 phosphorylation led to increased cDC numbers in the LNs of IL-6$^{-/-}$ animals [152]. STAT5 also plays an important role in DC development and activation and protection against liver fibrosis and lung injury [154, 155]. To explore if STAT3 and STAT5 played similar roles in the experimental conditions described here, the expression of phosphorylated STAT3 and STAT5 was assessed by flow cytometry. In agreement with already published data, there was a decrease of the frequency, as well as absolute cell numbers of cDC1 and cDC2 subsets expressing pSTAT3 in *Gpr183*$^{flox/flox}$-*Zbtb46*-cre^{+} animals when compared with the control groups **(Fig 3.6-E, F)**. However, expression of pSTAT5 was unchanged **(Fig 3.6-G, H)**. Furthermore, to establish if increased cDC proliferation was caused by a perturbation of their apoptotic abilities, the frequency and absolute cell numbers of hepatic cDC1 and cDC2 subsets undergoing apoptosis were assessed by measuring active caspase 3 with flow cytometry. These analyses revealed a significant decrease in the frequency as well as in the absolute cell numbers of cDC1 and cDC2 subsets undergoing apoptosis in the KO group when compared to control group, indicated by lower expression of active caspase 3 **(Fig 3.6-I, J)**. Taken together, these results confirmed that DC specific ablation resulted in increased proliferation of cDC1 and cDC2 subsets, which was concomitant with increased STAT3 phosphorylation and decreased apoptosis of cDC1 and cDC2 subsets.

3.7. Genetic ablation of *Ch25h* and *Cyp7b1* result in increased hepatic cDC abundance at steady state homeostasis

GPR183 functions via the oxysterol ligand 7α,25-OHC, which is synthesized by sequential hydroxylation of cholesterol *via* two enzymes called CH25H and CYP7B1. Mice deficient in these enzymes have impaired 7α,25-OHC synthesis, hence are unable to activate GPR183. Previous studies have shown that mice deficient of *Ch25h* had reduced cDC numbers and displayed an altered localization of splenic cDCs, which were not residing at the marginal zones as in WT mice. To further understand if CH25H and CYP7B1 enzymes played similar role in the frequency of cDC and homeostasis in the liver, *Ch25h*$^{-/-}$ and *Cyp7b1*$^{-/-}$ mouse lines were generated. The numbers of cDC, cDC1 and cDC2 subsets in the livers of *Ch25h*$^{-/-}$ and *Cyp7b1*$^{-/-}$ animals were subsequently analyzed as before, and this showed a significant increase in frequency as well as absolute cell numbers of cDC, cDC1 and cDC2 subsets in the liver when compared to the WT animals **(Fig 3.7-A, B, E, and F)**.

These results were further validated by visualizing frozen liver sections by using confocal microscopy. Immunostaining of DC markers showed increased CD11c^{+} MHCII^{+} F4/80^{-} cDCs around the portal regions of liver in *Ch25h*$^{-/-}$ animals when compared to the control group **(Fig 3.7-C, D)**. Overall, this data demonstrated that 7α,25-OHC is crucial for the maintenance of hepatic cDC subsets, and ablation of oxysterol enzymes, essential for its synthesis, phenocopies the increase of hepatic cDC numbers was observed upon *Gpr183* ablation.

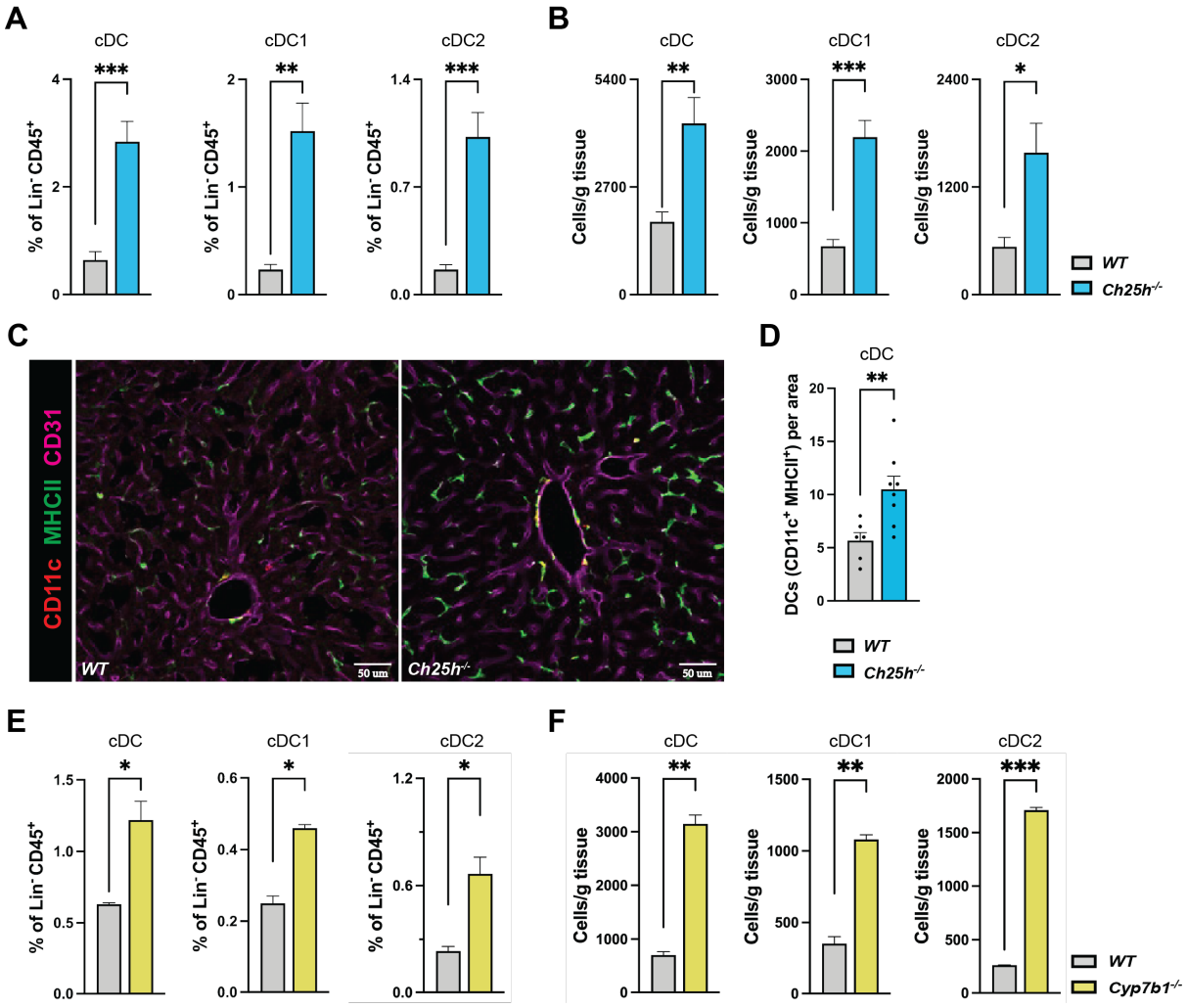

Figure 3.7: Genetic ablation of *Ch25h* and *Cyp7b1* result in increased hepatic cDC abundance in liver. The murine liver was enzymatically digested with collagenase type IV, cells were then stained with cell surface markers and analyzed with flow cytometry. **(A-B)** Frequency (A) and absolute cell numbers (B) of cDC, cDC1 and cDC2 subsets within the liver of WT and *Ch25h*$^{-/-}$ animals (*n*=12-14, error bars represent mean ± SEM). **(C)** Representative confocal microscopy images of fresh frozen liver sections (14 µm) from WT and *Ch25h*$^{-/-}$ animals. Sections were immunostained using anti-CD11c (red), anti-MHCII (green) and anti-CD31 (magenta) antibodies to visualize cDCs in the liver sections from WT and *Ch25h*$^{-/-}$ animals. Scale bars represent 50 µm. **(D)** Quantification of cDC cell numbers per area (425.10 x 425.10 µm) in fresh frozen liver sections (14 µm) from WT and *Ch25h*$^{-/-}$ animals (*n* = 6-8, each dot represents one area, error bars represent mean ± SEM). **(E-F)** Frequency (E) and absolute cell numbers (F) of cDC, cDC1 and cDC2 subsets within the liver of WT and *Cyp7b1*$^{-/-}$ animals (*n*=5-6, error bars represent mean ± SEM). *$P < 0.05$, **$P < 0.01$, ***$P < 0.001$.

3.8. Oxysterol production by radioresistant stromal niche cells is crucial for hepatic cDC homeostasis maintenance

The analyses of the livers of *Ch25h*$^{-/-}$ and *Cyp7b1*$^{-/-}$ mice suggested that the oxysterol synthesizing enzymes are crucial for controlling the DC pool size. However, it remains unclear if the oxysterol produced by the immune or the stromal compartments is crucial for controlling the DC pool within the liver microenvironment. To further explore this, *Ch25h* chimeras were generated in two different groups **(Fig 3.8-A)**. In group 1, 1 million CD45.2

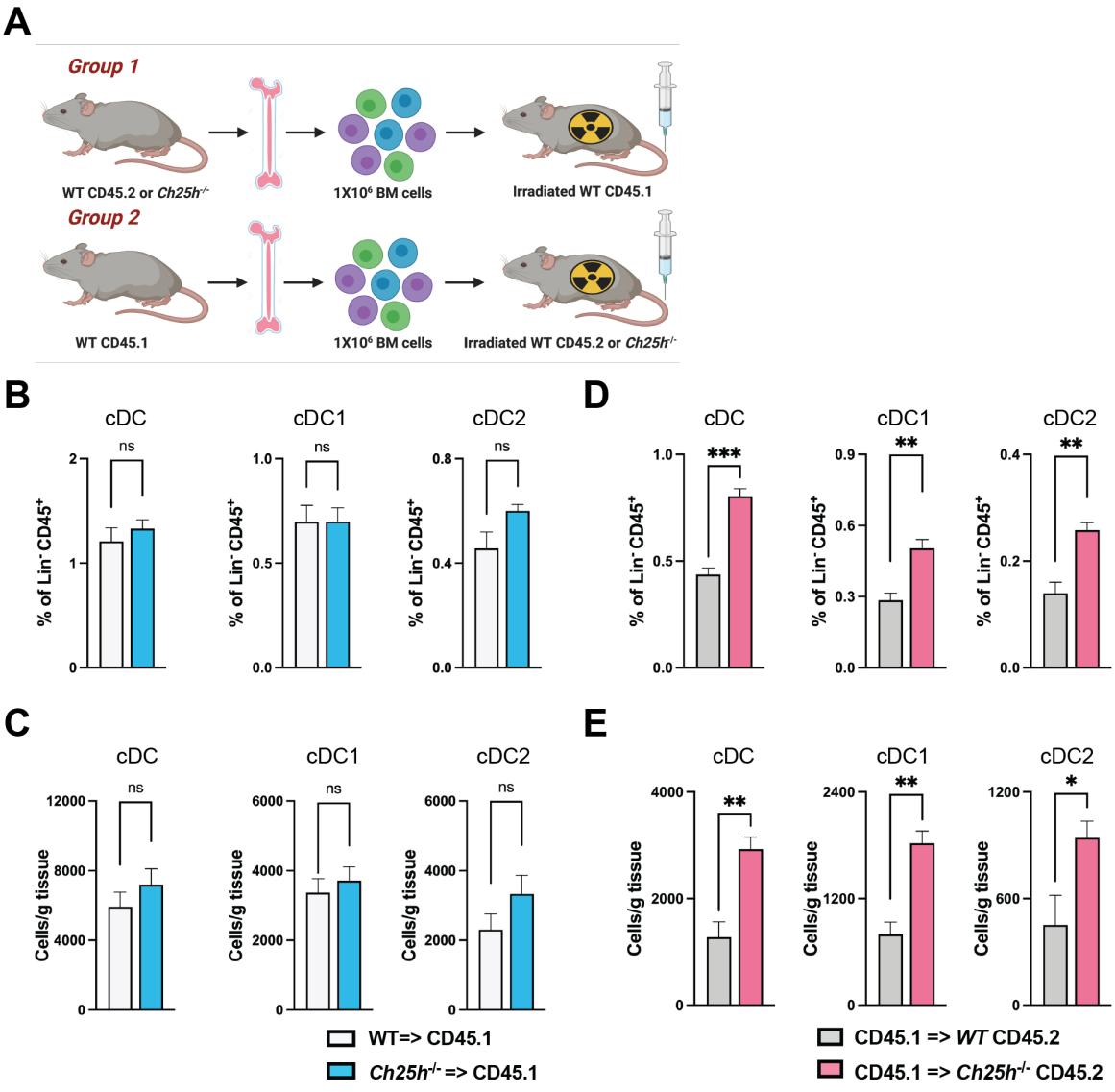

Figure 3.8: Oxysterol production by radioresistant stromal niche cells is crucial for hepatic cDC homeostasis maintenance. (A) Schematic illustration of *Ch25h* chimera generation. In group 1, one million CD45.2 WT or

Ch25h$^{-/-}$ donor BM cells were intravenously injected into lethally irradiated CD45.1 recipient mice. In group 2, 1 million CD45.1 WT donor BM cells were intravenously injected into lethally irradiated CD45.2 WT or *Ch25h*$^{-/-}$ recipient mice. After 8 weeks, recipients with more than 85% BM reconstitution were selected and number of cDC, cDC1 and cDC2 subsets were assessed in the livers of chimeras. **(B-C)** Frequency (B) and absolute cell numbers (C) of cDC, cDC1 and cDC2 subsets within the liver of group 1 chimera animals (*n*=6-7, error bars represent mean ± SEM). **(D-E)** Frequency (D) and absolute cell numbers (E) of cDC, cDC1 and cDC2 subsets within the liver of group 2 chimera animals (*n*=6-7, error bars represent mean ± SEM). **P < 0.05, **P < 0.01, ***P < 0.001.*

donor BM cells either from WT or from *Ch25h*$^{-/-}$ animals were injected into lethally irradiated CD45.1 host animals. In group 2, CD45.1 WT donor BM cells were injected into lethally irradiated either CD45.2 WT or *Ch25h*$^{-/-}$ host animals **(Fig 3.8-A)**. Both groups were analyzed for cDC abundance in liver 8 weeks after reconstitution. In group 1, the frequency and absolute cell numbers of cDC, cDC1 and cDC2 subsets showed no significant difference, regardless of the source of BM cells (WT BM cells or *Ch25h*$^{-/-}$ BM cells) **(Fig 3.8-B, C)**. Conversely, in the group 2, the *Ch25h*$^{-/-}$ hosts which received the BM cells from WT mice showed an increased frequency as well as absolute cells numbers of cDC, cDC1 and cDC2 subsets in the liver when compared to the WT hosts which received WT donor BM cells **(Fig 3.8-D, E)**. These results clearly indicated that oxysterol synthesis by the immune compartment is not solely crucial for maintaining the cDC pool size and homeostasis, but oxysterol synthesis by the radioresistant stromal niche compartment is important for controlling the hepatic DC pool and their homeostasis.

3.9 Endothelial cells produce the key enzymes for oxysterol synthesis and regulate cDC survival

As the data showed that the radioresistant stromal compartment is crucial for controlling the DC pool size within the liver, the source of oxysterols within the stromal compartment was further explored. First, it was determined which stromal subsets expressed the enzymes CH25H and CYP7B1 for the synthesis of oxysterol ligands. A publicly available sc-RNA seq dataset (GSE156059) [150] from the liver cell atlas was used for this purpose (https://www.livercellatlas.org). By using the Seurat package (V3.1.5) different subtypes of stromal cells were annotated based on their signature gene expression patterns, and the expression of *Ch25h* and *Cyp7b1* within these clusters was determined **(Fig 3.9-A, B)**. These *in-silico* analyses showed that the enzyme *Cyp7b1* was expressed by all the stromal subsets.

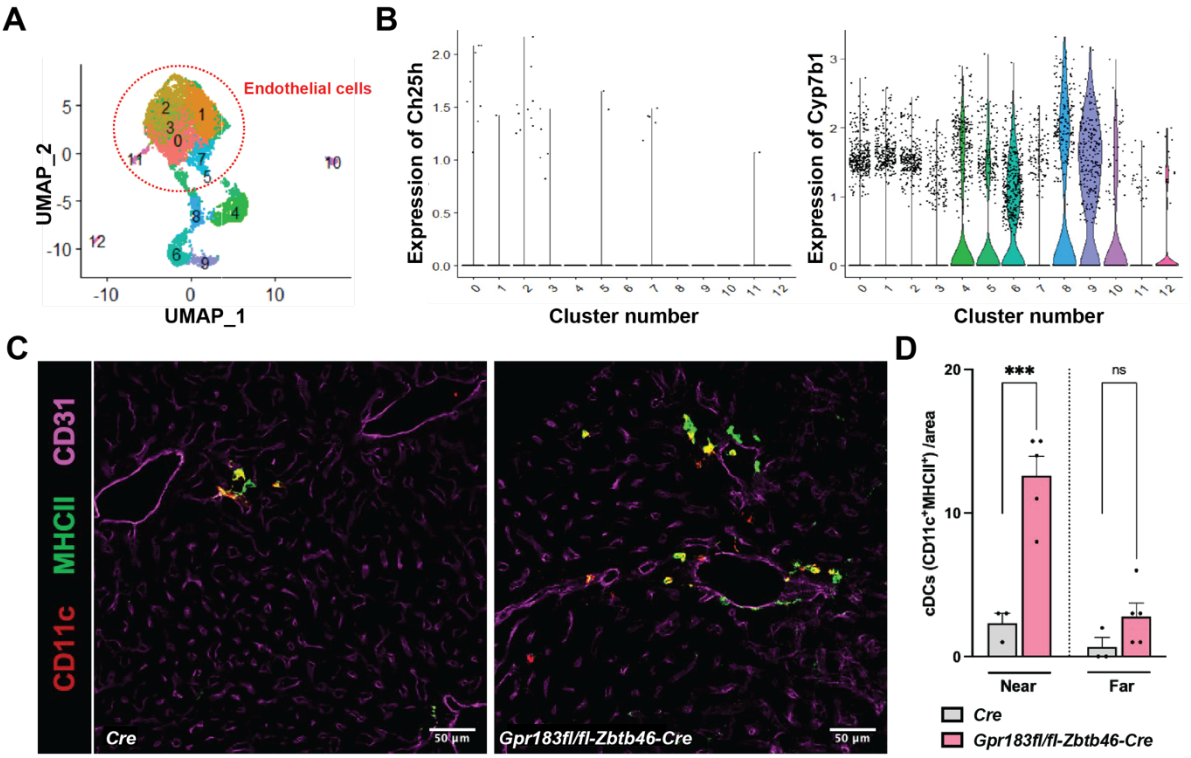

Figure 3.9: Endothelial cells in liver express key enzymes crucial for oxysterol production and are in close proximity to cDCs. Single cell sequencing data was analyzed by running Seurat package (V3.1.5) and various stromal cells clusters within the WT healthy murine liver were annotated and the expression of *Ch25h* and

Cyp7b1 was determined. **(A-B)** UMAP identification and annotation (A) of various stromal cell clusters and representative violin plots for the expression of *Ch25h* and *Cyp7b1* (B) within the stromal cell clusters in the WT healthy murine liver. **(C)** Representative confocal microscopy images of fresh frozen liver sections (14 µm) from *Zbtb46*-cre^{+} and *Gpr183*$^{flox/flox}$-*Zbtb46*-cre^{+} animals. Sections were immunostained using anti-CD11c (red), anti-MHCII (green) and anti-CD31 (magenta) antibodies to visualize cDCs in the liver sections from *Zbtb46*-cre^{+} and *Gpr183*$^{flox/flox}$-*Zbtb46*-cre^{+} animals. Scale bars represent 50 µm. **(D**) Quantification of cDC number which are near and far from endothelial cells per area (425.10 x 425.10 µm) in fresh frozen liver sections (14 µm) from *Zbtb46*-cre^{+} and *Gpr183*$^{flox/flox}$-*Zbtb46*-cre^{+} animals (*n* = 15, each dot represents one area, error bars represent mean ± SEM). **P < 0.05, **P < 0.01, ***P < 0.001.*

However, endothelial cell clusters were the only stromal cells which expressed both enzymes *Cyp7b1* and *Ch25h* **(Fig 3.9-B).** Since endothelial cells are the main source of oxysterol producing enzymes, we expected a close association of endothelial cells with DCs and we wanted to visualize this by confocal microscopy. To further validate the *in-silico* findings and examine whether hepatic cDCs are associated or in close contact with endothelial cells, liver sections were immunostained with antibodies against CD11c, MHCII, and CD31. The confocal imaging data showed that in the KO liver sections, cDCs were sitting in close proximity to CD31 expressing endothelial cells around the portal regions **(Fig 3.9-C)**. Furthermore, the frequencies of cDCs in close proximity (≤3µm) or far from CD31^{+} endothelial cells (>3µm) were quantified in randomly selected portal regions. This spatial analysis showed that the number of cDCs which were sitting near to endothelial cells were significantly increased in the KO livers when compared to the control groups **(Fig 3.9-D)**. Conversely, the cDCs which were far from the endothelial cells were not altered across KO and control groups **(Fig 3.9-D)**. Taken together, the *in-silico* data combined with spatial imaging analyses showed that only endothelial cells express the enzymes *Ch25h* and *Cyp7b1*, crucial for the biogenesis of GPR183

ligand 7α,25-OHC, and that cDCs are sitting in close proximity to endothelial cells in the hepatic portal regions, suggesting that the maintenance of hepatic cDCs is dependent on signals from the endothelial cells in the portal region.

3.10. Endothelial cells regulate hepatic cDC pool size and their survival via M-CSF-M-CSFR and Gas6-Axl interaction

Within the tissue or organ, cells are positioned in specific niches where they create a local microenvironment for themselves, depending on their surroundings and signaling ques they receive from the neighboring cells. Based on the signals immune cells receive and the niche they communicate with, their identity, function and tissue specific phenotype are influenced. For example, stellate cells, hepatocytes, and endothelial cells in liver imprint the KC identity on resident monocytes by inducing LXR-α in monocytes via the NOTCH-BMP pathway [125]. Cell-cell communication via ligand-receptor interaction is crucial, and tissue microenvironment enforces the identity in neighboring cells thereby regulating their function and maintenance. To understand what ligand-receptor interaction is controlling the endothelial and cDC communication, NicheNet algorithm was used on cDC subset expressing GPR183 and endothelial cells expressing the enzymes *Cyp7b1* and *Ch25h* on recently published datasets from healthy murine liver. These *in-silico* analyses showed that M-CSF-MCSFR and Gas6-Axl pairs had the highest interaction potentials **(Fig 3.10-A)**.

To validate this by immunostaining, fresh frozen liver sections from KO and control groups were immunostained with antibodies against M-CSF, Gas6 and a portal vein marker, EpCAM. We quantified the signals from $CD31^{+}$ endothelial cells and our confocal imaging results showed an increase in M-CSF **(Fig 3.10-B, D)** and Gas6 **(Fig 3.10-C, E)** signals *via* CD31

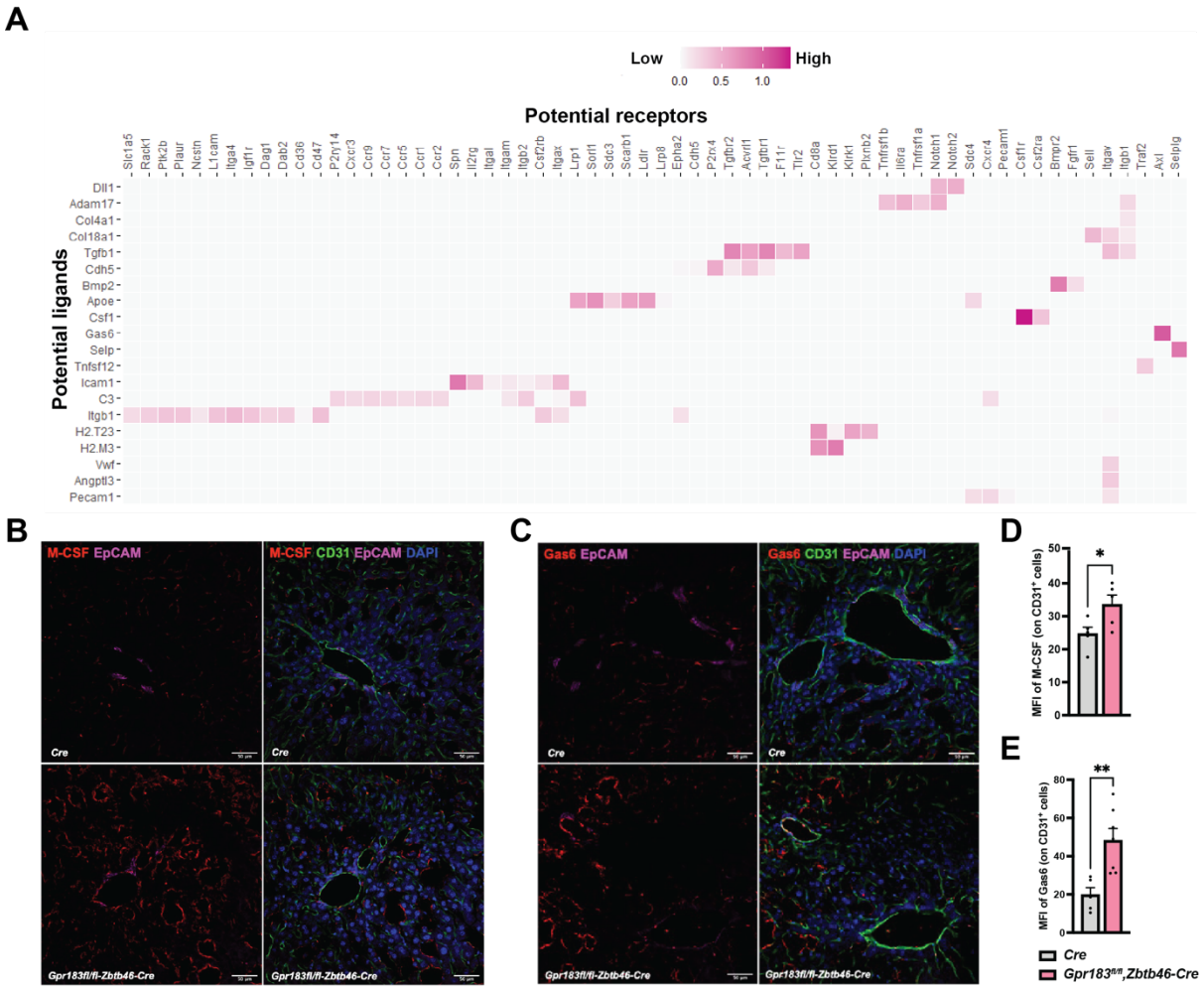

Figure 3.10: Endothelial cells regulate hepatic cDC pool size and their survival via M-CSF-M-CSFR and Gas6-Axl interaction. Single cell sequencing data was analyzed by running NicheNet algorithm to predict potential ligand-receptor interaction between endothelial cells and cDCs. **(A)** NicheNet *in-silico* analyses of potential ligand-receptor interactions between ligands from endothelial cells and receptors on cDC subset from WT healthy murine liver single cell sequencing datasets. **(B-C)** Representative confocal microscopy images of fresh frozen liver sections (14 µm) from *Zbtb46*-cre^{+} and *Gpr183*$^{flox/flox}$-*Zbtb46*-cre^{+} animals. Sections were immunostained using anti-M-CSF (B) and anti-Gas6 (C) (red), anti-CD31 (green) and EpCAM (magenta) antibodies to visualize the expression of M-CSF and Gas6 in *Zbtb46*-cre^{+} and *Gpr183*$^{flox/flox}$-*Zbtb46*-cre^{+} animals. Scale bars represent 50 µm. **(D-E**) Quantification of M-CSF (D) and Gas6 (E) MFI by endothelial cells in the portal regions of murine liver per area (425.10 x 425.10 µm) in fresh frozen liver sections (14 µm) from *Zbtb46*-cre^{+} and *Gpr183*$^{flox/flox}$-*Zbtb46*-cre^{+} animals (n = 5-7, each dot represents one area, error bars represent mean ± SEM). *$P < 0.05$, **$P < 0.01$.

expressing endothelial cells in the portal regions of KO mice when compared with the control groups in the hepatic portal regions. This data suggested that the endothelial cells in the portal region are the main producers of oxysterol ligand for GPR183 activation and they regulate the survival and maintenance of cDC subsets potentially via M-CSF-M-CSFR and Gas6-Axl interactions.

3.11. Blocking of gut-liver axis cholesterol transport results in increased hepatic cDC abundance and increased expression of M-CSF and Gas6 in endothelial cells

To further understand the role of cholesterol and its derivative oxysterols in maintaining cDC homeostasis in the liver, the role of dietary cholesterol for cDC maintenance and survival was studied. Cholesterol is synthesized by the enterocytes in the gut and is transported to the liver via the gut-portal vein axis **(Fig 3.11-A)**. In fact, the majority of cholesterol in the form of high-density lipoprotein cholesterol (HDL-C) in the liver is derived from the intestine. ApoA1 and the cholesterol transporter ABCA1 are crucial for the biogenesis of HDL-C from the enterocytes **(Fig 3.11-A)**. To investigate the role of gut derived cholesterol on hepatic cDCs, intestine specific knockout mouse line (*Abca1*$^{flox/flox}$-*Vil1*-cre) were generated to block the transport of gut-derived cholesterol to liver *via* portal blood. Liver sections of KO and control groups were immunostained as before and visualized by confocal microscopy. A significant increase in the number of cDCs around the portal regions of liver in KO animals when compared to the control group was observed **(Fig 3.11-B, C)**.

Next, the expression of M-CSF and Gas6 in endothelial cells was checked by confocal microscopy and a significant increase in the expression of M-CSF and Gas6 in endothelial cells around the portal regions of KO animals vs the control groups was observed **(Fig 3.11-D-G)**.

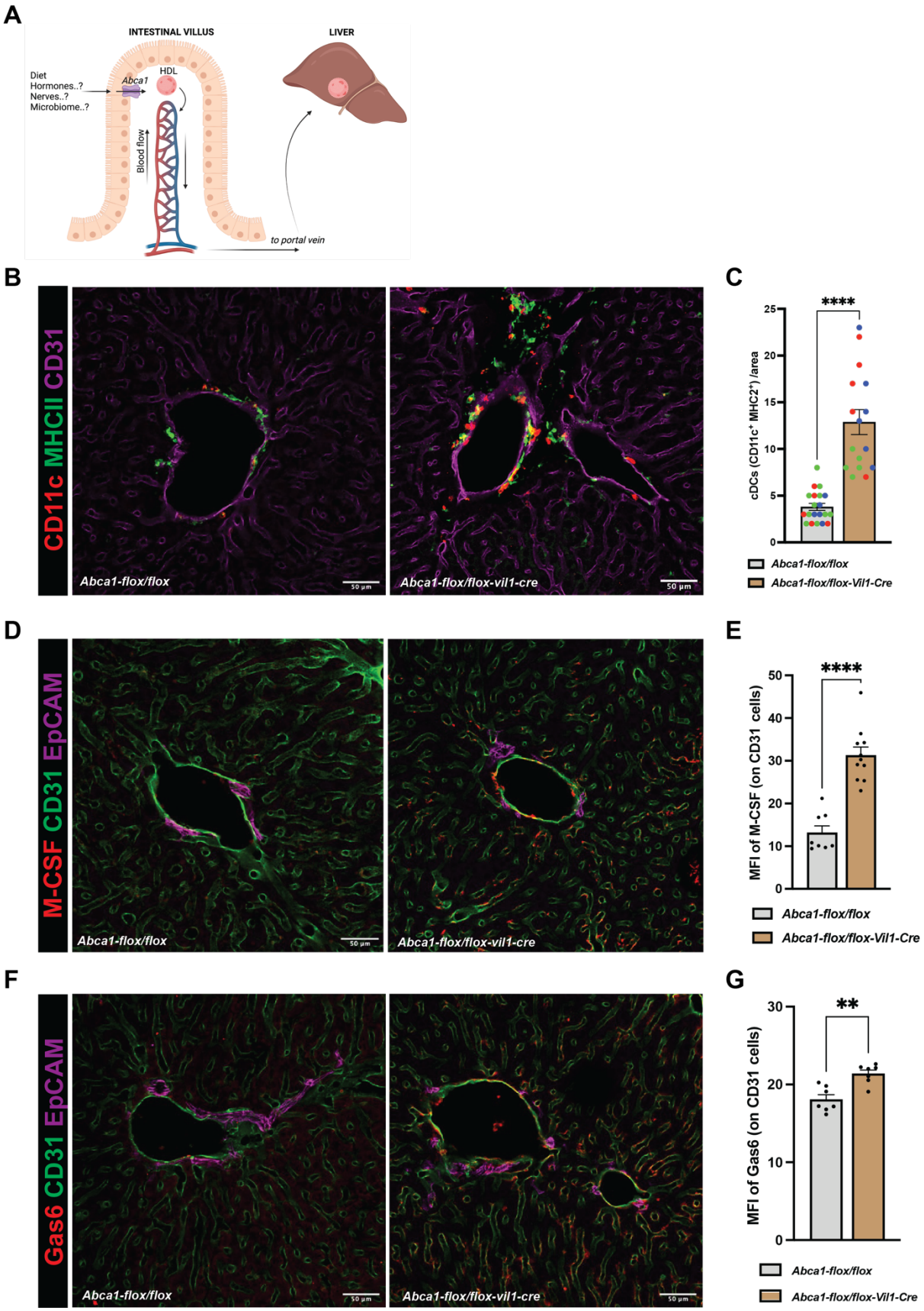

Figure 3.11: Dietary cholesterol from intestine is crucial for the maintenance of cDCs in liver. (A) Schematic illustration of cholesterol biogenesis in the intestine. Enterocytes express ABCA1 to promote HDL biogenesis in

the form of HDL which is then transported to the liver *via* portal vein blood circulation. To block the transport of gut derived cholesterol to the liver, we utilized vil1-cre to generate gut specific ablation of *Abca1* **(B)** Representative confocal microscopy images of fresh frozen liver sections (14 µm) from *Abca1*$^{flox/flox}$ and *Abca1*$^{flox/flox}$-*Vil1*-cre animals. Sections were immunostained using anti-CD11c (red), anti-MHCII (green) and anti-CD31 (magenta) antibodies to visualize cDC numbers in the liver sections from *Abca1*$^{flox/flox}$ and *Abca1*$^{flox/flox}$-*Vil1*-cre animals. Scale bars represent 50 µm. **(C)** Quantification of cDC cell numbers per area (425.10 x 425.10 µm) in fresh frozen liver sections (14 µm) from *Abca1*$^{flox/flox}$ and *Abca1*$^{flox/flox}$-*Vil1*-cre animals (*n* = 16-20, each dot represents one area, each color represents one mouse, error bars represent mean ± SEM). **(D)** Representative confocal microscopy images of fresh frozen liver sections (14 µm) from *Abca1*$^{flox/flox}$ and *Abca1*$^{flox/flox}$-*Vil1*-cre animals. Sections were immunostained using anti-M-CSF (red), anti-CD31 (green) and EpCAM (magenta) antibodies to visualize the expression and MFI of M-CSF in sections from *Abca1*$^{flox/flox}$ and *Abca1*$^{flox/flox}$-*Vil1*-cre animals. **(E)** Quantification of cDC cell numbers per area (425.10 x 425.10 µm) in fresh frozen liver sections (14 µm) from *Abca1*$^{flox/flox}$ and *Abca1*$^{flox/flox}$-*Vil1*-cre animals (*n* = 8-11, each dot represents one area, error bars represent mean ± SEM). **(F)** Representative confocal microscopy images of fresh frozen liver sections (14 µm) from *Abca1*$^{flox/flox}$ and *Abca1*$^{flox/flox}$-*Vil1*-cre animals. Sections were immunostained using anti-Gas6 (red), anti-CD31 (green) and EpCAM (magenta) antibodies to visualize the expression and MFI of M-CSF in sections from *Abca1*$^{flox/flox}$ and *Abca1*$^{flox/flox}$-*Vil1*-cre animals. **(G)** Quantification of cDC cell numbers per area (425.10 x 425.10 µm) in fresh frozen liver sections (14 µm) from *Abca1*$^{flox/flox}$ and *Abca1*$^{flox/flox}$-*Vil1*-cre animals (*n* = 6-7, each dot represents one area, error bars represent mean ± SEM). **P < 0.05, **P < 0.01, ***P < 0.001, ****P < 0.0001.*

Taken together, the imaging data showed that merely by blocking the transport of gut-derived cholesterol to the liver is sufficient to alter the cDC homeostasis in liver, phenocopying the phenotype observed in *Gpr183*$^{-/-}$, *Gpr183*$^{flox/flox}$-*Zbtb46*-cre^{+}, *Ch25h*$^{-/-}$ and *Cyp7b1*$^{-/-}$ mice indicating that dietary cholesterol is crucial for hepatic cDC homeostasis and maintenance.

3.12. DC specific *Gpr183* ablation results in increased lipid droplets deposition in liver and delayed progression of hepatic fibrosis upon CDAA-HFD feeding

To further establish the role of cDC subsets under pathophysiological conditions, *Gpr183*$^{flox/flox}$-*Zbtb46*-cre^{+} and *Zbtb46*-cre^{+} mice were challenged with choline-deficient, L-amino acid-defined high fat diet (CDAA-HFD) for 4 weeks to study the role of cDCs in development of NASH-induced fibrosis. Previous studies have demonstrated that CDAA-HFD model mimics the human NASH phenotype in both mice and rats by sequentially developing steatohepatitis, liver fibrosis and liver cancer without any loss of body weight [156-159]. Hepatic infiltration of T cells has been shown previously in NASH conditions [160, 161]. Therefore, the T cell and cDC phenotypes in the liver were profiled by flow cytometry. In line with already published data, our data showed a significant increase of infiltrating CD4^{+} T cells and CD8^{+} T cells, but no changes were observed in NK cells upon CDAA-HFD feeding **(Fig 3.12-A)**. Moreover, a significant increase in total cDC and cDC2 subsets frequency in the KO animals fed with CDAA-HFD was observed **(Fig 3.11-B)**. This increase was not evident in the control groups fed with CDAA-HFD. Interestingly, frequency of cDC1 subset was increased in control animals fed with CDAA-HFD and this was not observed in the KO group fed with CDAA-HFD **(Fig 3.12-B)**. Recent study has shown that cDC1s are the main contributors of NASH development by promoting the inflammatory T cell reprogramming during steatohepatitis [162]. As a selective increase of cDC1 subset in control group animals but not in KO animals when they were fed on CDAA-HFD was observed, the progression of liver fibrosis was investigated and compared across groups. Masson's trichrome staining on liver sections from the control and KO animals fed on CDAA-HFD revealed that the lipid droplet size and their content was significantly increased in the KO livers fed with CDAA-HFD when compared with

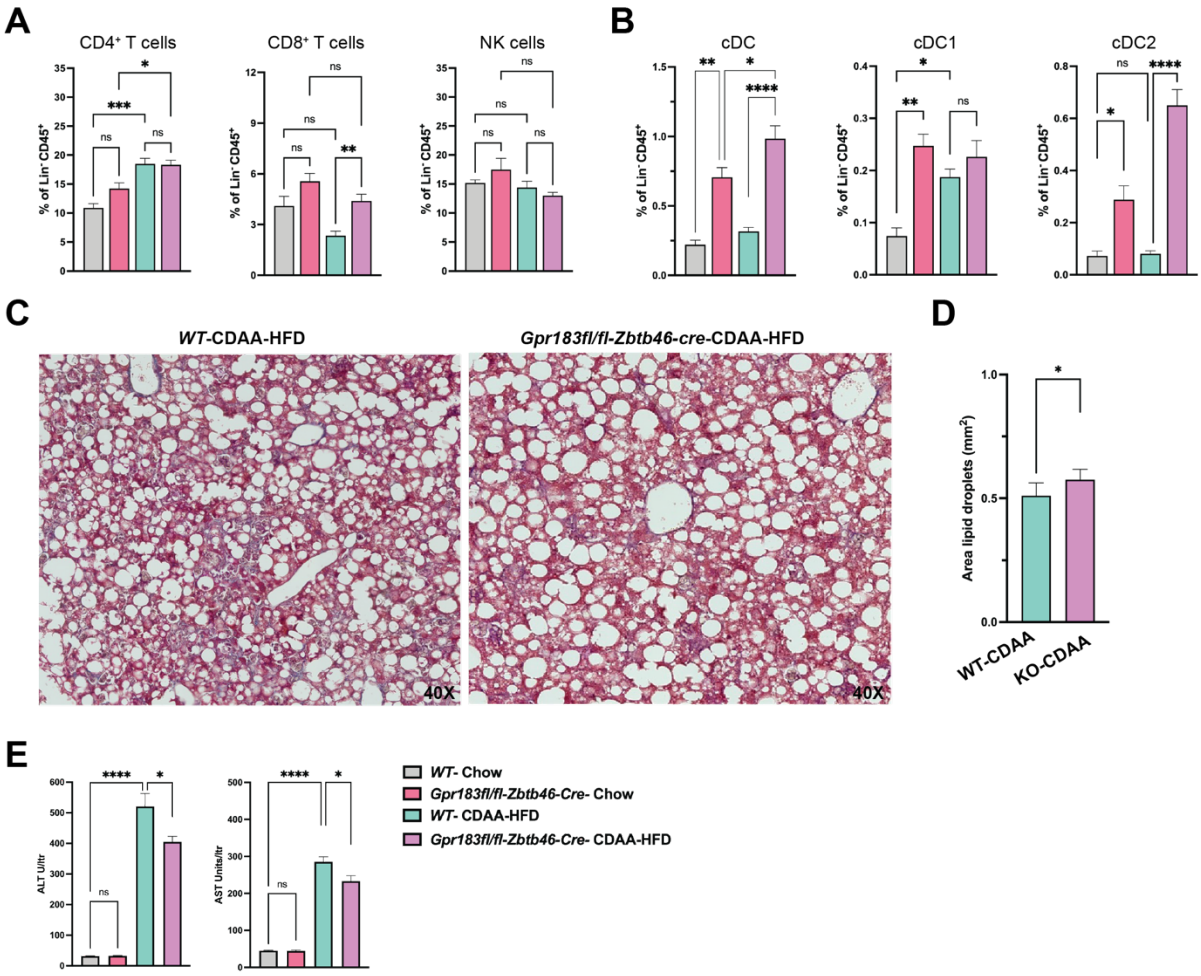

Figure 3.12: DC specific *Gpr183* ablation results in delayed progression of hepatic fibrosis upon CDAA-HFD feeding. WT and *Gpr183*$^{flox/flox}$-*Zbtb46*-cre^{+} animals were fed on chow and CDAA high fat diet for 4 weeks. **(A)** Frequency of CD4^{+} T cell, CD8+ T cell and NK cell subsets within the liver of WT and *Gpr183*$^{flox/flox}$-*Zbtb46*-cre^{+} animals fed on chow and CDAA-HFD (*n*=6-8, error bars represent mean ± SEM). **(B)** Frequency of cDC, cDC1, cDC2 subsets within the liver of WT and *Gpr183*$^{flox/flox}$-*Zbtb46*-cre^{+} animals fed on chow and CDAA-HFD (*n*=6-8, error bars represent mean ± SEM). **(C)** Representative Masson's trichrome staining images of fresh frozen liver sections (14 µm) from WT and *Gpr183*$^{flox/flox}$-*Zbtb46*-cre^{+} animals fed on CDAA-HFD for 4 weeks. **(D)** Quantification of lipid droplets in mm^2 area in the fresh frozen liver sections taken from the liver of WT and *Gpr183*$^{flox/flox}$-*Zbtb46*-cre^{+} animals fed on CDAA-HFD (*n*=3, error bars represent mean ± SEM). **(E)** Quantification of ALT and AST serum concentration in livers from WT and *Gpr183*$^{flox/flox}$-*Zbtb46*-cre^{+} animals fed on CDAA-HFD (*n*=7-8, error bars represent mean ± SEM). **P < 0.05, **P < 0.01, ***P < 0.001, ****P < 0.0001.*

the control groups **(Fig 3.12-C, D)**. Furthermore, the ALT and AST contents were measured to quantify liver damage after CDAA-HFD. Both, ALT and AST levels were significantly increased in the control animals after CDAA-HFD **(Fig 3.12-E, F)**. However, this increase in ALT and AST was significantly less in the KO animals fed on CDAA-HFD **(Fig 3.12-E, F)**. Taken together, these results suggested that the increase in cDC1 was selective to the control group fed on CDAA-HFD, which has been shown to be main driver of liver fibrosis. This increase of cDC1 subset was not observed in the KO animals fed on CDAA-HFD, which resulted in a delayed progression of NASH/fibrosis, as shown by increased lipid droplet size and significantly reduced ALT and AST levels in serum of KO animals fed on CDAA-HFD.

4. Discussion

In this study, the role of G protein coupled receptor GPR183 in hepatic cDC homeostasis, their survival, organization and their crosstalk with endothelial cells in the tissue microenvironment was investigated. First, we showed that lack of *Gpr183* results in increased hepatic cDC and cDC progenitors. Next, we showed that the increase of cDC numbers is due to their increased *in situ* proliferation and decreased apoptosis dependent on STAT3 phosphorylation. Our data from chimeric mice models showed that GPR183 played a cell intrinsic role in controlling the cDC pool size and that the expression of GPR183 on cDC subsets is crucial for maintenance of homeostasis and their abundance in the liver. Moreover, we demonstrated that oxysterol from the radioresistant stromal cells and not from the immune compartment is crucial for cDC maintenance and their abundance. Furthermore, our *in-silico* analyses combined with confocal imaging data showed an endothelial cell: cDC crosstalk *via* M-CSF-M-CSFR and Gas6-Axl signaling. Additionally, we showed that hindering the flow of dietary cholesterol from the gut to the liver through portal blood was sufficient to disturb the cDC homeostasis in the liver. Finally, we showed that DC specific KO animals were protected during the early phase from steatohepatitis and fibrosis development.

The liver is a crucial organ for the maintenance of body homeostasis, namely by performing several tasks such as synthesizing essential molecules, extracting and metabolizing several nutrients and xenobiotics, excretion of metabolic products, and most importantly neutralizing the microbes and microbial products from the gut entering the liver *via* the portal vein. As the liver is positioned adjacent to the gut and it receives the portal vein blood circulation from it, the liver provides a unique niche for the immune cells within the hepatic microenvironment. Immune cells are patrolling in the tissue to overcome the microbes or viral particles entering the liver *via* the portal blood and play a crucial role in host defense and maintenance of

cellular homeostasis. To perform their tasks, immune cells are positioned in a specific niche within the organ. How are immune cells strategically positioned in secondary lymphoid organs such as spleen has been well studied. For example, the positioning of cDCs within murine spleen was dependent on chemotactic receptor GPR183. Our unpublished data on the role of GPR183 on lung cDCs showed that it regulates the positioning of cDC2 within the adventitial cuffs of the murine lung in a TSLP-dependent manner [163]. However, whether such niche specific signals also regulate the immune cell homeostasis in the cholesterol-rich hepatic environment still remains elusive. Therefore, this study aimed to investigate the role of GPR183 in maintenance of hepatic cDC subsets.

4.1. Flow cytometry based phenotypic characterization of hepatic mononuclear phagocytes and expression of GPR183 in myeloid cell subsets

The murine liver harbors a variety of immune cell subsets such as T cells, B cells, NK cells, KCs, monocytes, and DCs. The myeloid compartment is characterized by the diverse, yet redundant, expression of multiple surface markers which hinders an accurate distinction between the multiple myeloid cell types. Thus, a better phenotypic characterization strategy to discriminate myeloid cells based on the combination of cell surface markers they express is needed. To circumvent this challenge in order to study the role of GPR183 on regulation of hepatic cDC homeostasis in murine liver, in this project we proposed a comprehensive multi-color flow cytometry panel comprising of markers for cDC, cDC1, cDC2, KCs and monocytes, which was proved to be accurate for the discrimination of myeloid cells in the liver. A first step consisted in separating macrophages from cDCs, as they usually express overlapping markers, by excluding $CD64^{+}$ macrophages. cDCs in the liver express high levels of CD11c and MHCII. To further improve their identification CD26 was also added in addition to gold

standard pan cDC markers and around 85% of hepatic cDCs were found to be expressing CD26 in homeostasis and inflammation, in agreement with previous studies [45]. To further split them into cDC1 and cDC2 subsets, cDCs were discriminated based on the expression of XCR1 and CD172α for cDC1s and cDC2s, respectively [55]. Taken together, designing the flow cytometry panel and the comprehensive gating strategy to gate cDCs and their subclasses without the contamination of macrophages and other myeloid cells was a relevant starting point for the development of this project.

Recent studies have shown that GPR183 is expressed by various immune cells in spleen, lung, LNs and intestine. Within these tissues, GPR183 is expressed by B cells, T cells and cDCs [132, 145]. However, the expression patterns of GPR183 in other organs, and especially in a tissue with a high cholesterol environment such as the liver had not been studied yet. In this thesis, for the first time we showed that within the murine liver, cDCs express high level of GPR183. Moreover, within the cDC compartment, cDC1 and cDC2 subclasses expressed high levels of GPR183. Conversely, other myeloid cells within the murine liver did not express high levels of GPR183. Although, the exact role of GPR183 in the liver had not been studied so far, the high expression of GPR183 in cDC subsets hints towards a similar role of homeostasis maintenance in liver as previously shown in other tissues [132, 137, 148].

4.2. GPR183 controls the hepatic cDC subsets pool size in a cell-intrinsic manner

Existing data on the role of GPR183 on immune functions and homeostasis is limited to the chemotactic role of GPR183 and regulation of the positioning and organization of T cells, B cells and DCs within the murine spleen [132, 145]. The role of GPR183 in cDC homeostasis in the liver has not been explored yet. Here we showed that global ablation of *Gpr183* resulted

in increased cDC pool size within the murine liver. DC-specific ablation of *Gpr183* phenocopied the results of global KO animals. Furthermore, our chimeric data in combination with spatial analyses showed that increased DC abundance in the liver was a cell-intrinsic process which requires the expression of GPR183 on cDCs. Contrary to the previously published data, where only splenic cDC2 abundance were affected in the *Gpr183* deficient mice [132, 143], our data showed that both cDC1 and cDC2 numbers were altered. This could be because (i) unlike the liver, the expression of GPR183 on splenic cDCs is limited to cDC2 subset, as shown before [132] or (ii) because of a different tissue specific niche and microenvironment.

4.3. Increase in cDCs number is because of their increased proliferation and impaired apoptosis

Cellular homeostasis is maintained by a finely tuned balance between proliferation and apoptosis. Any imbalance between proliferation and apoptosis may lead to impaired tissue homeostasis [164]. As we observed an increase in cDC numbers, we hypothesized that this could be a result of imbalance in proliferation and apoptosis. As expected, our results have shown an increased proliferation and significantly decreased apoptosis of cDC1 and cDC2 subsets. Additionally, we observed an increase in pre-cDC1 and pre-cDC2 precursor cells in the KO murine livers and decreased phosphorylation of STAT3 in cDC1 and cDC2 subsets was observed. Previously published studies have shown that STAT3 modulates DC maintenance and their immune functions [151, 152] and decreased STAT3 phosphorylation led to increased cDC numbers in the LNs of IL-6$^{-/-}$ animals [152]. Taken together, these results clearly demonstrate that increase in cDC numbers is due to the imbalance in proliferation to apoptosis ratio. These results are in contrary to previously published study, where it has been

shown that ablation of *Gpr183* did not affect the proliferation and survival of splenic cDC2s, as they did not observe any changes in the proliferation and apoptosis of splenic cDC2s between KO and WT animals [132]. This discrepancy could be because the cDC1 subset in the spleen does not express GPR183 as shown by published data [132] and cDCs in different tissues behave differently and require different signaling queues depending on their local tissue microenvironment.

4.4. *Gpr183* ablation does not affect migratory capacity of hepatic cDCs to the hepatic draining LN

DCs act as the bridging antigen presenting cells between the innate and adaptive immune responses to link them together. The uptake of any foreign antigen results in DC maturation, allowing them to migrate to the LN *via* lymphatic vessels [165, 166]. Upon activation and migration to LNs, DCs prime the T cells *via* MHCII antigen presentation within the LN [167, 168]. Since we observed an increase in DC abundance in the liver in DC-specific KO animals along with an increased expression of activation markers (i.e., CD80 and CD86), we further investigated whether deficiency of GPR183 altered their migration capacity to the draining hepatic LN. As expected, we found a significant increase in m-cDC, m-cDC1 and m-cDC2 subsets within the draining LNs in KO animals. These results demonstrate that lack of *Gpr183* in DCs does not alter their migratory capacity to the draining LNs. Prior data have shown that splenic DCs lacking *Gpr183* were functionally capable of presenting antigen and interacting with T cells but were unable to acquire blood-borne antigen trapped in the marginal zone due to their inability to locate themselves close to this region in the spleen [132]. This was because the remaining cDC1s in the *Gpr183*-deficient animals were not able to compensate for the very few remaining cDC2s in the marginal zone. Our data showed an increase in cDC activation

and increased migration of cDCs to the LN, but whether they are able to prime and interact with T cells in the LN requires further detailed *in-vitro* experimental studies.

4.5. Oyxsterol-GPR183 axis in radio-resistant stromal cells is crucial for the maintenance of cDC pool size within the liver

Oxysterol 7α,25-OHC is one of the most potent ligands for GPR183, which is a derivative of cholesterol synthesized by sequential hydroxylation of cholesterol by the enzymes CH25H and CYP7B1. Previous studies have shown that *Ch25h*$^{-/-}$ animals lacking the oxysterol ligand 7α,25-OHC have defects in the correct positioning of cDCs within the marginal zones of spleen [132]. As expected, our data on *Ch25h*$^{-/-}$ and *Cyp7b1*$^{-/-}$ animals showed a significant increase of cDC, cDC1 and cDC2 subsets because of the absence of key enzymes for the synthesis of GPR183 ligand. Unlike previously published data where the DC phenotype (decrease in splenic cDC2 subset) in spleen was less prominent in *Ch25h*$^{-/-}$ animals, our data showed a similar phenotype as the one of *Gpr183*$^{-/-}$ animals [132]. These results indicate that oxysterols-GPR183 axis is required for hepatic cDC maintenance.

It is crucial to determine the source of GPR183 ligands/oxysterols in order to establish which cell population interacts with hepatic cDCs within the tissue microenvironment and where the spatial niche exists in the liver. It has been shown that stromal cells, such as fibroblasts are the main source of oxysterol ligands in lymphoid tissues [134, 135, 137] and in the murine gut [169]. To explore whether the stromal or the immune compartment is the main source of oxysterol ligands in the murine liver, we generated *Ch25h* chimeric animals. Our results demonstrate that the radio-resistant stromal compartment and not the immune compartment is the main source of oxysterol ligands which can activate GPR183. Taken

together, these results demonstrate that similar to lymphoid organs and the gut, the stromal compartment in the liver is the main producer of ligands responsible for GPR183 activation.

4.6. Endothelial cells control the maintenance and survival of hepatic cDCs via M-CSF and Gas6

Although from our chimeric experiments it was clear that radio-resistant stromal cells are the key source of ligand for GPR183, it was still not clear which stromal cells are the main ligand source. To investigate this further, we utilized the publicly available single cell RNA-seq data and we checked for the expression of *Ch25h* and *Cyp7b1* in WT murine liver. In line with previously published data, *Cyp7b1* is highly expressed in liver by all the stromal cells [170]. However, *Ch25h* is specifically expressed only by the endothelial cells in the liver. Importantly, endothelial cells were the only cells which express both *Cyp7b1* and *Ch25h* together. This data suggested that the endothelial cells are the candidates guiding hepatic cDCs to their niche. Therefore, we further validated this by spatial analysis and found that indeed cDCs in the portal regions of liver were sitting next to the endothelial cells in the liver.

Recent studies have shown that GPR183 acts as a chemotactic guiding factor which directs the immune cells based on the oxysterol gradients and promotes their localization maintenance and survival within the spleen [132]. By sensing the 7α,25-OHC gradient in the spleen, cDCs migrate to the marginal zones and bridging channels *via* sensing the lymphotoxin-α1β2 produced by B cells, which is required for the maintenance and homeostasis of cDCs in the spleen. Similarly, in the murine gut, 7α,25-OHC chemotactic gradient maintained by fibroblast cells in the intestine attracts the GPR183-expressing ILC3s at the site of crypto patch formation, thereby positioning the lymphotoxin-α1β2^{+} ILC3s in proximity to the lymphotoxin-βR^{+} stromal cells in the gut [142]. This ILC3: stromal crosstalk

promotes the recruitment of GPR183-expressing B cells, to complete isolated lymphoid follicles (ILF) formation [142]. These studies indicate that in addition to the oxysterol-GPR183 signaling axis, other niche-specific guiding factors might play a key role in immune cell homeostasis within the tissue microenvironment.

Depending on the signaling queues from the neighboring niche cells, immune cells strategically locate and position themselves within their favorable niche for their maintenance and survival. If such guiding niche factor which can regulate the DC homeostasis and survival is indeed also functioning in liver in a similar fashion, the endothelial cells can be the source, as they express the key enzymes for the synthesis of GPR183 ligand. To determine the potential ligand-receptor communication between the endothelial cells and cDCs, we took advantage of publicly available single cell RNA-seq data from healthy mice liver [150] and performed a NicheNet prediction analysis on endothelial cells and cDCs. NicheNet models and predicts potential intercellular communication by linking ligands to target receptor genes in the public domain. It also considers the already published ligand-receptor interactions [171]. We found that M-CSF and Gas6 ligands from the endothelial cells and M-CSFR and Axl receptors from cDCs had the highest interaction potential amongst others. Furthermore, our spatial analysis also validated these *in-silico* results, where we observed an increased expression of M-CSF and Gas6 in endothelial cells around the portal regions of KO murine livers. A wide range of cell types, such as endothelial cells, fibroblasts, and monocyte/macrophages produce M-CSF, which serves as a chemotactic tonic factor for immune cell survival and maintenance [172]. Gas6, a ligand for TAM receptor (Tyro3, Axl, and Mer) is expressed by endothelial cells [173], bone marrow stromal cells [174] and vascular smooth muscle cells [175]. Several studies have described various functions of Gas6-TAM receptor signaling, such as inhibition of apoptosis [176], stimulation of cell growth and

proliferation [175, 177], stimulation of hemostasis [178], modulation of inflammation [179] and mediation of efferocytosis [180]. Taken together these results indicate that endothelial cells in the portal regions of murine liver are the key producers of oxysterol ligands and that M-CSF and Gas6 from endothelial cells communicate *via* M-CSF-M-CSFR and Gas6-Axl signaling to control the DC pool size potentially *via* controlling their cell proliferation, survival and apoptotic potential.

4.7. Dietary cholesterol from the gut-liver axis is crucial for hepatic DC homeostasis

We sought to investigate whether the cholesterol from dietary source is essential for the maintenance and survival of DCs in liver. The role of peripheral circulating cholesterol in the form of HDL has been widely studied in metabolic disorders, inflammation and atherosclerosis [181, 182]. However, the role of gut derived HDL in DC survival and maintenance has not been explored so far. The gut and the liver are two distinct sources of HDL. The gut alone accounts for 25% of the total circulating HDL in the body [183]. A recently published study unveiled the physiological function of enterically-derived HDL3 as a portal guardian of intestinal-leaked lipopolysaccharide (LPS), which forms a disease tolerance strategy to protect the liver from damage caused by gut-derived LPS [184]. However, whether the cholesterol synthesized in the gut plays any role in the maintenance of immune cell homeostasis in the liver still remains largely unknown. The biogenesis of HDL requires apoA1 and the cholesterol transporter ABCA1 [184]. To understand the role of enterically-derived cholesterol in hepatic DC maintenance, we used mice conditionally deficient for *Abca1* in the intestine (*Vil*-Cre). Our spatial results from *Abca1*-$^{flox\text{-}flox}$-*vil-1*-cre animals showed a significant increase of cDCs in the portal regions of the liver when compared to the control groups and

phenocopied the results from DC specific *Gpr183*$^{-/-}$, *Ch25h*$^{-/-}$ and *Cyp7b1*$^{-/-}$ animals. Furthermore, we also observed a similar increase of M-CSF and Gas6 in the portal region endothelial cells in the liver.

Collectively, these results suggest that the dietary cholesterol from the gut is crucial for the maintenance of cDCs in the liver and for the first time we show that only blocking the transport of cholesterol from the gut to the liver results in increased hepatic cDC abundance in a M-CSF and Gas6-dependent manner.

4.8. *Gpr183* deficient mice showed delayed fibrosis progression and less tissue damage upon short-term CDAA high fat diet feeding

NASH is the primary cause of liver disease, which leads to further complications such as fibrosis, cirrhosis, and progression towards hepato-carcinoma. Oxysterols are oxidized cholesterol molecules that are formed in the early steps of cholesterol metabolism and bile acid synthesis. They control lipid metabolism and perform significant metabolic tasks such as activating crucial bile acid pathway enzymes, promoting reverse cholesterol transport, and controlling hepatic cholesterol and fatty acid production [185]. Importantly, recent studies have shown that non-alcoholic fatty liver disease (NAFLD) patients have elevated serum concentrations of oxysterols such as 25-hydroxycholesterol (25-HC) and 27-hydroxycholesterol (27-HC) [186, 187]. However, despite these evidences, it still remains elusive and poorly understood whether the oxysterols-GPR183 axis is an active player under pathophysiological conditions such as NASH. To understand the role of GPR183 in the development of liver fibrosis, we fed the *Gpr183*$^{flox/flox}$-*Zbtb46*-cre^{+} animals on CDAA-HFD and our results showed that the KO animals had the higher tendency to develop more and bigger lipid droplets when compared to their control counterparts. Importantly, the ALT and AST

concentration in serum, which is a sign of liver damage, was significantly lower in the KO animals fed on CDAA-HFD when compared to the control group fed on CDAA-HFD. A recent study has shown that XCR1$^+$ cDCs in liver contribute to the development of NASH [162]. Taking this study in account, we observed that in the KO animals fed with CDAA-HDF, the abundance of XCR1$^+$ cDC1s was not altered and only cDC2s were increased. Since, XCR1$^+$ cDC1s drive the NASH phenotype in liver, this could be the reason behind the delayed NASH progression in our experimental settings.

Taken together, our data demonstrates that DC specific ablation of *Gpr183* results in delayed progression of NASH development and this can be further explored as therapeutic target for NAFLDs. Further research on long term effect of feeding of CDAA-HFD is required to consider this in therapeutic settings.

5. Conclusion and working model

Based on the above evidences, we propose a model of GPR183 directed control of cDC homeostasis maintenance *via* M-SCF and Gas6 within the murine liver **(Fig 4.1)**. Pre-cDCs from the blood circulation enter the liver *via* portal vein blood and differentiate into cDCs. Lack of GPR183 in DCs results in increased pre-cDCs number along with increased proliferation and decreased apoptosis of cDCs. cDCs migrate towards *Ch25h*$^+$ *Cyp7b1*$^+$ endothelial cells which produce the GPR183 ligand, 7α,25-OHC. DCs lacking GPR183 are not able to sense the 7α,25-OHC gradient and accumulate around the portal vein regions within the liver microenvironment where they have access to M-CSF and Gas6 produced by endothelial cells. M-CSF and Gas6 control the maintenance and survival of cDCs *via* M-CSF-M-CSFR and Gas6-Axl interaction and position them around the portal vein regions within the liver.

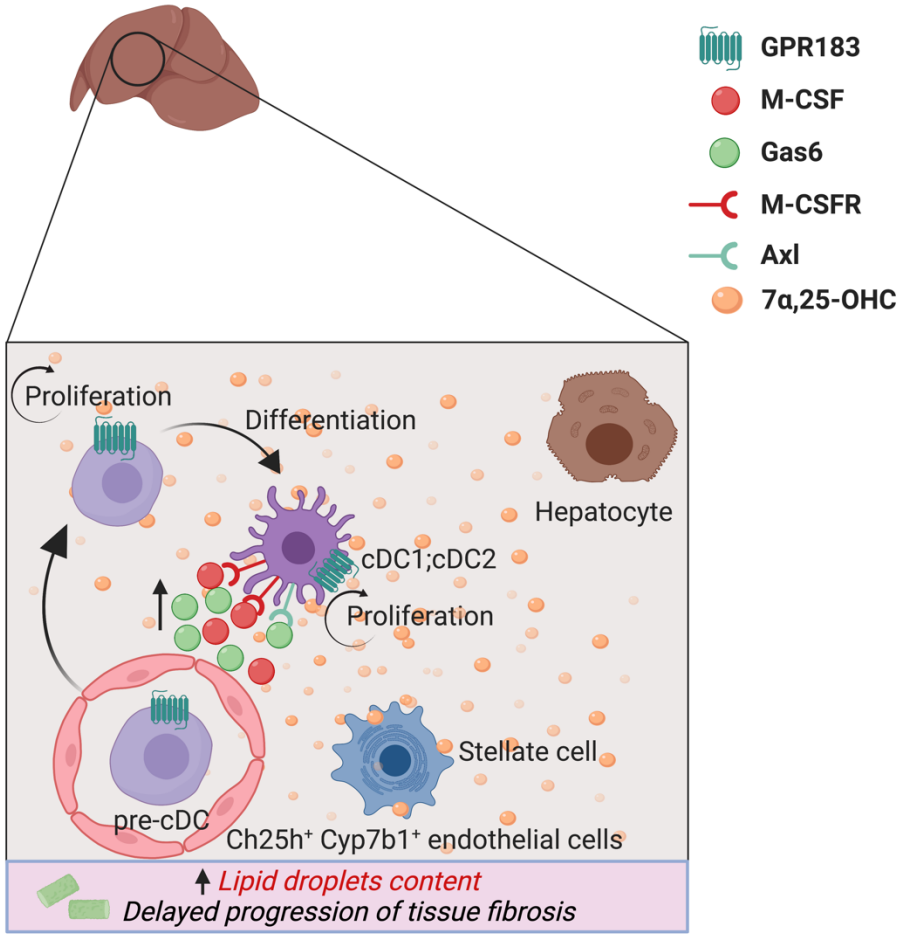

Figure 4.1: Graphical abstract of working model of positioning and maintenance of cDCs within the murine liver. pre-cDCs from the blood circulation enter the liver via portal vein blood and differentiate into cDCs. Lack of GPR183 results in increased pre-cDCs number along with increased proliferation and decreased apoptosis of cDCs. cDCs migrate towards *Ch25h*$^{+}$ *Cyp7b1*$^{+}$ endothelial cells which produce GPR183 ligand, 7α,25-OHC. DCs lacking *Gpr183* are not able to sense the 7α,25-OHC gradient and accumulate around the portal vein regions within the liver microenvironment and communicate with endothelial cells via M-CSF and Gas6.

Our study has provided new insights on the role of GPR183 in regulation of hepatic DC homeostasis. Here we show that in addition to secondary lymphoid organs, GPR183 acts as a chemotactic receptor in the liver which is responsible for maintenance and survival of cDCs near portal vein regions within the liver. We also show here that M-CSF and Gas6 are the guiding niche factors required for the maintenance and survival of hepatic cDCs. Furthermore,

we have shown that dietary cholesterol from the gut-liver axis is crucial for the maintenance of steady state homeostasis of hepatic cDCs. Lastly, we also showed that mice lacking the expression of GPR183 in cDCs had delayed progression of fibrosis development upon short-term CDAA-HDF feeding. These evidences will pave ways to design novel therapeutic strategies for NAFLD and designing DC-based vaccines.

6. References

1. Chaplin, D.D., *Overview of the immune response.* J Allergy Clin Immunol, 2010. **125**(2 Suppl 2): p. S3-23.
2. Rosenblum, M.D., K.A. Remedios, and A.K. Abbas, *Mechanisms of human autoimmunity.* J Clin Invest, 2015. **125**(6): p. 2228-33.
3. Belkaid, Y. and T.W. Hand, *Role of the microbiota in immunity and inflammation.* Cell, 2014. **157**(1): p. 121-41.
4. Batista, F.D. and M.L. Dustin, *Cell:cell interactions in the immune system.* Immunol Rev, 2013. **251**(1): p. 7-12.
5. Commins, S.P., L. Borish, and J.W. Steinke, *Immunologic messenger molecules: cytokines, interferons, and chemokines.* J Allergy Clin Immunol, 2010. **125**(2 Suppl 2): p. S53-72.
6. Kumar, H., T. Kawai, and S. Akira, *Pathogen recognition by the innate immune system.* Int Rev Immunol, 2011. **30**(1): p. 16-34.
7. Bonilla, F.A. and H.C. Oettgen, *Adaptive immunity.* J Allergy Clin Immunol, 2010. **125**(2 Suppl 2): p. S33-40.
8. Hoebe, K., E. Janssen, and B. Beutler, *The interface between innate and adaptive immunity.* Nat Immunol, 2004. **5**(10): p. 971-4.
9. Iwasaki, A. and R. Medzhitov, *Control of adaptive immunity by the innate immune system.* Nat Immunol, 2015. **16**(4): p. 343-53.
10. Medzhitov, R., *Recognition of microorganisms and activation of the immune response.* Nature, 2007. **449**(7164): p. 819-26.
11. Liu, Y. and C.A. Janeway, Jr., *Cells that present both specific ligand and costimulatory activity are the most efficient inducers of clonal expansion of normal CD4 T cells.* Proc Natl Acad Sci U S A, 1992. **89**(9): p. 3845-9.
12. Burnet, F.M., *A modification of Jerne's theory of antibody production using the concept of clonal selection.* CA Cancer J Clin, 1976. **26**(2): p. 119-21.
13. Boehm, T., *Design principles of adaptive immune systems.* Nat Rev Immunol, 2011. **11**(5): p. 307-17.
14. Litman, G.W., J.P. Rast, and S.D. Fugmann, *The origins of vertebrate adaptive immunity.* Nat Rev Immunol, 2010. **10**(8): p. 543-53.
15. Nagasawa, T., *Microenvironmental niches in the bone marrow required for B-cell development.* Nat Rev Immunol, 2006. **6**(2): p. 107-16.
16. Miller, J.F., *Revisiting thymus function.* Front Immunol, 2014. **5**: p. 411.
17. LeBien, T.W. and T.F. Tedder, *B lymphocytes: how they develop and function.* Blood, 2008. **112**(5): p. 1570-80.
18. Reinherz, E.L. and S.F. Schlossman, *The differentiation and function of human T lymphocytes.* Cell, 1980. **19**(4): p. 821-7.
19. Banchereau, J. and R.M. Steinman, *Dendritic cells and the control of immunity.* Nature, 1998. **392**(6673): p. 245-52.
20. Steinman, R.M. and Z.A. Cohn, *Identification of a novel cell type in peripheral lymphoid organs of mice. I. Morphology, quantitation, tissue distribution.* J Exp Med, 1973. **137**(5): p. 1142-62.
21. Steinman, R.M. and M.D. Witmer, *Lymphoid dendritic cells are potent stimulators of the primary mixed leukocyte reaction in mice.* Proc Natl Acad Sci U S A, 1978. **75**(10): p. 5132-6.

22. Metlay, J.P., et al., *The distinct leukocyte integrins of mouse spleen dendritic cells as identified with new hamster monoclonal antibodies.* J Exp Med, 1990. **171**(5): p. 1753-71.
23. Takeuchi, S. and M. Furue, *Dendritic cells: ontogeny.* Allergol Int, 2007. **56**(3): p. 215-23.
24. Merad, M., et al., *The dendritic cell lineage: ontogeny and function of dendritic cells and their subsets in the steady state and the inflamed setting.* Annu Rev Immunol, 2013. **31**: p. 563-604.
25. Balan, S., M. Saxena, and N. Bhardwaj, *Dendritic cell subsets and locations.* Int Rev Cell Mol Biol, 2019. **348**: p. 1-68.
26. Traver, D., et al., *Development of CD8alpha-positive dendritic cells from a common myeloid progenitor.* Science, 2000. **290**(5499): p. 2152-4.
27. Manz, M.G., et al., *Dendritic cell potentials of early lymphoid and myeloid progenitors.* Blood, 2001. **97**(11): p. 3333-41.
28. Manz, M.G., et al., *Dendritic cell development from common myeloid progenitors.* Ann N Y Acad Sci, 2001. **938**: p. 167-73; discussion 173-4.
29. D'Amico, A. and L. Wu, *The early progenitors of mouse dendritic cells and plasmacytoid predendritic cells are within the bone marrow hemopoietic precursors expressing Flt3.* J Exp Med, 2003. **198**(2): p. 293-303.
30. Karsunky, H., et al., *Flt3 ligand regulates dendritic cell development from Flt3+ lymphoid and myeloid-committed progenitors to Flt3+ dendritic cells in vivo.* J Exp Med, 2003. **198**(2): p. 305-13.
31. Mende, I., et al., *Flk2+ myeloid progenitors are the main source of Langerhans cells.* Blood, 2006. **107**(4): p. 1383-90.
32. Fogg, D.K., et al., *A clonogenic bone marrow progenitor specific for macrophages and dendritic cells.* Science, 2006. **311**(5757): p. 83-7.
33. Liu, K., et al., *In vivo analysis of dendritic cell development and homeostasis.* Science, 2009. **324**(5925): p. 392-7.
34. Naik, S.H., et al., *Development of plasmacytoid and conventional dendritic cell subtypes from single precursor cells derived in vitro and in vivo.* Nat Immunol, 2007. **8**(11): p. 1217-26.
35. Miller, J.C., et al., *Deciphering the transcriptional network of the dendritic cell lineage.* Nat Immunol, 2012. **13**(9): p. 888-99.
36. Sichien, D., et al., *Development of conventional dendritic cells: from common bone marrow progenitors to multiple subsets in peripheral tissues.* Mucosal Immunol, 2017. **10**(4): p. 831-844.
37. Poltorak, M.P. and B.U. Schraml, *Fate mapping of dendritic cells.* Front Immunol, 2015. **6**: p. 199.
38. Murphy, T.L., et al., *Transcriptional Control of Dendritic Cell Development.* Annu Rev Immunol, 2016. **34**: p. 93-119.
39. Schlitzer, A., et al., *Identification of cDC1- and cDC2-committed DC progenitors reveals early lineage priming at the common DC progenitor stage in the bone marrow.* Nat Immunol, 2015. **16**(7): p. 718-28.
40. Sichien, D., et al., *IRF8 Transcription Factor Controls Survival and Function of Terminally Differentiated Conventional and Plasmacytoid Dendritic Cells, Respectively.* Immunity, 2016. **45**(3): p. 626-640.

41. Grajales-Reyes, G.E., et al., *Batf3 maintains autoactivation of Irf8 for commitment of a CD8alpha(+) conventional DC clonogenic progenitor.* Nat Immunol, 2015. **16**(7): p. 708-17.
42. Persson, E.K., et al., *IRF4 transcription-factor-dependent CD103(+)CD11b(+) dendritic cells drive mucosal T helper 17 cell differentiation.* Immunity, 2013. **38**(5): p. 958-69.
43. Nussenzweig, M.C., et al., *Studies of the cell surface of mouse dendritic cells and other leukocytes.* J Exp Med, 1981. **154**(1): p. 168-87.
44. Steinman, R.M., et al., *Identification of a novel cell type in peripheral lymphoid organs of mice. V. Purification of spleen dendritic cells, new surface markers, and maintenance in vitro.* J Exp Med, 1979. **149**(1): p. 1-16.
45. Guilliams, M., et al., *Unsupervised High-Dimensional Analysis Aligns Dendritic Cells across Tissues and Species.* Immunity, 2016. **45**(3): p. 669-684.
46. Meredith, M.M., et al., *Expression of the zinc finger transcription factor zDC (Zbtb46, Btbd4) defines the classical dendritic cell lineage.* J Exp Med, 2012. **209**(6): p. 1153-65.
47. Satpathy, A.T., et al., *Zbtb46 expression distinguishes classical dendritic cells and their committed progenitors from other immune lineages.* J Exp Med, 2012. **209**(6): p. 1135-52.
48. Guilliams, M., et al., *Dendritic cells, monocytes and macrophages: a unified nomenclature based on ontogeny.* Nat Rev Immunol, 2014. **14**(8): p. 571-8.
49. Sung, S.S., et al., *A major lung CD103 (alphaE)-beta7 integrin-positive epithelial dendritic cell population expressing Langerin and tight junction proteins.* J Immunol, 2006. **176**(4): p. 2161-72.
50. del Rio, M.L., et al., *CD103- and CD103+ bronchial lymph node dendritic cells are specialized in presenting and cross-presenting innocuous antigen to CD4+ and CD8+ T cells.* J Immunol, 2007. **178**(11): p. 6861-6.
51. Bedoui, S., et al., *Cross-presentation of viral and self antigens by skin-derived CD103+ dendritic cells.* Nat Immunol, 2009. **10**(5): p. 488-95.
52. Ginhoux, F., et al., *The origin and development of nonlymphoid tissue CD103+ DCs.* J Exp Med, 2009. **206**(13): p. 3115-30.
53. Edelson, B.T., et al., *Peripheral CD103+ dendritic cells form a unified subset developmentally related to CD8alpha+ conventional dendritic cells.* J Exp Med, 2010. **207**(4): p. 823-36.
54. Shortman, K. and W.R. Heath, *The CD8+ dendritic cell subset.* Immunol Rev, 2010. **234**(1): p. 18-31.
55. Dorner, B.G., et al., *Selective expression of the chemokine receptor XCR1 on cross-presenting dendritic cells determines cooperation with CD8+ T cells.* Immunity, 2009. **31**(5): p. 823-33.
56. Crozat, K., et al., *Comparative genomics as a tool to reveal functional equivalences between human and mouse dendritic cell subsets.* Immunol Rev, 2010. **234**(1): p. 177-98.
57. Cancel, J.C., et al., *Are Conventional Type 1 Dendritic Cells Critical for Protective Antitumor Immunity and How?* Front Immunol, 2019. **10**: p. 9.
58. Bachem, A., et al., *Superior antigen cross-presentation and XCR1 expression define human CD11c+CD141+ cells as homologues of mouse CD8+ dendritic cells.* J Exp Med, 2010. **207**(6): p. 1273-81.

59. Crozat, K., et al., *The XC chemokine receptor 1 is a conserved selective marker of mammalian cells homologous to mouse CD8alpha+ dendritic cells.* J Exp Med, 2010. **207**(6): p. 1283-92.
60. Jongbloed, S.L., et al., *Human CD141+ (BDCA-3)+ dendritic cells (DCs) represent a unique myeloid DC subset that cross-presents necrotic cell antigens.* J Exp Med, 2010. **207**(6): p. 1247-60.
61. Chiang, M.C., et al., *Differential uptake and cross-presentation of soluble and necrotic cell antigen by human DC subsets.* Eur J Immunol, 2016. **46**(2): p. 329-39.
62. Lauterbach, H., et al., *Mouse CD8alpha+ DCs and human BDCA3+ DCs are major producers of IFN-lambda in response to poly IC.* J Exp Med, 2010. **207**(12): p. 2703-17.
63. Aliberti, J., et al., *Essential role for ICSBP in the in vivo development of murine CD8alpha + dendritic cells.* Blood, 2003. **101**(1): p. 305-10.
64. Tailor, P., et al., *The BXH2 mutation in IRF8 differentially impairs dendritic cell subset development in the mouse.* Blood, 2008. **111**(4): p. 1942-5.
65. Hacker, C., et al., *Transcriptional profiling identifies Id2 function in dendritic cell development.* Nat Immunol, 2003. **4**(4): p. 380-6.
66. Chandra, J., et al., *Batf3 selectively determines acquisition of CD8(+) dendritic cell phenotype and function.* Immunol Cell Biol, 2017. **95**(2): p. 215-223.
67. Balan, S., et al., *Large-Scale Human Dendritic Cell Differentiation Revealing Notch-Dependent Lineage Bifurcation and Heterogeneity.* Cell Rep, 2018. **24**(7): p. 1902-1915 e6.
68. Kirkling, M.E., et al., *Notch Signaling Facilitates In Vitro Generation of Cross-Presenting Classical Dendritic Cells.* Cell Rep, 2018. **23**(12): p. 3658-3672 e6.
69. Scharton-Kersten, T., et al., *Interferon consensus sequence binding protein-deficient mice display impaired resistance to intracellular infection due to a primary defect in interleukin 12 p40 induction.* J Exp Med, 1997. **186**(9): p. 1523-34.
70. Liu, C.H., et al., *Cutting edge: dendritic cells are essential for in vivo IL-12 production and development of resistance against Toxoplasma gondii infection in mice.* J Immunol, 2006. **177**(1): p. 31-5.
71. Mashayekhi, M., et al., *CD8alpha(+) dendritic cells are the critical source of interleukin-12 that controls acute infection by Toxoplasma gondii tachyzoites.* Immunity, 2011. **35**(2): p. 249-59.
72. Hildner, K., et al., *Batf3 deficiency reveals a critical role for CD8alpha+ dendritic cells in cytotoxic T cell immunity.* Science, 2008. **322**(5904): p. 1097-100.
73. Sancho, D., et al., *Identification of a dendritic cell receptor that couples sensing of necrosis to immunity.* Nature, 2009. **458**(7240): p. 899-903.
74. Durai, V. and K.M. Murphy, *Functions of Murine Dendritic Cells.* Immunity, 2016. **45**(4): p. 719-736.
75. Lewis, K.L., et al., *Notch2 receptor signaling controls functional differentiation of dendritic cells in the spleen and intestine.* Immunity, 2011. **35**(5): p. 780-91.
76. Kasahara, S. and E.A. Clark, *Dendritic cell-associated lectin 2 (DCAL2) defines a distinct CD8alpha- dendritic cell subset.* J Leukoc Biol, 2012. **91**(3): p. 437-48.
77. Bogunovic, M., et al., *Origin of the lamina propria dendritic cell network.* Immunity, 2009. **31**(3): p. 513-25.
78. Varol, C., et al., *Intestinal lamina propria dendritic cell subsets have different origin and functions.* Immunity, 2009. **31**(3): p. 502-12.

79. Burkly, L., et al., *Expression of relB is required for the development of thymic medulla and dendritic cells.* Nature, 1995. **373**(6514): p. 531-6.
80. Weih, F., et al., *Multiorgan inflammation and hematopoietic abnormalities in mice with a targeted disruption of RelB, a member of the NF-kappa B/Rel family.* Cell, 1995. **80**(2): p. 331-40.
81. Briseno, C.G., et al., *Deficiency of transcription factor RelB perturbs myeloid and DC development by hematopoietic-extrinsic mechanisms.* Proc Natl Acad Sci U S A, 2017. **114**(15): p. 3957-3962.
82. Satpathy, A.T., et al., *Notch2-dependent classical dendritic cells orchestrate intestinal immunity to attaching-and-effacing bacterial pathogens.* Nat Immunol, 2013. **14**(9): p. 937-48.
83. Kabashima, K., et al., *Intrinsic lymphotoxin-beta receptor requirement for homeostasis of lymphoid tissue dendritic cells.* Immunity, 2005. **22**(4): p. 439-50.
84. Gao, Y., et al., *Control of T helper 2 responses by transcription factor IRF4-dependent dendritic cells.* Immunity, 2013. **39**(4): p. 722-32.
85. Schlitzer, A., et al., *IRF4 transcription factor-dependent CD11b+ dendritic cells in human and mouse control mucosal IL-17 cytokine responses.* Immunity, 2013. **38**(5): p. 970-83.
86. Bajana, S., et al., *IRF4 promotes cutaneous dendritic cell migration to lymph nodes during homeostasis and inflammation.* J Immunol, 2012. **189**(7): p. 3368-77.
87. Tussiwand, R., et al., *Klf4 expression in conventional dendritic cells is required for T helper 2 cell responses.* Immunity, 2015. **42**(5): p. 916-28.
88. Kumamoto, Y., et al., *CD301b(+) dermal dendritic cells drive T helper 2 cell-mediated immunity.* Immunity, 2013. **39**(4): p. 733-43.
89. Kumamoto, Y., et al., *CD301b(+) dendritic cells suppress T follicular helper cells and antibody responses to protein antigens.* Elife, 2016. **5**.
90. Brown, C.C., et al., *Transcriptional Basis of Mouse and Human Dendritic Cell Heterogeneity.* Cell, 2019. **179**(4): p. 846-863 e24.
91. Lennert, K. and W. Remmele, *[Karyometric research on lymph node cells in man. I. Germinoblasts, lymphoblasts & lymphocytes].* Acta Haematol, 1958. **19**(2): p. 99-113.
92. Colonna, M., G. Trinchieri, and Y.J. Liu, *Plasmacytoid dendritic cells in immunity.* Nat Immunol, 2004. **5**(12): p. 1219-26.
93. Liu, Y.J., *IPC: professional type 1 interferon-producing cells and plasmacytoid dendritic cell precursors.* Annu Rev Immunol, 2005. **23**: p. 275-306.
94. Reizis, B., *Plasmacytoid Dendritic Cells: Development, Regulation, and Function.* Immunity, 2019. **50**(1): p. 37-50.
95. Zhan, Y., et al., *Plasmacytoid dendritic cells are short-lived: reappraising the influence of migration, genetic factors and activation on estimation of lifespan.* Sci Rep, 2016. **6**: p. 25060.
96. Musumeci, A., et al., *What Makes a pDC: Recent Advances in Understanding Plasmacytoid DC Development and Heterogeneity.* Front Immunol, 2019. **10**: p. 1222.
97. Wolf, A.I., et al., *Plasmacytoid dendritic cells are dispensable during primary influenza virus infection.* J Immunol, 2009. **182**(2): p. 871-9.
98. Swiecki, M., et al., *Plasmacytoid dendritic cell ablation impacts early interferon responses and antiviral NK and CD8(+) T cell accrual.* Immunity, 2010. **33**(6): p. 955-66.

99. Cervantes-Barragan, L., et al., *Plasmacytoid dendritic cells control T-cell response to chronic viral infection.* Proc Natl Acad Sci U S A, 2012. **109**(8): p. 3012-7.
100. Puttur, F., et al., *Conventional Dendritic Cells Confer Protection against Mouse Cytomegalovirus Infection via TLR9 and MyD88 Signaling.* Cell Rep, 2016. **17**(4): p. 1113-1127.
101. Kaminsky, L.W., et al., *Redundant Function of Plasmacytoid and Conventional Dendritic Cells Is Required To Survive a Natural Virus Infection.* J Virol, 2015. **89**(19): p. 9974-85.
102. Cervantes-Barragan, L., et al., *Control of coronavirus infection through plasmacytoid dendritic-cell-derived type I interferon.* Blood, 2007. **109**(3): p. 1131-7.
103. Swiecki, M., et al., *Plasmacytoid dendritic cells contribute to systemic but not local antiviral responses to HSV infections.* PLoS Pathog, 2013. **9**(10): p. e1003728.
104. Cisse, B., et al., *Transcription factor E2-2 is an essential and specific regulator of plasmacytoid dendritic cell development.* Cell, 2008. **135**(1): p. 37-48.
105. Ghosh, H.S., et al., *Continuous expression of the transcription factor e2-2 maintains the cell fate of mature plasmacytoid dendritic cells.* Immunity, 2010. **33**(6): p. 905-16.
106. Grajkowska, L.T., et al., *Isoform-Specific Expression and Feedback Regulation of E Protein TCF4 Control Dendritic Cell Lineage Specification.* Immunity, 2017. **46**(1): p. 65-77.
107. Ippolito, G.C., et al., *Dendritic cell fate is determined by BCL11A.* Proc Natl Acad Sci U S A, 2014. **111**(11): p. E998-1006.
108. Scott, C.L., et al., *The transcription factor Zeb2 regulates development of conventional and plasmacytoid DCs by repressing Id2.* J Exp Med, 2016. **213**(6): p. 897-911.
109. Wu, X., et al., *Transcription factor Zeb2 regulates commitment to plasmacytoid dendritic cell and monocyte fate.* Proc Natl Acad Sci U S A, 2016. **113**(51): p. 14775-14780.
110. Corrales, L., et al., *The host STING pathway at the interface of cancer and immunity.* J Clin Invest, 2016. **126**(7): p. 2404-11.
111. Dos Santos, V.G., et al., *Evidence of regulatory myeloid dendritic cells and circulating inflammatory epidermal dendritic cells-like modulated by Toll-like receptors 2 and 7/8 in adults with atopic dermatitis.* Int J Dermatol, 2017. **56**(6): p. 630-635.
112. Goldeck, D., et al., *Altered dendritic cell subset distribution in patients with Parkinson's disease: Impact of CMV serostatus.* J Neuroimmunol, 2016. **290**: p. 60-5.
113. Segura, E. and S. Amigorena, *Inflammatory dendritic cells in mice and humans.* Trends Immunol, 2013. **34**(9): p. 440-5.
114. Schlitzer, A., et al., *Recent advances in understanding dendritic cell development, classification, and phenotype.* F1000Res, 2018. **7**.
115. Hammad, H., et al., *Inflammatory dendritic cells--not basophils--are necessary and sufficient for induction of Th2 immunity to inhaled house dust mite allergen.* J Exp Med, 2010. **207**(10): p. 2097-111.
116. Plantinga, M., et al., *Conventional and monocyte-derived CD11b(+) dendritic cells initiate and maintain T helper 2 cell-mediated immunity to house dust mite allergen.* Immunity, 2013. **38**(2): p. 322-35.
117. Bottcher, J.P., P.A. Knolle, and D. Stabenow, *Mechanisms balancing tolerance and immunity in the liver.* Dig Dis, 2011. **29**(4): p. 384-90.
118. Racanelli, V. and B. Rehermann, *The liver as an immunological organ.* Hepatology, 2006. **43**(2 Suppl 1): p. S54-62.

119. Tacke, F. and H.W. Zimmermann, *Macrophage heterogeneity in liver injury and fibrosis.* J Hepatol, 2014. **60**(5): p. 1090-6.
120. Varol, C., S. Yona, and S. Jung, *Origins and tissue-context-dependent fates of blood monocytes.* Immunol Cell Biol, 2009. **87**(1): p. 30-8.
121. Gomez Perdiguero, E., et al., *Tissue-resident macrophages originate from yolk-sac-derived erythro-myeloid progenitors.* Nature, 2015. **518**(7540): p. 547-51.
122. Yona, S., et al., *Fate mapping reveals origins and dynamics of monocytes and tissue macrophages under homeostasis.* Immunity, 2013. **38**(1): p. 79-91.
123. Schulz, C., et al., *A lineage of myeloid cells independent of Myb and hematopoietic stem cells.* Science, 2012. **336**(6077): p. 86-90.
124. Guilliams, M., et al., *Spatial proteogenomics reveals distinct and evolutionarily conserved hepatic macrophage niches.* Cell, 2022. **185**(2): p. 379-396 e38.
125. Bonnardel, J., et al., *Stellate Cells, Hepatocytes, and Endothelial Cells Imprint the Kupffer Cell Identity on Monocytes Colonizing the Liver Macrophage Niche.* Immunity, 2019. **51**(4): p. 638-654 e9.
126. Crispe, I.N., *The liver as a lymphoid organ.* Annu Rev Immunol, 2009. **27**: p. 147-63.
127. Eckert, C., et al., *The complex myeloid network of the liver with diverse functional capacity at steady state and in inflammation.* Front Immunol, 2015. **6**: p. 179.
128. Link, A., et al., *Association of T-zone reticular networks and conduits with ectopic lymphoid tissues in mice and humans.* Am J Pathol, 2011. **178**(4): p. 1662-75.
129. Connolly, M.K., et al., *In liver fibrosis, dendritic cells govern hepatic inflammation in mice via TNF-alpha.* J Clin Invest, 2009. **119**(11): p. 3213-25.
130. Henning, J.R., et al., *Dendritic cells limit fibroinflammatory injury in nonalcoholic steatohepatitis in mice.* Hepatology, 2013. **58**(2): p. 589-602.
131. Jiao, J., et al., *Dendritic cell regulation of carbon tetrachloride-induced murine liver fibrosis regression.* Hepatology, 2012. **55**(1): p. 244-55.
132. Gatto, D., et al., *The chemotactic receptor EBI2 regulates the homeostasis, localization and immunological function of splenic dendritic cells.* Nat Immunol, 2013. **14**(5): p. 446-53.
133. Birkenbach, M., et al., *Epstein-Barr virus-induced genes: first lymphocyte-specific G protein-coupled peptide receptors.* J Virol, 1993. **67**(4): p. 2209-20.
134. Hannedouche, S., et al., *Oxysterols direct immune cell migration via EBI2.* Nature, 2011. **475**(7357): p. 524-7.
135. Liu, C., et al., *Oxysterols direct B-cell migration through EBI2.* Nature, 2011. **475**(7357): p. 519-23.
136. Russell, D.W., *The enzymes, regulation, and genetics of bile acid synthesis.* Annu Rev Biochem, 2003. **72**: p. 137-74.
137. Yi, T., et al., *Oxysterol gradient generation by lymphoid stromal cells guides activated B cell movement during humoral responses.* Immunity, 2012. **37**(3): p. 535-48.
138. Rosenkilde, M.M., et al., *Molecular pharmacological phenotyping of EBI2. An orphan seven-transmembrane receptor with constitutive activity.* J Biol Chem, 2006. **281**(19): p. 13199-13208.
139. Benned-Jensen, T., et al., *Ligand modulation of the Epstein-Barr virus-induced seven-transmembrane receptor EBI2: identification of a potent and efficacious inverse agonist.* J Biol Chem, 2011. **286**(33): p. 29292-29302.
140. Benned-Jensen, T., et al., *Small molecule antagonism of oxysterol-induced Epstein-Barr virus induced gene 2 (EBI2) activation.* FEBS Open Bio, 2013. **3**: p. 156-60.

141. Rutkowska, A., et al., *The EBI2 signalling pathway plays a role in cellular crosstalk between astrocytes and macrophages.* Sci Rep, 2016. **6**: p. 25520.
142. Emgard, J., et al., *Oxysterol Sensing through the Receptor GPR183 Promotes the Lymphoid-Tissue-Inducing Function of Innate Lymphoid Cells and Colonic Inflammation.* Immunity, 2018. **48**(1): p. 120-132 e8.
143. Yi, T. and J.G. Cyster, *EBI2-mediated bridging channel positioning supports splenic dendritic cell homeostasis and particulate antigen capture.* Elife, 2013. **2**: p. e00757.
144. Pereira, J.P., et al., *EBI2 mediates B cell segregation between the outer and centre follicle.* Nature, 2009. **460**(7259): p. 1122-6.
145. Gatto, D., et al., *Guidance of B cells by the orphan G protein-coupled receptor EBI2 shapes humoral immune responses.* Immunity, 2009. **31**(2): p. 259-69.
146. Gatto, D., K. Wood, and R. Brink, *EBI2 operates independently of but in cooperation with CXCR5 and CCR7 to direct B cell migration and organization in follicles and the germinal center.* J Immunol, 2011. **187**(9): p. 4621-8.
147. Li, J., et al., *EBI2 augments Tfh cell fate by promoting interaction with IL-2-quenching dendritic cells.* Nature, 2016. **533**(7601): p. 110-4.
148. Lu, E., et al., *Distinct oxysterol requirements for positioning naive and activated dendritic cells in the spleen.* Sci Immunol, 2017. **2**(10).
149. Wyss, A., et al., *The EBI2-oxysterol axis promotes the development of intestinal lymphoid structures and colitis.* Mucosal Immunol, 2019. **12**(3): p. 733-745.
150. Remmerie, A., et al., *Osteopontin Expression Identifies a Subset of Recruited Macrophages Distinct from Kupffer Cells in the Fatty Liver.* Immunity, 2020. **53**(3): p. 641-657 e14.
151. Melillo, J.A., et al., *Dendritic cell (DC)-specific targeting reveals Stat3 as a negative regulator of DC function.* J Immunol, 2010. **184**(5): p. 2638-45.
152. Park, S.J., et al., *IL-6 regulates in vivo dendritic cell differentiation through STAT3 activation.* J Immunol, 2004. **173**(6): p. 3844-54.
153. Bell, B.D., et al., *The transcription factor STAT5 is critical in dendritic cells for the development of TH2 but not TH1 responses.* Nat Immunol, 2013. **14**(4): p. 364-71.
154. Eddy, W.E., et al., *Stat5 Is Required for CD103(+) Dendritic Cell and Alveolar Macrophage Development and Protection from Lung Injury.* J Immunol, 2017. **198**(12): p. 4813-4822.
155. Hosui, A., et al., *Loss of STAT5 causes liver fibrosis and cancer development through increased TGF-beta and STAT3 activation.* J Exp Med, 2009. **206**(4): p. 819-31.
156. Nakae, D., et al., *Production of both 8-hydroxydeoxyguanosine in liver DNA and gamma-glutamyltransferase-positive hepatocellular lesions in rats given a choline-deficient, L-amino acid-defined diet.* Jpn J Cancer Res, 1990. **81**(11): p. 1081-4.
157. Nakae, D., et al., *High incidence of hepatocellular carcinomas induced by a choline deficient L-amino acid defined diet in rats.* Cancer Res, 1992. **52**(18): p. 5042-5.
158. Sakaida, I., et al., *Prevention of fibrosis reduces enzyme-altered lesions in the rat liver.* Carcinogenesis, 1994. **15**(10): p. 2201-6.
159. Denda, A., et al., *Expression of inducible nitric oxide (NO) synthase but not prevention by its gene ablation of hepatocarcinogenesis with fibrosis caused by a choline-deficient, L-amino acid-defined diet in rats and mice.* Nitric Oxide, 2007. **16**(1): p. 164-76.

160. Wolf, M.J., et al., *Metabolic activation of intrahepatic CD8+ T cells and NKT cells causes nonalcoholic steatohepatitis and liver cancer via cross-talk with hepatocytes.* Cancer Cell, 2014. **26**(4): p. 549-64.
161. Grohmann, M., et al., *Obesity Drives STAT-1-Dependent NASH and STAT-3-Dependent HCC.* Cell, 2018. **175**(5): p. 1289-1306 e20.
162. Deczkowska, A., et al., *XCR1(+) type 1 conventional dendritic cells drive liver pathology in non-alcoholic steatohepatitis.* Nat Med, 2021. **27**(6): p. 1043-1054.
163. Zhang, L., *GPR183 expression on pulmonary conventional dendritic cell type 2 dictates subtissular localisation and instructs their survival via the thymic stromal lymphopoietin (TSLP) - TSLP receptor (TSLPR) axis*. 2021, Rheinische Friedrich-Wilhelms-Universität Bonn: Bonn.
164. Sun, Z., et al., *The influence of apoptosis on intestinal barrier integrity in rats.* Scand J Gastroenterol, 1998. **33**(4): p. 415-22.
165. Granucci, F., et al., *Early events in dendritic cell maturation induced by LPS.* Microbes Infect, 1999. **1**(13): p. 1079-84.
166. Larsen, C.P., et al., *Migration and maturation of Langerhans cells in skin transplants and explants.* J Exp Med, 1990. **172**(5): p. 1483-93.
167. Bousso, P. and E. Robey, *Dynamics of CD8+ T cell priming by dendritic cells in intact lymph nodes.* Nat Immunol, 2003. **4**(6): p. 579-85.
168. Ingulli, E., et al., *In vivo detection of dendritic cell antigen presentation to CD4(+) T cells.* J Exp Med, 1997. **185**(12): p. 2133-41.
169. Chu, C., et al., *Anti-microbial Functions of Group 3 Innate Lymphoid Cells in Gut-Associated Lymphoid Tissues Are Regulated by G-Protein-Coupled Receptor 183.* Cell Rep, 2018. **23**(13): p. 3750-3758.
170. Schwarz, M., et al., *Identification and characterization of a mouse oxysterol 7alpha-hydroxylase cDNA.* J Biol Chem, 1997. **272**(38): p. 23995-4001.
171. Browaeys, R., W. Saelens, and Y. Saeys, *NicheNet: modeling intercellular communication by linking ligands to target genes.* Nat Methods, 2020. **17**(2): p. 159-162.
172. Green, M. and M.A. Harrington, *A comparison of macrophage colony-stimulating factor (M-CSF) gene expression in primary and immortalized endothelial cells.* J Hematother Stem Cell Res, 2000. **9**(2): p. 237-46.
173. Manfioletti, G., et al., *The protein encoded by a growth arrest-specific gene (gas6) is a new member of the vitamin K-dependent proteins related to protein S, a negative coregulator in the blood coagulation cascade.* Mol Cell Biol, 1993. **13**(8): p. 4976-85.
174. Avanzi, G.C., et al., *GAS6, the ligand of Axl and Rse receptors, is expressed in hematopoietic tissue but lacks mitogenic activity.* Exp Hematol, 1997. **25**(12): p. 1219-26.
175. Nakano, T., et al., *Vascular smooth muscle cell-derived, Gla-containing growth-potentiating factor for Ca(2+)-mobilizing growth factors.* J Biol Chem, 1995. **270**(11): p. 5702-5.
176. Goruppi, S., E. Ruaro, and C. Schneider, *Gas6, the ligand of Axl tyrosine kinase receptor, has mitogenic and survival activities for serum starved NIH3T3 fibroblasts.* Oncogene, 1996. **12**(3): p. 471-80.
177. Valverde, P., M.S. Obin, and A. Taylor, *Role of Gas6/Axl signaling in lens epithelial cell proliferation and survival.* Exp Eye Res, 2004. **78**(1): p. 27-37.

178. Angelillo-Scherrer, A., et al., *Role of Gas6 receptors in platelet signaling during thrombus stabilization and implications for antithrombotic therapy.* J Clin Invest, 2005. **115**(2): p. 237-46.
179. Camenisch, T.D., et al., *A novel receptor tyrosine kinase, Mer, inhibits TNF-alpha production and lipopolysaccharide-induced endotoxic shock.* J Immunol, 1999. **162**(6): p. 3498-503.
180. Anderson, H.A., et al., *Serum-derived protein S binds to phosphatidylserine and stimulates the phagocytosis of apoptotic cells.* Nat Immunol, 2003. **4**(1): p. 87-91.
181. Tall, A.R. and L. Yvan-Charvet, *Cholesterol, inflammation and innate immunity.* Nat Rev Immunol, 2015. **15**(2): p. 104-16.
182. Chen, S. and D. Wang, *Intestinal-derived HDL: The portal guardian of the liver.* Immunity, 2021. **54**(9): p. 1903-1905.
183. Brunham, L.R., et al., *Intestinal ABCA1 directly contributes to HDL biogenesis in vivo.* J Clin Invest, 2006. **116**(4): p. 1052-62.
184. Han, Y.H., et al., *Enterically derived high-density lipoprotein restrains liver injury through the portal vein.* Science, 2021. **373**(6553).
185. Schroepfer, G.J., Jr., *Oxysterols: modulators of cholesterol metabolism and other processes.* Physiol Rev, 2000. **80**(1): p. 361-554.
186. Ikegami, T., et al., *Increased serum liver X receptor ligand oxysterols in patients with non-alcoholic fatty liver disease.* J Gastroenterol, 2012. **47**(11): p. 1257-66.
187. Raselli, T., et al., *Elevated oxysterol levels in human and mouse livers reflect nonalcoholic steatohepatitis.* J Lipid Res, 2019. **60**(7): p. 1270-1283.

7. Summary

Our data shows that lack of GPR183 resulted in increased abundance of hepatic cDC and DC progenitors due to their increased in-situ proliferation and impaired apoptosis. Next, we investigated whether an active production of 7α,25-OHC is needed to maintain normal DC numbers in the liver and we assessed the liver-resident DC compartment of *Ch25h*$^{-/-}$ and *Cyp7b1*$^{-/-}$ mice. Here we observed an increased abundance of hepatic DCs within these mice. Furthermore, analysis of chimeric experiments revealed that the radioresistant stromal compartment is crucial for maintaining the DC pool size and that DCs are closely associated with 7α,25-OHC producing endothelial cells in the portal regions of the liver. Next, our single-cell transcriptomics data and NIchenet-based in-silico receptor-ligand inference alongside spatial analyses identified M-CSF-M-CSFR and Gas6-Axl endothelial cell-DC interactions as crucial to the control of DC pool size within the murine liver. Additionally, blocking the gut-liver axis cholesterol transport also showed similar M-CSF and Gas6 dependent increase in hepatic DC numbers. Finally, to understand the role of GPR183 in disease and pathophysiological conditions we fed WT and *Gpr183*$^{flox/flox}$-*Zbtb46*-cre^{+} animals on CDAA-HFD and our data showed a significantly increased lipid content and decreased ALT and AST serum concentration in KO animals compared to their WT counterparts.

Taken together, these findings demonstrate that GPR183 plays a cell-intrinsic role in organization and survival of hepatic DCs in murine liver. Additionally, M-CSF and Gas6 produced by endothelial cells in the portal regions act as the guiding niche factor for positioning and survival of cDCs within the portal regions of liver. Our data also shows possible implication of GPR183 in health and disease and could pave ways for developing novel therapeutic targets for liver diseases.